INFORMATION TO USERS

This manuscript has been reproduced from the microfilm master. UMI films the text directly from the original or copy submitted. Thus, some thesis and dissertation copies are in typewriter face, while others may be from any type of computer printer.

The quality of this reproduction is dependent upon the quality of the copy submitted. Broken or indistinct print, colored or poor quality illustrations and photographs, print bleedthrough, substandard margins, and improper alignment can adversely affect reproduction.

In the unlikely event that the author did not send UMI a complete manuscript and there are missing pages, these will be noted. Also, if unauthorized copyright material had to be removed, a note will indicate the deletion.

Oversize materials (e.g., maps, drawings, charts) are reproduced by sectioning the original, beginning at the upper left-hand corner and continuing from left to right in equal sections with small overlaps.

Photographs included in the original manuscript have been reproduced xerographically in this copy. Higher quality 6" x 9" black and white photographic prints are available for any photographs or illustrations appearing in this copy for an additional charge. Contact UMI directly to order.

Bell & Howell Information and Learning
300 North Zeeb Road, Ann Arbor, MI 48106-1346 USA
800-521-0600

UMI®

EFFECT OF SUBSTITUTIONAL ELEMENTS ON DYNAMIC STRAIN AGING IN STEEL

by

Sandra Cunningham

A Thesis Submitted to the Faculty of Graduate Studies and
Research in Partial Fulfillment of the Requirements for the
Degree of Master of Engineering

Department of Mining and Metallurgical Engineering
McGill University
Montreal, Canada
June 1999
©

0-612-55019-2

ABSTRACT

Distinct serrations had been observed on the stress-strain curves of various steels tested previously at high temperatures (950-1100°C) at McGill University. An explanation proposed for this behavior was that dynamic strain aging (DSA), caused by the presence of *substitutional* elements, was taking place. To investigate the possibility that the jerky flow was caused by an interaction between dislocations and substitutional elements, the conditions of temperature and strain rate under which serrated yielding had previously been observed were explored. In addition, some of the same material was utilized in the testing. 5

Much of the previous work on DSA in steel has focused on the effect of interstitials, namely, carbon and nitrogen, rather than that of substitutional elements. These studies have been conducted in the blue brittle region (i.e. 100-400°C), where the diffusivity of the interstitial elements is sufficiently rapid for them to keep up with the moving dislocations. However, for substitutional elements to obtain enough mobility to induce DSA, the temperature range must be significantly higher.

The effect of substitutional elements on DSA in steel was examined in torsion and, although numerous tests were formulated and carried out in an attempt to gather evidence for this phenomenon, no firm data for the occurrence of DSA were obtained. Further experiments and analysis will be required to gain a better understanding of the behavior of DSA at elevated temperatures, particularly for the case where dynamic recrystallization is taking place. A testing method might then be devised that could make the effect of DSA more evident.

RÉSUMÉ

Des pics très particuliers ont été observés sur les courbes contrainte-déformation de différents aciers déformés à haute température (950-1000°C) à l'Université McGill. L'existence d'un phénomène de vieillissement dynamique sous déformation causé par les éléments *substitutionnels* a été proposé pour expliquer ce comportement. Afin de vérifier si les oscillations brutales des courbes de déformation étaient dues à une interaction entre les dislocations et les éléments substitutionnels, les conditions de température et de vitesse de déformation pour lesquelles ce phénomène avait été observé ont été explorées. De plus, les tests ont en partie été effectués avec ces mêmes matériaux.

La plupart des travaux précédents sur le phénomène de vieillissement dynamique sous déformation des aciers se sont intéressés à l'effet des interstitiels, c'est-à-dire le carbone et l'azote, plutôt qu'à celui des substitutionnels. Ces études ont été effectuées dans le domaine de fragilité au bleu (100-400°C), où la vitesse de diffusion des interstitiels est suffisante pour accompagner les dislocations en mouvement. Toutefois, dans le cas des substitutionnels, il est nécessaire d'augmenter la température de manière significative pour que la vitesse de diffusion soit suffisante pour induire le vieillissement dynamique sous déformation.

L'effet des éléments substitutionnels sur le vieillissement dynamique sous déformation a été étudié à l'aide d'essai de torsion et, bien que de nombreux test aient été effectués, aucun résultat n'a permis de mettre en évidence de façon certaine la réalité du phénomène. De nouveaux essais et analyses seront donc nécessaire pour obtenir une meilleure compréhension du vieillissement dynamique sous déformation à haute température, en particulier dans le cas où le métal subit une recristallisation dynamique. Il est donc nécessaire d'imaginer une nouvelle méthode d'étude qui permette de mettre en évidence de manière plus claire l'effet du vieillissement dynamique sous déformation.

ACKNOWLEDGEMENTS

I would like to express my gratitude to my thesis supervisor, Professor John J. Jonas, for giving me the opportunity to work under him and for his collaboration throughout the course of this work. I would also like to thank Visiting Professor René Le Gall and Laurent Gavard for their innovative ideas and suggestions. Their extensive theoretical knowledge and perspective allowed me to approach the work from different angles, which may have otherwise been overlooked. Their assistance was greatly appreciated.

I would like to recognize Edwin Fernandez, for all his technical help in numerous laboratory complications and bringing lightness to them, and Lorraine Mello for her administrative help and cheerful smile.

I am also grateful to my friends, past and present office mates included, within the department; their presence has made my studies all the more enjoyable. My memories from McGill will be forever cherished. I also want to acknowledge my friend, Janice, for all the great times we have had over the years. Finally, I would like to express my deepest thanks to my family: mummy, Marianne and Ben. Their unconditional love and support have made me what I am today.

TABLE OF CONTENTS

LIST OF FIGURES

CHAPTER II

CHAPTER III

CHAPTER IV

LIST OF TABLES

CHAPTER III

CHAPTER IV

CHAPTER I

INTRODUCTION

There are two types of strain aging that can be distinguished: static strain aging (SSA) and dynamic strain aging (DSA). Static strain aging refers to the hardening of a material that has undergone plastic deformation and which is subsequently aged for a period of time. The strengthening effect results from the diffusion of solute atoms to dislocations during aging. The formation of solute atmospheres around dislocations effectively pins, at least temporarily, the dislocations and restrains them from further movement upon reloading; these events consequently lead to an increase in the yield strength. A higher stress is then required to tear the dislocations away from the solute atmospheres. Strain aging may also increase the ultimate tensile strength, reduce the ductility, and raise the ductile-to-brittle transition temperature. Generally, in steel, the elements responsible for strain aging are carbon and nitrogen. This is due to the significantly higher diffusivities of interstitial solutes compared to substitutional solutes. The diffusivities are also a strong function of temperature and thus, the extent of strengthening depends on the aging temperature as well as the aging time.

In the case of dynamic strain aging, the aging process occurs *during* deformation. Solute atoms possess enough mobility to catch up with the moving dislocations and impede dislocation motion during deformation. Dislocations become temporarily pinned by obstacles, at which time solute atoms diffuse to the dislocations and lock them. The repeated pinning and unpinning of dislocations within the DSA domain is manifested on a stress-strain curve by serrations, also known as jerky flow or as the Portevin-LeChatelier (PLC) effect. DSA develops when the diffusivity of the solute atoms approaches the dislocation velocity. The occurrence of DSA is therefore dependent on temperature and strain rate: the diffusivity is a function of temperature while the dislocation velocity is governed by the strain rate.

Although serrated yielding is the most visible evidence of DSA, there are also other manifestations of DSA. These include an increase in the flow stress, an increase in the work hardening rate and more importantly, a negative strain rate sensitivity. In fact, it has been shown that these properties are affected over wider conditions of temperature and strain rate than of serrated yielding[1,2].

There has been extensive work on DSA over the last forty years, particularly on the effect of interstitial elements in steel and of substitutional elements in aluminum and zinc alloys. One area that remains vague and unexplored is the DSA caused by substitutional elements in steel. Some workers have alluded to the possibility of evidence for DSA[3,4]. Kirihata et al. have reported the occurrence of serrated flow over certain temperature and strain rate ranges in a Cr-Mo-V-Ni-Nb steel, suggesting that DSA originating from *substitutional* elements was responsible for the jerky flow[3]. It was reasoned that, over the temperatures explored, 900° to 1100°C, the diffusion rates of the interstitial elements were too high to contribute to DSA and so, it was deduced that the serrations were a result of substitutional element-dislocation interaction. A similar account of serrated yielding over a comparable temperature range was noted by Bai et al.[4] They observed serrations on the stress-strain curves of low carbon Nb-B steels tested in compression at a strain rate of $5 \times 10^{-4}\ s^{-1}$. The element they believed to be responsible for DSA was niobium.

The present study attempts to gain an understanding of solute-dislocation interactions at elevated temperatures (> 900°C) and to confirm early reports of evidence for the occurrence of DSA caused by substitutional elements. Several types of tests were formulated to extract evidence for the firm substantiation of DSA. The conditions of temperature and strain rate explored were similar to those where what was taken to be

long winded

serrated yielding had been previously observed[3]. The Cr-Mo-V-Ni-Nb steel used in the work of Kirihata et al. was utilized in the testing, as well as several other steels.

Chapter II provides the reader with a literature review on dynamic strain aging. An introduction to static strain aging is given, followed by the cause and manifestations of dynamic strain aging. A brief history of the discovery of DSA is presented, after which some of the definitions and mechanisms employed to describe DSA are identified. Basically, the pertinent work of various investigators over the last forty years is highlighted.

Chapter III describes the experimental techniques and materials used in the study. The chemical compositions as well as the geometry of the specimen are given. All mechanical testing procedures were based on torsion as the testing mode. The procedure for each type of test is elaborated with a brief justification.

Chapter IV presents the experimental results and discusses the relevance of the findings. Observations are made with regards to the testing procedure together with a rationale for each method that was chosen. Finally, the conclusions drawn from this study are given in Chapter V.

CHAPTER II

LITERATURE REVIEW

2.1 Static Strain Aging

The aging process can occur during or after deformation. The aging that takes place after deformation is better known as static strain aging (SSA). The general features describing SSA are illustrated in **Figure 2.1**, which depicts a typical normalized steel stress-strain curve (*curve A*), a pre-strained steel stress-strain curve (*curve B*) and an aged steel stress-strain (*curve C*). *Curve A* represents a typical mild steel curve with an upper and lower yield point. If the steel is then strained to *point X* and immediately retested, it will yield stress-strain *curve B*. The upper and lower yield point are no longer evident and the yield strength has increased. If, however, the specimen is allowed to age at room temperature or above for a period of time and then tested, *curve C* would be obtained. In this case, the upper and lower yield point as well as the Lüders extension are present. The yield point is now higher than that of the pre-strained steel because of aging.

SSA is most clearly manifested by an increase in yield stress upon aging after straining. Nevertheless, other properties can also be affected by SSA. These include the ultimate tensile strength, the ductility, the ductile-to-brittle transition, the high temperature strength, the fatigue strength and the electrical and magnetic properties[6]. As indicated in Chapter I, SSA is caused by the migration of solute atoms to dislocations and their subsequent locking. Generally, the elements responsible for SSA in steel are carbon and nitrogen. These interstitial elements have significantly higher diffusivities than the substitutional elements and can produce aging effects at relatively low temperatures and short periods of holding. The effect of nitrogen in strain aging is more pronounced as it has a higher solubility and diffusion coefficient in steel.

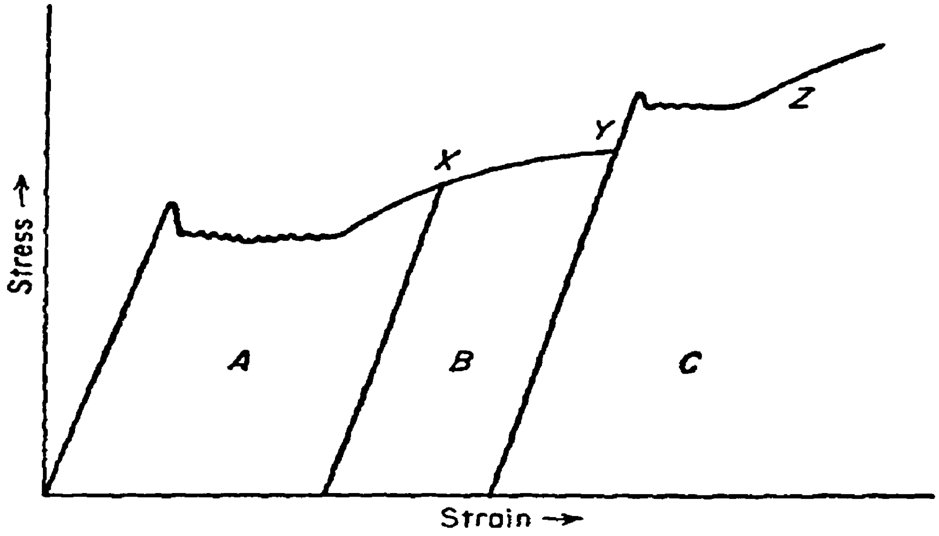

Figure 2.1: Stress-strain curves of normalized steel (*curve A*), pre-strained steel (*curve B*) and aged steel (*curve C*)[5].

It has been suggested by Hundy (cited in ref. 6) that the aging process occurs in two stages. The first stage includes the diffusion of solute species to the dislocation to form atmospheres. Stage two involves the formation of precipitates on the dislocations. The dislocation atmospheres form ideal sites for the nucleation of precipitates. According to Bilby (cited in ref. 7), solutes are drawn to the dislocation core and diffuse along the core to feed the precipitate particles spaced at intervals along the dislocation (i.e. by a process of pipe diffusion). The precipitates contribute to the overall strength of the material, raising the UTS and work hardening rate but lowering the elongation to fracture. If, however, there is a low concentration of solutes, only stage one occurs.

The practical significance of strain aging can be manifold. For example, it can affect cold forming operations by reducing the material's ductility or modify the toughness properties during cold working. Another processing problem that can arise is the formation of stretcher strain markings on the surface during deep-drawing due to inhomogeneous deformation. This behavior can usually be remedied by performing skin pass rolling or roller leveling, which applies a strain to the material (i.e. it brings it to *point X* in **Figure 2.1**) prior to the forming operation. If the material is not allowed to age, then the yield point phenomenon will disappear and will not produce the irregular surface markings. Aging can also have a positive application. For example, bake hardening involves heating a preformed product and allowing for diffusion of the interstitial elements in solution, such as carbon and nitrogen in steel, to dislocations in order to harden the material. It utilizes the strengthening effects of aging to improve the mechanical properties of a component.

2.2 Dynamic Strain Aging

Dynamic strain aging (DSA) involves strain aging *during* deformation. It occurs because of an interaction between the moving dislocations and solute atoms. It appears when the solute atoms, interstitial or substitutional, obtain enough mobility to keep up with the moving dislocations and form solute atmospheres. Thus, DSA develops in a certain temperature range where the diffusivity of the solute atoms is sufficient to impede and disturb dislocation motion. Alternate aging and breaking away from the atmospheres occurs as the band front extends along the gauge. The result and most obvious manifestation of DSA is serrated yielding. The pinning and unpinning of dislocations creates jerky flow on a stress-strain curve, as illustrated in **Figure 2.2**.

Serrated yielding was first observed by LeChatelier in 1909 when studying the properties of mild steel at elevated temperatures. LeChatelier and Portevin then investigated an aluminum alloy (3.5% Cu - 0.5% Mg - 0.5% Mn) and discovered the same behavior[1]. Serrated flow was subsequently referred to as the Portevin-LeChatelier or PLC effect.

The temperature range within which serrated yielding occurs is known as the DSA or PLC region. Below this temperature range, the diffusivity is too low for the solute atoms to segregate to the dislocations and lock them during deformation. Above this range, the diffusivity of the solute atoms is fast enough to keep up with the moving dislocations without causing a drag force or impeding their motion. The two are said to move in phase under the influence of their interaction energy[9].

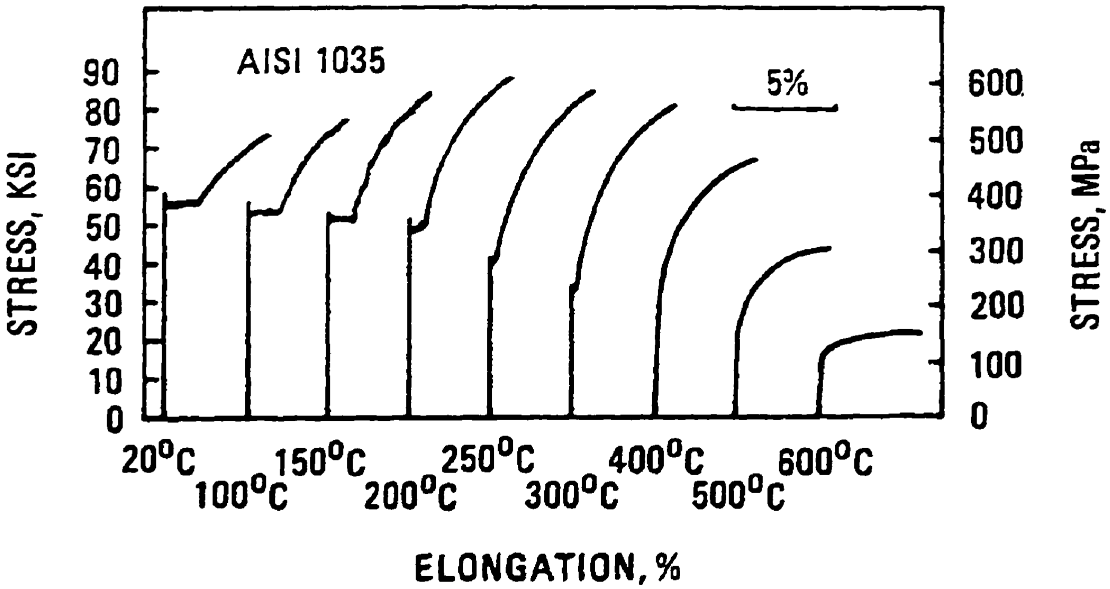

Figure 2.2: Stress-strain curve exhibiting the PLC effect in the temperature range 100 to 200°C of a carbon steel strained in tension at $d\varepsilon/dt = 1.75 \times 10^{-4}$ s^{-1} (8).

There have been several theories presented to explain the DSA process. According to Baird, DSA can be explained in terms of solute atoms segregating to dislocations to form Cottrell atmospheres; alternatively, Snoek ordering (stress induced) may be involved[10]. Snoek ordering refers to solute atoms jumping into lower energy sites lying within the stress fields of dislocations. The solute atmospheres and ordering of the solutes are said to cause a drag force and to reduce the dislocation velocity in this way[10-13]. That is, as the dislocation slows down from solute drag, more time is provided for additional solute atoms to migrate to the dislocation and in turn to slow it down even further. The stress required to move the dislocation is subsequently increased and, as this occurs, the dislocation begins to speed up again. This leads to the 'shedding' of solute atoms as they can no longer keep up with the accelerating dislocation.

The phenomena of solute drag and solid solution hardening are best illustrated by the diagram re-constructed from that of Blanc and Strudel and shown in **Figure 2.3**[14]. *Curve 1* represents the lattice friction force as a function of the dislocation velocity while *Curve 2* depicts the solute drag force. Both of these curves increase with increasing dislocation velocity, particularly the drag force curve which rises drastically. Conversely *Curve 3*, denoting the concentration of diffusing solute atoms, decreases with higher dislocation velocities. The behavior of the dislocation velocity during DSA is illustrated by *Curve 4*. At low speeds ($< V_M$), the solute atoms are capable of keeping up with the moving dislocations and the dislocation is considered to be in the drag regime. As the dislocation velocity increases (i.e. $> V_M$), it enters an instability regime and the dislocations begin to pull away from the solute atmospheres because the solute atmospheres can no longer keep up with the accelerating dislocations. As the dislocation velocity continues to increase to V_3, it begins to encounter obstacles such as dislocation substructures and grain boundaries, which tend to slow it down and bring it into the friction regime. When the dislocations reach a velocity of V_m, the dislocations once again reach a point of instability causing the dislocations to slow down even further and re-enter the drag regime. This repeated cycle is what causes the stress-strain curve to be serrated.

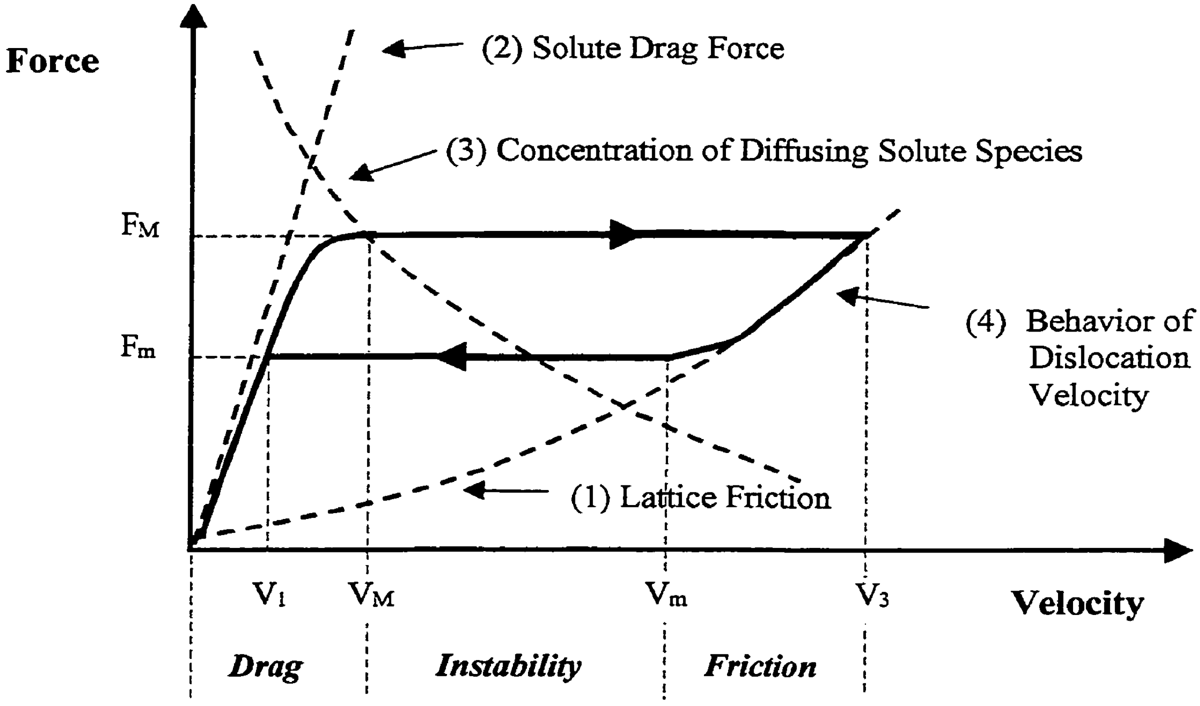

Figure 2.3: Stress-velocity diagram for mobile dislocation in the presence of impurities[14].

Within the solute drag regime, the drag force is said to be at a maximum when the dislocation proceeds at:

$$v_c = \frac{4D}{h} \qquad (2.1)$$

where D is the diffusion coefficient of the solute and h is the effective radius of the atmosphere[10,15]. Expressing this speed in terms of strain rate:

$$\dot{\varepsilon} = \rho_m b v_c = (4 b \rho_m / h) D = A D \qquad (2.2)$$

where ρ_m is the mobile dislocation density, b is the Burgers vector and A is a proportionality term that depends on solute concentration[16].

Another theory explaining the mechanism of DSA is that the dislocations are pinned by solute atoms and new dislocations must be generated in order to maintain the imposed strain rate[12]. According to Zeghib and Klepaczko, this is now the accepted explanation for the increased work hardening rate observed in the interstitial alloys[17]. Section 2.5.2 deals further with this theory.

A more recent theory, recognizing that dislocation motion is jerky, states that it is during the dislocation's waiting time at obstacles that the solute atoms migrate to the dislocations and if their mobility is sufficiently high or the waiting time long enough, the solutes atoms can create dislocation atmospheres and in effect cause DSA[18-20]. That is, a dislocation will advance freely for a time (t_f) until it encounters an obstacle (i.e. a precipitate or a dislocation forest), where it is temporarily arrested for a time (t_w). Thus, the dislocation velocity can be expressed as follows:

$$v = \frac{l}{t_f + t_w} \qquad (2.3)$$

where l is the distance between obstacles. If the diffusivity of the solute atoms is high enough, the solute atoms may lock onto the dislocation during the waiting time and increase the pinning strength[18-21]. If this occurs, a higher stress is required to move the dislocation line with solute atoms attached compared to when the dislocations have no solute atoms attached to them. The result of the pinning and unpinning of the solute atoms on the dislocations translates into serrations on the stress-strain curve.

2.3 Appearance and Disappearance of the Serrations Caused by DSA

The dependence on temperature of the appearance and disappearance of serrations is often expressed in terms of an Arrhenius-type equation:

$$\dot{\varepsilon} = A \exp \frac{-Q}{R\,T} \qquad (2.4)$$

where $\dot{\varepsilon}$ is the strain rate, A is a frequency factor, Q is the activation energy, R is the rate constant and T is the absolute temperature[2,16]. By constructing a plot of the strain rate vs the inverse temperature, one can obtain the conditions (i.e. temperature and strain rate) associated with the appearance and disappearance of the serrations. An example of such a plot is presented in **Figure 2.4**, where the filled squares symbolize a completely serrated stress-strain curve, the open squares indicate smooth stress-strain curves and the half filled squares relate to stress-strain curves with an intermediate degree of serrations.

At low temperatures, the solutes atoms are immobile with respect to the moving dislocations and do not impede their motion. At the other extreme, at high temperatures, the mobility of the solute atoms is such that they can follow the dislocations without any drag or disruption. At intermediate temperatures (i.e. the region where the squares are filled in **Figure 2.4**), the solute atoms interact with the moving dislocations and influence the flow properties. This region is known as the DSA region or domain.

The slopes of the two lines bounding the region where serrations are observed in **Figure 2.4** are proportional to the activation energies associated with the appearance and disappearance of serrations. The curve on the right denotes the appearance of serrations while the curve on the left represents the disappearance of serrations. In many cases, the activation energy for the appearance of serrations has been reported to be similar to the activation energy of the diffusing solute species[6,11,12,22,23]. The activation energy for the disappearance of serrations is hypothesized to be equal to the activation energy of the diffusing solute plus the binding energy of the solute species to the dislocation core[11,12]. As the solute atoms move with the dislocations, they have to jump to adjacent sites to keep up with the dislocations as well as make their normal diffusion jumps. Various methods of calculating the activation energies for the onset and termination of serrations are outlined in a paper by de Almeida[21].

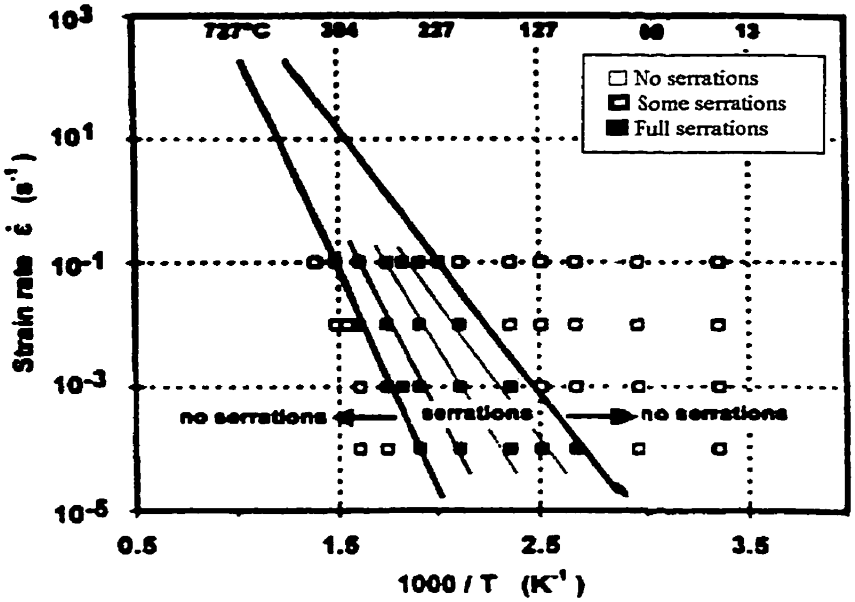

Figure 2.4: Temperature and strain rate range over which serrations are observed[22].

2.4 Effect of Temperature and Strain Rate on the DSA Domain

As the strain rate increases, so does the dislocation velocity and the time the dislocation spends arrested at obstacles is shortened. The diffusivity of the solute atoms must therefore be greater in order to catch up with the faster moving dislocations and sustain DSA. The diffusion coefficient increases exponentially with temperature and thus, an increase in temperature will result in an increase in diffusivity of the solute atoms. The effect of strain rate on the location of the DSA region is clearly illustrated in the work of Karimi Taheri et al. on low carbon steel[22]. They observed that the DSA region shifts to higher temperatures when the strain rate is increased from 10^{-4} s^{-1} to 10^{-1} s^{-1} in tensile tests.

2.5 Other Manifestations of DSA

Serrated yielding is an extreme and visible manifestation of DSA. However, there are also other mechanical properties that are affected by DSA. These include the flow stress, σ, the work hardening rate, θ, the Hall-Petch constant, K_ε, the strain rate sensitivity, γ, and the ductility. **Figure 2.5** illustrates how these properties are influenced within the DSA region[35]. The diagram also illustrates the trend of the affected parameters at temperatures *below* and *above* the DSA region. Within the DSA region, a peak or plateau in strength at a given strain can be observed as well as a peak in the work hardening rate and most importantly, a negative strain rate sensitivity. Many studies have shown that serrated yielding only occurs over a confined narrow temperature and strain rate region compared to the relatively wider conditions under which other evidence of DSA has been identified[1,2].

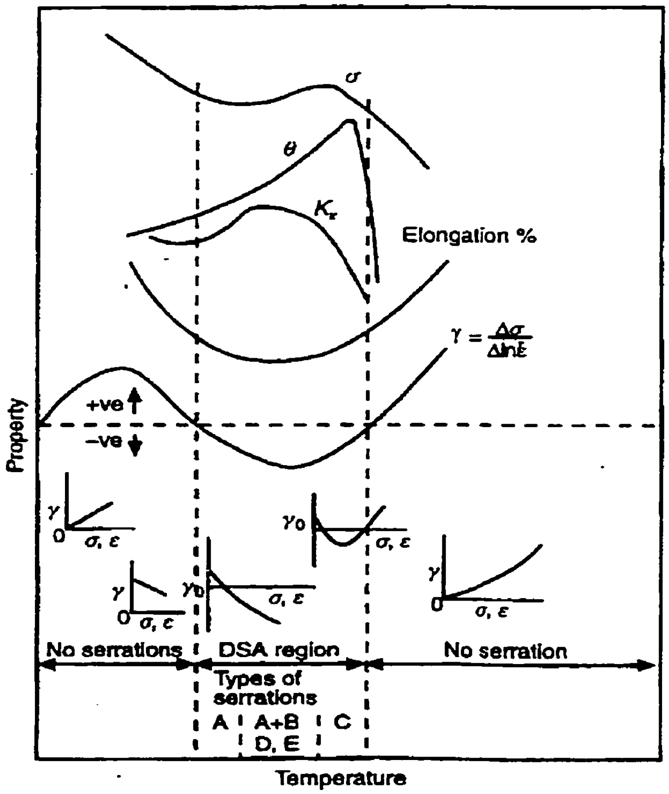

Figure 2.5: Schematic representations of different manifestations of DSA[35].

2.5.1 Peak or Plateau in Strength

The yield stress, σ_{ys}, can be considered as the strength of the initial obstacle substructure of a material prior to work hardening and the flow stress, σ_f, is the yield stress of the strain hardened material. Therefore, the strain hardening contribution, $\Delta\sigma$, can be considered as the change in strength that results from plastic deformation and is calculated as follows:

$$\Delta\sigma = \sigma_f - \sigma_{ys} \qquad (2.5)$$

The strain hardening contribution can be subdivided into individual contributions[24]. That is, flow stress increases due to dislocation-dislocation interactions ($\Delta\sigma_{dd}$), dislocation-precipitate interactions ($\Delta\sigma_{dp}$), and dislocation-solute interactions ($\Delta\sigma_{ds}$) are observed. If the sum of all these contributions is calculated, the overall work hardening or strain hardening contribution is obtained:

$$\Delta\sigma = \Delta\sigma_{dd} + \Delta\sigma_{dp} + \Delta\sigma_{ds} \qquad (2.6)$$

The $\Delta\sigma_{ds}$ component encompasses the DSA contribution and becomes significant in the DSA region..

A common method of demonstrating the effect of DSA on flow stress is to plot the change in magnitude of work hardening with respect to the magnitude of work hardening at room temperature as a function of temperature[2]:

$$\Delta\sigma' = \Delta\sigma - \Delta\sigma_o \qquad (2.7)$$

where $\Delta\sigma_o$ is $\Delta\sigma$ at room temperature (the flow stress, σ_f, is generally taken as the UTS or the peak stress). Lou et al. have utilized this method, as shown in **Figure 2.6**, to establish the DSA behavior on a construction grade steel (0.19% C, 1.2% Mn)[2].

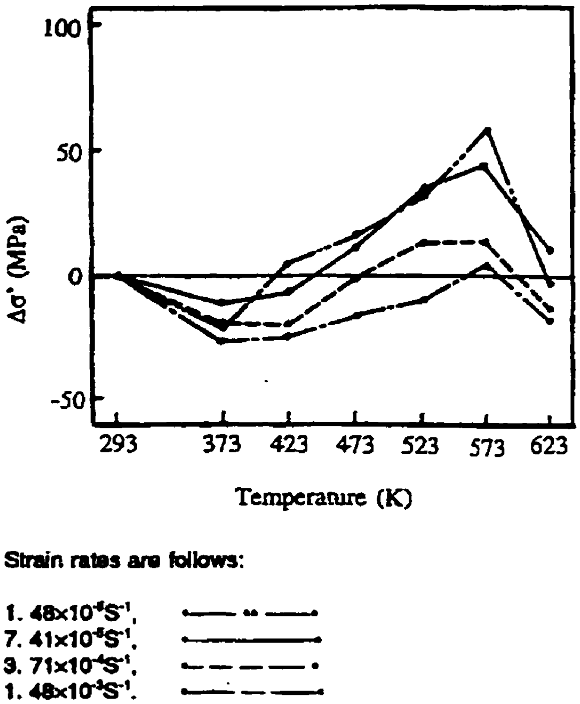

why not in sequence

Figure 2.6: Increase with respect to the room temperature value of work hardening, $\Delta\sigma$, in a construction grade steel[2].

2.5.2 Peak in the Work Hardening Rate

Keh et al. were the first investigators to study DSA dislocation structures through the use of transmission microscopy[11]. They showed that the increase in flow stress in the serrated region was attributable to significantly higher dislocation densities. This enhanced rate of dislocation multiplication with strain within the DSA region is due to the solute pinning. **Figure 2.7** illustrates the evolution of the average dislocation density with strain of mild steel deformed in tension at two different temperatures. A significant increase in the rate of dislocation generation in going from 25°C to 200°C is observed.

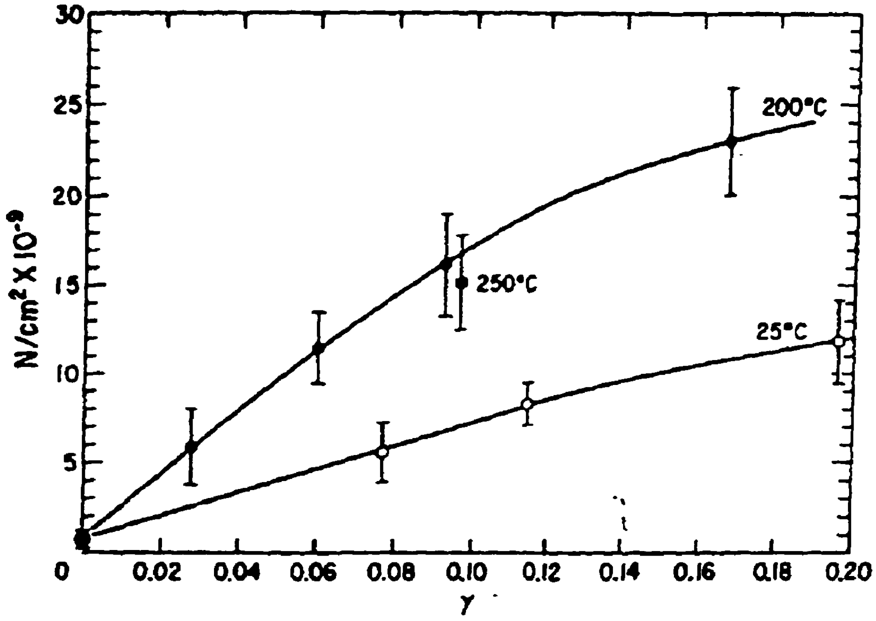

Figure 2.7: Evolution of dislocation density with strain and temperature[11].

2.5.3 Negative Strain Rate Sensitivity

In a normal thermally activated process, the response to a decrease in dislocation velocity would be a decrease in the resistance to motion. In other words, the flow stress decreases as the strain rate decreases. However, within the DSA region, the opposite holds true. The resistance to motion is raised as the strain rate or dislocation velocity decreases. This is due to the longer time the dislocation spends arrested at obstacles when moving at a lower average velocity, which results in more solute atoms diffusing to the dislocation. Consequently, the higher solute concentration around the dislocation produces a strengthening effect and thus, a higher stress is required to move the dislocation. According to Bouchaud et al., the hardening or aging is proportional to the 2/3 power of the waiting time before reaching saturation[25].

The net consequence of this 'antithermal' aging contribution phenomenon is a negative SRS occurring within the DSA region. **Figure 2.8** depicts the flow stress versus temperature curves of two materials, a pure one that does not exhibit DSA (dashed line) and the other that does (solid line), at both a low and high strain rate. The former continuously softens with increasing temperature, while the latter features a hump in the curve. The negative strain rate sensitivity is found in the temperature range of *region b*. When going from a low strain rate to a higher strain rate in this region, a flow stress decrease is observed. This is due to the hump in the flow stress-temperature curve observed in the presence of DSA. Conversely in *region c*, when going from a low strain rate to a high strain rate, the material undergoes an unusually high increase in flow stress. Again, this is attributable to the hump in the flow stress curve with increasing temperature.

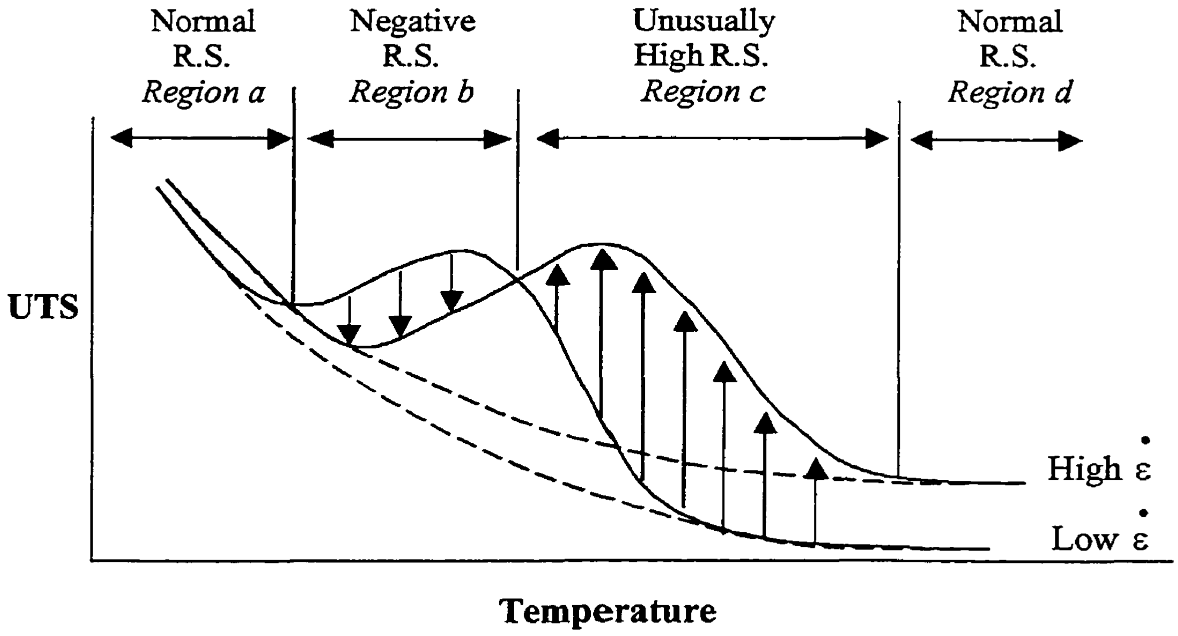

Figure 2.8: Stress versus temperature curves at a low and high strain rate of a material with and without exhibiting DSA showing different rate sensitivities (R.S.).

The significance of having a negative strain rate sensitivity is that deformation can proceed at a lower stress with an increase in strain rate and this can lead to flow localization (i.e. unstable deformation) brought about by shear bands and ultimately can result in catastrophic low-strain fracture.

Another interpretation given by Baird and Jamieson suggests that the negative strain rate sensitivity results from the localized exhaustion of sufficient solute atoms to lock the dislocations[26]. The material is weaker is these areas and therefore will tend to deform preferentially over the solute-rich areas.

2.6 Interaction Effects of Solutes and Precipitates on DSA

There are two classes of alloying elements that can be distinguished with respect to DSA. In the first class, we encounter elements that contribute to DSA by diffusing quickly enough through the lattice to dislocations and locking onto them. The effectiveness of an element in producing strain aging is a function of the following characteristics:

-its solubility
-its diffusion coefficient
-the severity with which it locks dislocations (i.e. its interaction energy).

The second class involves elements that alter the behavior of the first class and therefore affect DSA indirectly. The second class affects the first class by changing the latter's mobility or free concentration.

Examples of the second class include substitutional elements such as titanium, zirconium and niobium in steel that have an affinity for interstitial elements. These elements interact with carbon and nitrogen to form carbides, nitrides and/or carbonitrides. The presence of these elements appears to shift the DSA region to higher temperatures[12]. Another possible interaction of substitutional solute atoms (i.e. Mn, Mo, Cr) is the stress-induced ordering of substitutional-interstitial pairs or complexes, which effectively lowers the mobility of carbon and nitrogen[10].

The interaction effect of solutes, namely hydrogen, in commercial-purity titanium on the variables affected by DSA is evident in the work of Senkov et al.[16]. Their work demonstrated that hydrogen not only influenced the position of the work hardening peaks with respect to temperature but also their heights. In addition, the strain rate sensitivity increased with the addition of hydrogen. Therefore, the magnitude of DSA attributable to elements such as carbon, oxygen and iron was decreased with the addition of hydrogen. The explanation provided for this behavior was that hydrogen in solution hindered other solute atoms from 'latching on' to mobile dislocations because hydrogen dislocation atmospheres had already formed (due to its higher mobility). Furthermore, hydrogen was found to decrease the diffusivity of the other solute elements.

Another study conducted by Kishore et al. using a modified 9Cr-1Mo steel demonstrated that the size and distribution of precipitates can also affect the extent of DSA[27]. They compared their steel under two microstructural conditions. The steel was heat treated under similar conditions (normalized at 1000°C) except that one batch of specimens was subjected to a tempering temperature of 550°C while the other was held at 710°C. They found that the 550°C specimens were much less sensitive to DSA and this was attributed to the presence of finer second phase particles (0.04 μm in diameter and allegedly Cr_2C) compared to the coarser carbide particles (0.1 μm diameter) in the 710°C specimens. It was proposed that the finer precipitates acted as more effective carbon sinks than the coarser particles and, therefore, depleted the solute atmospheres much more rapidly. As plastic deformation proceeds, the solute atoms are depleted from the arrested dislocations and diffuse, via pipe diffusion, to the precipitate sinks. Consequently, the severity of DSA was considerably reduced in the 550°C specimens.

2.7 Controlling DSA

It appears that the most effective way of minimizing the DSA caused by interstitial solutes in steel is through the addition of microalloying elements such that carbides, nitrides and carbonitrides are formed[28]. The idea is to 'trap' the interstitials in the form of carbides, nitrides and carbonitrides so that the concentration of carbon and nitrogen in solution is greatly reduced; this therefore reduces the sensitivity to DSA. Boron additions have proven to be useful in decreasing the deleterious effects of DSA in low carbon steels subjected to cold deformation during production[29]. The effects of several other alloying elements on strain aging can be reviewed in a paper by Baird[30]. W/Cr

2.8 Implications of DSA

The effect of DSA on manufacturing processes has been reported in many papers[6,22,28,31]. Examples include the reduced drawability resulting from the unstable deformation due to negative strain rate sensitivity and the cracking due to lower ductility. The domain where DSA exists must be considered when selecting operating conditions (i.e. temperature, strain rate). Parameters such as composition and microstructure should also be considered because the existence of DSA is strongly dependent on if and how the solute species are present in the material. The processing conditions under which DSA can occur are therefore not the only consideration. Prior treatment can affect whether DSA will occur at all. For example, in drawing, the cooling rate after hot rolling will affect the amount of the solute species in solution and therefore the susceptibility to DSA. If the amount of solute species in solution is carefully controlled during the cooling stage, the extent of DSA may be greatly reduced. Any pre-treatment which increases the amount of solute species in solution will increase the susceptibility to DSA and vice versa.

The addition of alloying elements to a material can also affect the DSA behavior. As highlighted in section 2.6, the addition of nitride, carbide and carbonitride formers to steel will generally reduce the sensitivity to DSA caused by the presence of carbon and nitrogen.

DSA can also be a positive phenomenon if its domain is well known. For example, it can be used as a thermomechanical treatment to increase the room temperature strength[12]. It can also serve as a strengthener at elevated temperatures because of the associated increased strength, higher work hardening rate as well as better resistance to creep and fatigue.

2.9 Modelling DSA

The importance of reliably detecting and predicting DSA beyond the range where it is visible as a result of serrated yielding must be emphasized. It is through modelling that it may be predicted, controlled and accounted for before establishing forming or processing operating parameters that may be greatly affected by DSA.

Kubin and Estrin have modelled the critical strains associated with the PLC effect in terms of strain dependence and the densities of both the mobile and forest dislocations[32,33]. They have also addressed and tried to account for the occasional observation of two PLC regimes within the same deformation curve. **Figure 2.9** shows the strain dependence of the mobile and forest dislocation densities obtained for a specific set of parameters outlined in the paper's appendix. Based on these two dislocation density evolutions, they were able to predict DSA domains and explain the experimental observation of two PLC regimes within the same stress-strain curve, such as demonstrated in the work of Schwink and Nortmann[34].

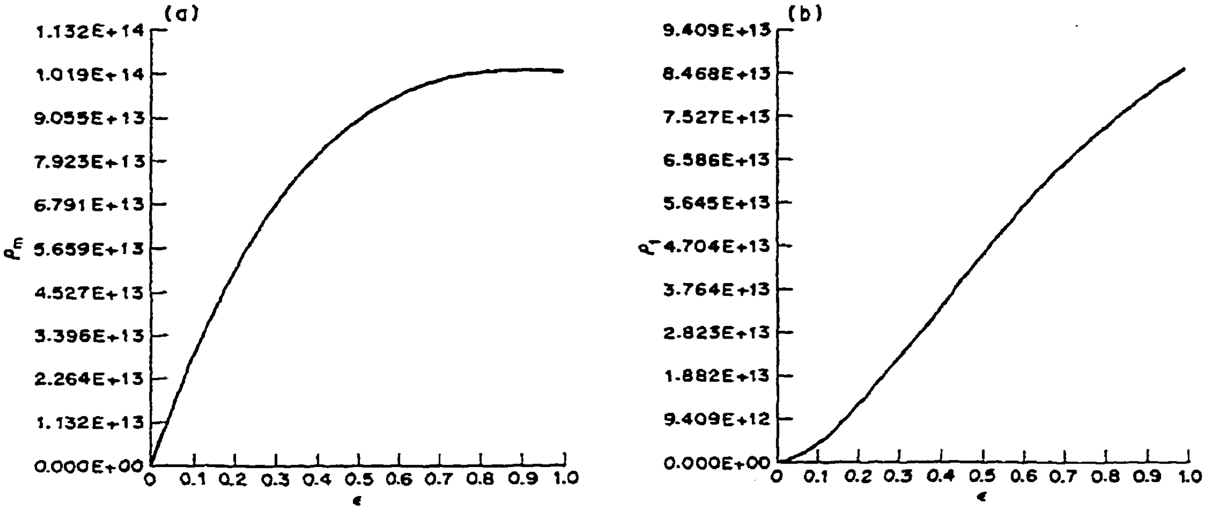

Figure 2.9: Strain dependence of (a) the mobile dislocation density ρ_m and (b) the forest dislocation density ρ_f[32].

2.10 DSA Caused by Substitutional Elements

The elements responsible for DSA can be either interstitial, substitutional or complexes of the two. This section deals with the latter two. The temperature at which the DSA caused by substitutional elements appears must be significantly higher than that for the DSA brought about by interstitial elements. This is due to the considerably lower diffusivities of the substitutional elements. Thus, in order for substitutional atoms to gain enough mobility, the temperature must be raised such that the diffusivity approaches the dislocation velocity.

Much of the work on DSA has focused on the effect of interstitial elements in steel (or BCC alloys). Some work has been conducted on the DSA caused by substitutional elements, although most of it has concentrated on FCC materials such as aluminum or the HCP zinc alloys. There appears to be little research on the DSA caused by substitutional elements in steel, specifically at high temperatures (> 900°C).

2.10.1 Types of DSA Serrations

Serrations have been classified into five classes according to their appearance[1]. **Figure 2.10** depicts the patterns of the different types of serrations. These classifications have been made based on FCC materials containing substitutional solutes. Type A consists of periodic locking serrations with a sharp increase in flow stress followed by a drop below the general level of the curve. Type A serrations arise from the propagation of Lüders bands from one end of the gauge to the other. Type B serrations appear when there is an irregular movement of the Lüders band front and manifest themselves by small oscillations about the general level of the flow curve. Type C serrations occur when many Lüders bands form at various locations on the gauge and lead to abrupt drops below the stress level, known as unlocking serrations. Type D serrations are manifested by plateaus on the curve with no evidence of work hardening. Type E serrations are harder to recognize as they are less structured and often appear after type A serrations and at higher strains. Types C and D generally occur at higher temperatures, while types A, B and E present themselves at lower temperatures and high strain rates[35]. It should be noted that more than one type of serration can appear simultaneously. For example, in the inset of **Figure 2.10**, type A and type B serrations as well as type B and type D are all occurring concurrently.

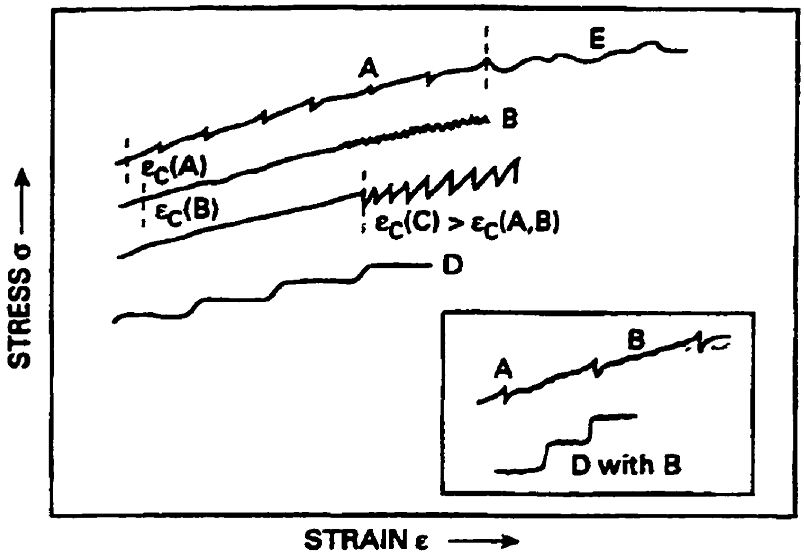

Figure 2.10: Types or classes of serrations commonly observed in the deformation of substitutional solid solution alloys[1].

2.10.2 Homogeneous Strain

A critical strain that precedes the first appearance of serrations has been recorded in certain alloys; it has been shown to vary with solute concentration, strain rate and temperature[10,18,36,37]. The dependences on the latter two are illustrated in **Figure 2.11**. An explanation for the delay in the appearance of the first serrations offered by Cottrell was that an enhanced diffusion coefficient is obtained in the presence of vacancies[37]. He postulated that serrated flow could occur at a much lower temperature than that predicted using the lattice diffusion coefficients of the solute atom responsible for DSA. For example, it was shown that the activation energy for the appearance and growth of serrations was about half the activation energy for the bulk diffusion of nickel and silicon in iron, the substitutional elements believed to be responsible for DSA[9]. Cottrell rationalized that the diffusion coefficient is enhanced by the vacancies introduced during deformation according to the relation:

$$D = k_1 C_v \exp(-Q/kT) \qquad (2.8)$$

where C_v is the concentration of vacancies, which varies with strain according to the following relationship:

$$C_v = B\varepsilon^m \qquad (2.9)$$

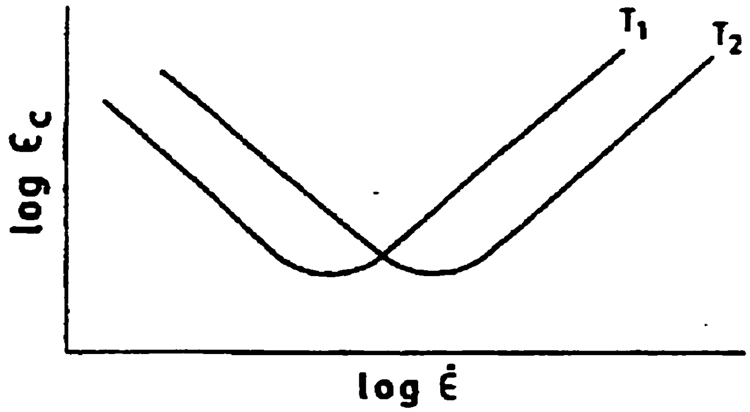

Figure 2.11: Effect of strain rate and temperature on critical strain[35].

The bulk diffusion of substitutional solute atoms is enhanced by the creation of vacancies during deformation. That is, a material must be initially strained to a point such that the diffusion coefficient is sufficiently accelerated by the presence of vacancies to induce DSA. The mobile dislocation density also changes as a function of strain according to the following equation:

$$\rho_m = x \quad \varepsilon^{\beta} \qquad (2.10)$$

where x and β are constants. Thus, equation 2.4 can now be modified to account for the critical strain and evolution of the mobile dislocation density:

$$\dot{\varepsilon} = k \quad \varepsilon_c^{\,(m+\beta)} \quad \exp\frac{-Q}{R\,T} \qquad (2.11)$$

where k is a constant, ε_c is the critical strain, and m and β are also constants defined by equations 2.9 and 2.10, respectively.

Equation 2.11 has been shown to be in good agreement with the work of Winstone et al. (as cited in ref. 28), who studied the mechanical properties of an Fe-1.1 at% Nb alloy over a wide temperature range. Typically, m + β varies between 0.5 and 1 for interstitial elements and 2 and 3 for substitutional elements[38].

However, this interpretation, even with modifications to account for other effects (i.e. grain size, thermal effects, etc.), does not explain all the experimental results satisfactorily[10,39,40]. In fact, there exists work that contradicts this theory. Experiments involving straining an alloy, subsequently aging it so as to allow for complete or partial annealing and then restraining, showed that the critical strain was not affected by the intermediate annealing stage[41,42]. According to the theory proposed by Baird, the critical strain should have increased considering that the vacancies were removed by the annealing stage and, therefore, a higher strain would be required to produce serrated yielding.

An alternative explanation offered by Cuddy and Leslie was that, rather than the vacancies enhancing diffusion, the DSA observed at lower temperatures was due to solute pipe diffusion along dislocations; the latter raised the diffusivity and allowed for the redistribution of solute atoms at much lower temperatures[9]. Thus, the diffusion mechanism proposed was core or pipe diffusion rather than lattice diffusion. It explained why serrations appeared at much lower temperatures than those predicted by using the substitutional lattice diffusivities. They found that the activation energy of pinning was roughly half that of lattice solute diffusion

Thus, there is no general agreement about the diffusion mechanism involved in substitutional DSA. However, experiments have demonstrated in certain cases that the activation energy associated with DSA is significantly lower than that of volume or bulk diffusion. The elements responsible for DSA have also been disputed. Some workers have argued that it is interstitial-substitutional complexes that form and lock the dislocations causing DSA rather than the interstitial or substitutional elements themselves[9,35]. The appearance of serrations in some cases is probably due to complexes or clusters, with a combination of interstitial and substitutional elements forming atmospheres around the moving dislocations rather than individual free substitutional elements. In other instances, it can be solely due to interstitial or substitutional elements, as proved by many investigators.

2.11 Summary

Dynamic strain aging involves strain aging *during* deformation and results from the interaction of moving dislocations and solute atoms. DSA arises from the repeated pinning and unpinning of mobile dislocations by solute atoms. It develops when the mobility of solute atoms is sufficient to keep up with moving dislocations and impede dislocation motion. The elements responsible for DSA may be interstitial or substitutional depending on the temperature and imposed deformation rate. In some cases, it has been suggested that complexes are responsible for DSA. The most obvious manifestation of DSA is serrated yielding on a stress-strain curve. Other properties can also be affected by DSA and these include the flow stress, the work hardening rate, and more importantly, the strain rate sensitivity.

This chapter has highlighted the results and findings regarding dynamic strain aging of several investigators. However, there are areas that still remain vague, speculative or simply unknown. For example, little research has been carried out on the DSA caused by substitutional elements in steel. Some of this work is described in the chapters that follow.

CHAPTER III

EXPERIMENTAL DETAILS

The experimental technique employed was torsion testing as it allowed for testing over a wide range of strain rates and the attainment of large strains. It was also chosen because it provided a starting block of the temperature and strain rate conditions under which serrated yielding had previously been observed in torsion and over which the DSA domain could hopefully be mapped.

3.1 Materials

The materials tested were acquired as transfer bars supplied by Sumitomo Metal Industries in Japan in the form of plates approximately 20 cm x 20 cm x 2 cm. The first material, steel A, consisted of a high carbon Mn-Cr steel. The second and more important material, steel B, was a medium carbon steel containing various alloying elements in significant quantities. The chemical compositions of the two steels are listed in **Table 3.1**.

Table 3.1: Chemical compositions of the experimental materials in wt%.

Steel	C	N	Mn	P	S	Si	Cu	Ni	Cr	Mo	V	Nb	Ti	Sol Al
A	0.24	0.003	0.64	0.018	0.009	0.13	<.01	0.07	0.19	<.004	<.01	0.013	0.031	0.03
B	0.45	0.003	0.67	0.0014	0.005	0.19	0.02	0.47	0.99	0.96	0.12	0.014	0.014	0.049
C	0.07	<.001	0.270	0.028	0.004	0.20	N/A	N/A	N/A	0.010	N/A	<.001	N/A	N/A
D	0.155	0.0005	0.01	0.002	0.001	0.03	N/A	30.5	N/A	N/A	N/A	0.005	N/A	N/A
E	0.28	N/A	0.52	0.016	0.004	0.22	N/A	N/A	0.83	0.15	N/A	N/A	N/A	N/A
F	0.05	N/A	0.37	0.006	0.006	0.03	N/A	N/A	N/A	N/A	N/A	0.03	N/A	N/A
Iron	0.03	N/A	0.054	<.002	<.003	<.001	0.018	0.009	0.22	<.017	N/A	<.002	N/A	N/A

N/A = Not Available

The material utilized to verify the background "noise" level produced by the torsion machine was electrolytic iron and its chemical composition is also shown in **Table 3.1**. The electrolytic iron bars (7.5 cm x 7.5 cm x 15 cm) were provided by CANMET in Ottawa. Although the chemical analysis of the "pure" iron revealed it to contain some impurities, it served the purpose of demonstrating the difference between fairly pure material vs. the steels tested. In addition, other materials, whose chemical compositions are listed in **Table 3.1**, were tested to evaluate the level of scatter on the stress-strain curve as a function of the level of alloying or impurity elements.

Torsion specimens were prepared from the steel plates and iron bars with the geometry shown in **Figure 3.1**. Samples were taken such that the longitudinal axis corresponded to the rolling direction of the plate.

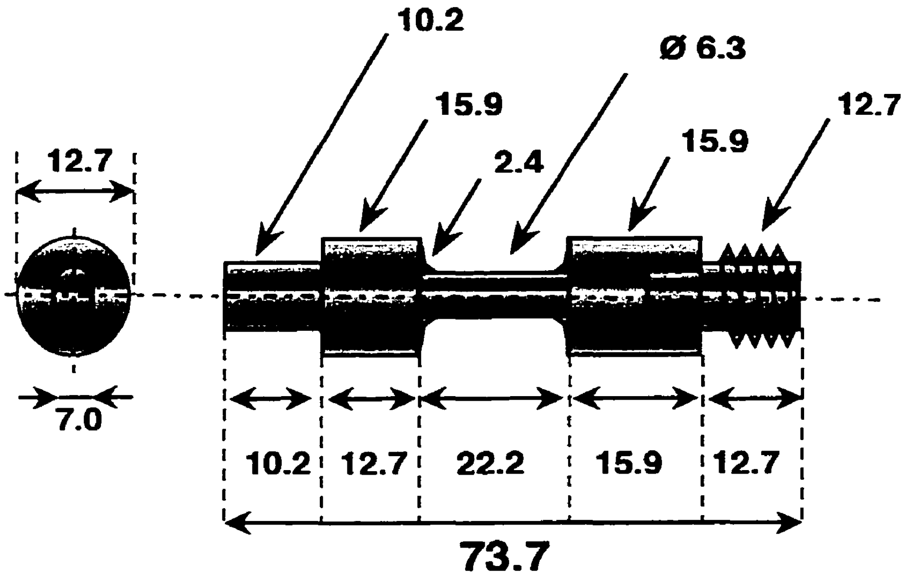

Figure 3.1: Geometry of the torsion specimens (in mm).

3.2 Instrumentation

Torsion tests were performed on a servo-hydraulic computer-controlled Materials Testing System (MTS) torsion machine. The torsion machine rests on a lathe bed, as shown in **Figure 3.2**. The hydraulic power is supplied by an MTS 501 series Hydraulic Power Supply. The power is fed through a servovalve and transmitted to the rotating hydraulic actuator. The specimen is screwed into the stationary grip while the other end is fitted into the slot of the rotating grip that provides the couple to the specimen. A 2 mm gap was left between the specimen and the rotating grip to allow for thermal expansion. The angular displacement was measured by either a 10-turn or a 50-turn potentiometer. Tests were initially performed on the latter and it was only later recognized that the 10-turn potentiometer could be utilized for smaller strains. The 10-turn potentiometer allows for more accurate control of the twist. The torque cell on the right recorded the torque. Two types of torque cells were utilized: a 112.98 N-m (1000 in-lb$_f$) cell and an 11.30 N-m (100 in-lb$_f$) cell. The lower torque cell was employed when the material was believed to be soft enough so as not to exceed the maximum allowable torque (i.e. when the testing conditions corresponded to high temperatures and/or low strain rates).

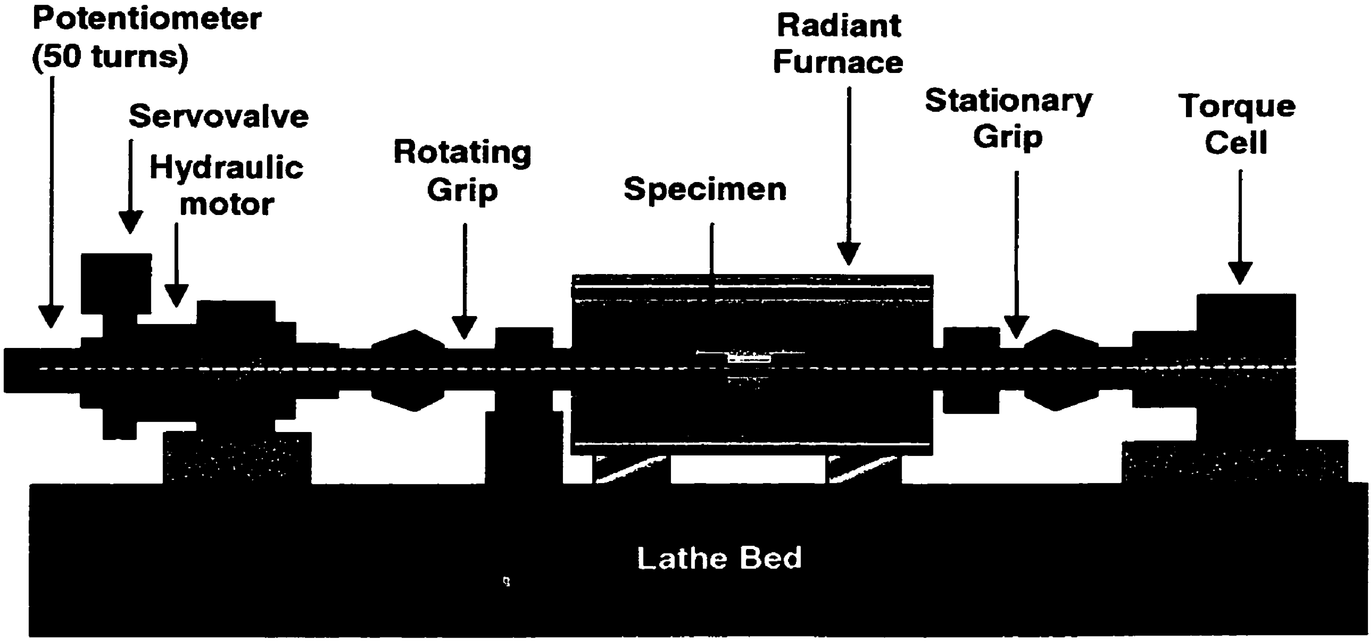

Figure 3.2: Schematic diagram of the torsion machine.

3.3 Furnace and Temperature Control

The sample is enclosed in a radiant furnace heated by four tungsten filament lamps manufactured by Research Inc. The temperature is controlled through a feedback control circuit consisting of a Leeds & Northrup Electromax V Controller while temperature programming is carried out using a 1300 Leeds & Northrup Process

Programmer. The temperature is detected by an Omega 1.5 mm (1/16") Type K enclosed thermocouple in contact with the gage length of the specimen at about 7 mm from its shoulder. The sample was contained in a quartz tube with high purity argon flowing through it to prevent oxidation.

3.4 Data Acquisition and Data Processing

The TestWare-SX™ program operates under Operating System/2™ (OS/2®) using a 486 generation PC. The TestStar™ software allows for the programming of the deformation schedule (i.e. strain, strain rate, time). The test templates and procedures can be saved and stored in the TestWare-SX program. The program also allows for the prescription of a data acquisition rate up to a maximum of 1000 data point/s. The twist-temperature-torque data could be viewed on the TestStar workstation while the complete twist-time-temperature-torque data were acquired by the microcomputer connected to the digital control feature of the TestStar.

The output data file from the TestStar software was converted to spreadsheet format for further processing and graphical representation. There were two software packages utilized to interpret the data: EXCEL and ORIGINAL. The latter is a much more powerful software, which allows for data manipulation beyond the capabilities of EXCEL.

The measured angular rotation or twist, θ, of the specimen was manipulated to express the deformation in terms of the equivalent von Mises strain, ε, using the following equations:

$$\gamma = \frac{\theta D}{2L} \qquad (3.1)$$

$$\varepsilon = \frac{\gamma}{\sqrt{3}} \qquad (3.2)$$

$$\varepsilon = \frac{\theta D}{2\sqrt{3}\,L} \qquad (3.3)$$

where γ is the shear strain, and D and L are the diameter and length of the specimen gauge, respectively. In a similar manner, the twist rate could be converted into the equivalent strain rate, $\dot{\varepsilon}$:

$$\dot{\varepsilon} = \frac{\dot{\theta} D}{2\sqrt{3}\, L} \tag{3.4}$$

The torque, T, was converted into the equivalent stress, σ, using the equation of Fields and Backofen[43]:

$$\sigma = \frac{4\sqrt{3}\, T}{\pi D^3}(3 + m + n) \tag{3.5}$$

where T is the torque, m is the macroscopic strain rate sensitivity and n is the macroscopic strain hardening coefficient. For simplicity, the variables m and n were set constant at 0.17 and 0.13, respectively. Although m is approximately constant during a given high temperature test, n is first positive, then negative, and finally zero when dynamic recrystallization takes place. Here, the negative and zero values of n were overlooked.

3.5 Temperature Selection

The diffusivity of substitutional elements is significantly slower than that of interstitial elements. Much higher temperatures are therefore required in order to develop the type of DSA caused by substitutional elements compared to when DSA is generated by the diffusion of interstitial elements. Thus, testing temperatures were selected over the range where the diffusivity of substitutional elements becomes appreciable (i.e. > 900°C). By recognizing that the DSA caused by the interstitial elements, carbon and nitrogen, occurs between the temperatures of 150 and 300°C, depending on the strain rate, and knowing their diffusivities within this temperature range, an equivalent temperature range can be found for the substitutional elements. This is illustrated in **Figure 3.3**, which allows for the direct comparison of the diffusion coefficients of carbon and nitrogen to those of the substitutional elements. By assuming that the diffusion coefficients for the substitutional elements should equal those of carbon and nitrogen for DSA to occur, the temperature range is found to be 900 to 1350°C, depending on the substitutional element of interest.

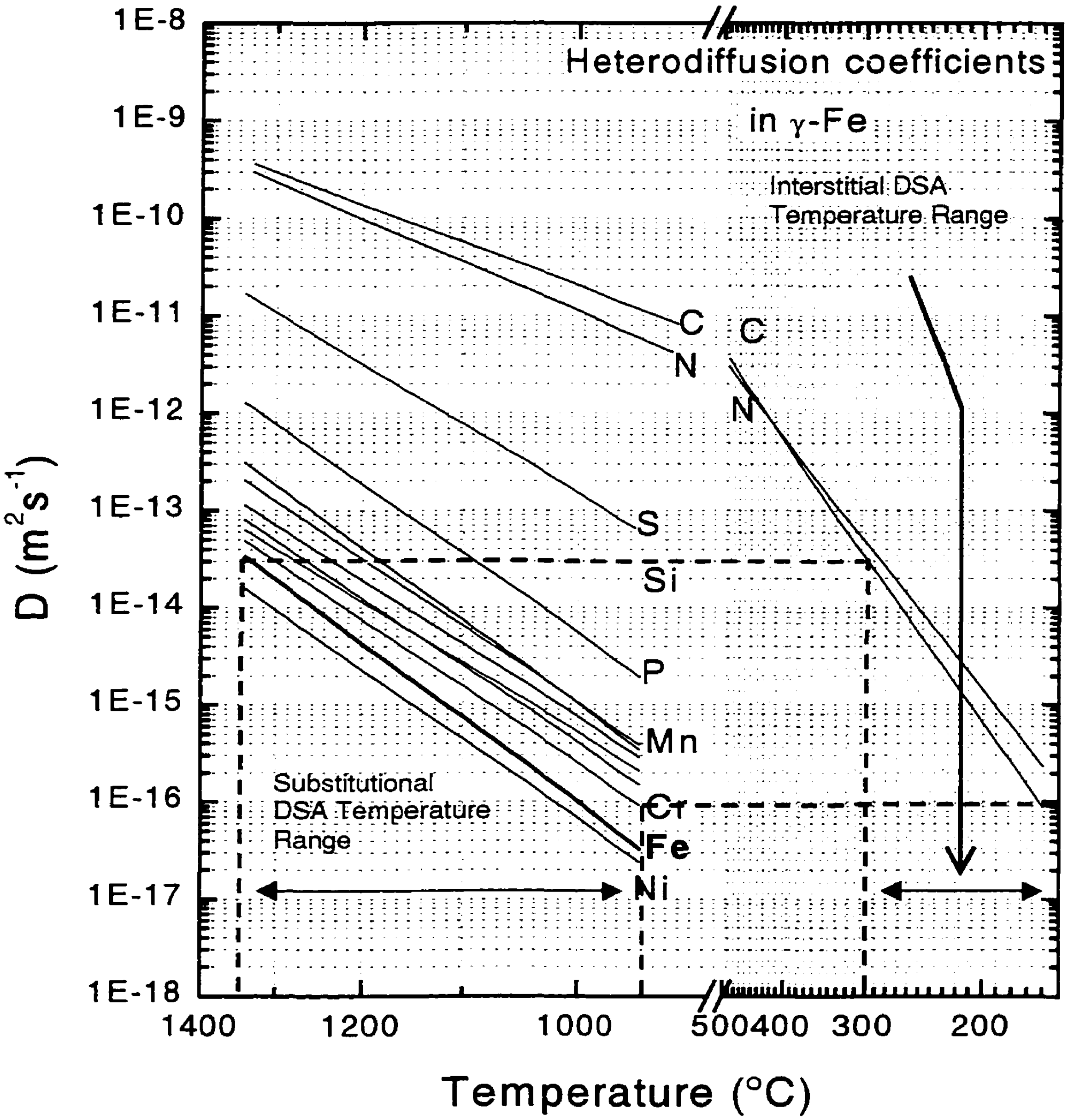

Figure 3.3: Diffusion coefficients of interstitial and substitutional elements in iron[44].

3.6 Test Techniques

There were several types of tests performed in attempting to extract evidence of DSA caused by substitutional elements in the austenite phase. All tests were configured such that they could be performed in torsion since all the specimens were already machined for this testing mode. The first set of tests examined the stress scatter level on the stress-strain curves of various alloys. Single pass torsion tests carried out at a constant strain rate constituted the second class of tests. The following experiments were formulated because initial results were inconclusive, as discussed in Chapter IV. Subsequent tests were conceived based on speculative initial results or devised from previously established methods used to reveal evidence of DSA[33,45]. The rationale and justification of the experiments are briefly covered in the experimental techniques below but they are detailed in more depth in Chapter IV.

The third group of tests entailed changing the strain rate during deformation. The fourth set of experiments varied the temperature during deformation in order to determine the conditions of instability where DSA occurs. The next approach was modifying the stress at a constant rate and observing the effects on the strain rate. The final class of tests consisted of again going through strain rate changes during the deformation, only this time, the strain rate changes were much smaller. The testing techniques and parameters of each test are elaborated in the following sections.

3.6.1 Single Pass Torsion Tests

Single pass deformation is the simplest of all the tests and entails deforming at a constant strain rate to a specified strain. Steel A, steel B and the iron underwent this type of test. Steel A was tested with the intent of getting familiar with the torsion machine and to observe evidence of DSA. The temperatures investigated ranged from 900 to 1100°C, in 50°C increments, at the following strain rates: 10^{-4}, 10^{-2}, 1, 5 s^{-1}. In the case of the iron, the purpose was to evaluate the background "noise" level of the machine. The temperatures explored ranged from 900 to 1150°C using strain rates of 10^{-2} and 1 s^{-1}.

Steel B was the material of greater importance as it contained more alloying elements and exhibited more distinct serrations in previous tests. The conditions examined for steel B are summarized in **Figure 3.4**. The temperatures ranged from 900 to 1200°C and the strain rate began at 10^{-3} s^{-1} and extended to $1s^{-1}$, with jumps of one order of magnitude.

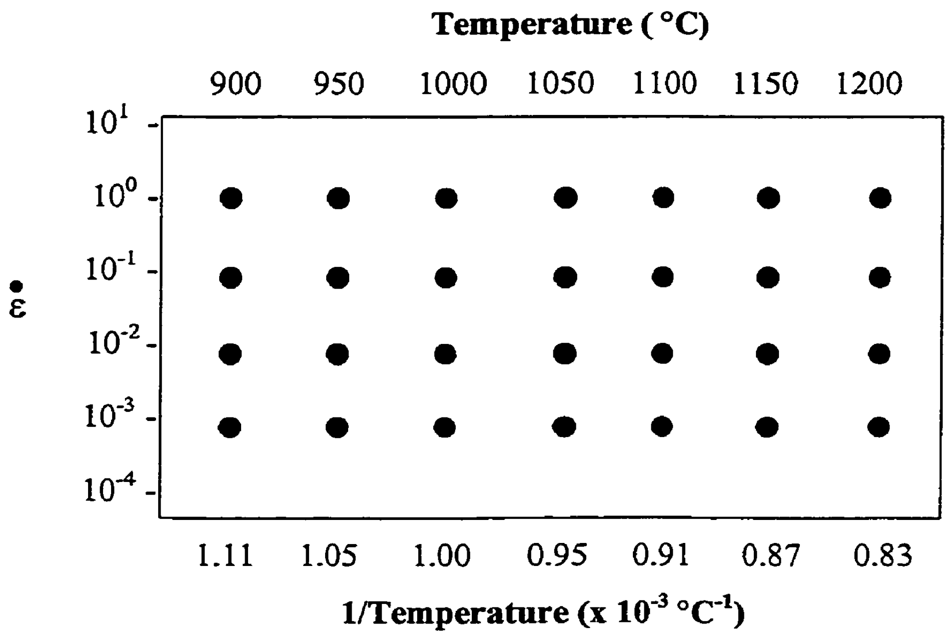

Figure 3.4: Test conditions examined for steel B for single pass deformation.

The thermal and deformation cycle for each individual test is illustrated in **Figure 3.5**. Each sample underwent the same pre-deformation thermal cycle: heat to 1200°C at a rate of 1.5°C/s, soak for 15 minutes and then cool to the deformation test temperature at a rate of 1°C/s.

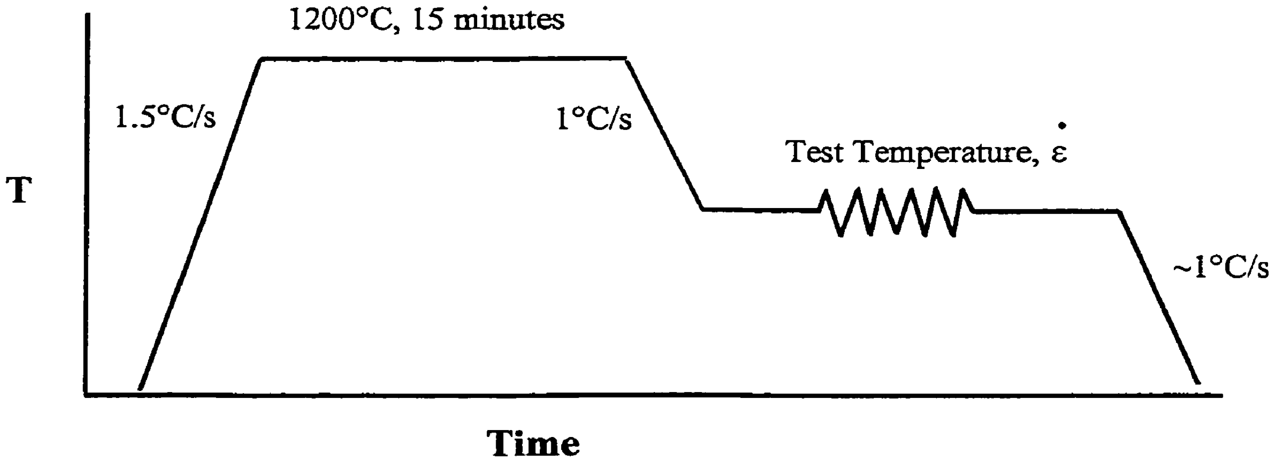

Figure 3.5: Schematic diagram of the thermal cycle employed.

In order to ensure that the tests were performed in the austenite phase, the following equation, based on chemical composition and plate thickness, was utilized to calculate the A_{r3} temperature[46]:

$$A_{r3} = 910 - 310C - 80Mn - 20Cu - 15Cr - 80Mo + 0.35\,(t - 8) \qquad (3.6)$$

where t is the plate thickness in mm. According to the above equation and given a plate thickness of 23 mm, the A_{r3} temperature for steel A is 780°C and, therefore, testing at temperatures of 900°C and above ensured that the steel was in the austenite phase. In the case of Steel B, the A_{r3} temperature was found to be 630°C, again assuring that at temperatures of 900°C and above, the material was in the austenite phase.

In the case of steels C to F and the iron, they were only tested at one temperature, 1050°C, and one strain rate, 10^{-3} s^{-1}. The purpose of these tests was to compare the scatter level on the stress-strain curves as well as the variation of the strain rate of various steels containing different degrees of alloying elements.

3.6.2 Strain Rate Change Tests

Strain rate change tests involve changing the strain rate during deformation and observing the material's response. In a normal thermally activated process, the response to a decrease in the deformation rate would be a decrease in the flow stress. However, within the DSA region associated with the presence of interstitial elements, the opposite is observed. Thus, if negative values of strain rate sensitivity are observed, these provide a good indication that DSA is occurring. The purpose of these tests was therefore to determine if steel B exhibits negative strain rate sensitivity under the conditions of the test.

The thermal cycle was the same as that shown in **Figure 3.4**. The temperatures investigated ranged from 950 to 1200°C, increasing by 50°C increments. The strain rate change test involved straining to a strain of about one and then increasing the strain rate by one order of magnitude. After an additional applied strain of about one, the strain rate was decreased back to its original value. Thus, both positive and negative strain rate changes were performed on the same specimen. An example of a deformation cycle is shown in **Figure 3.6**.

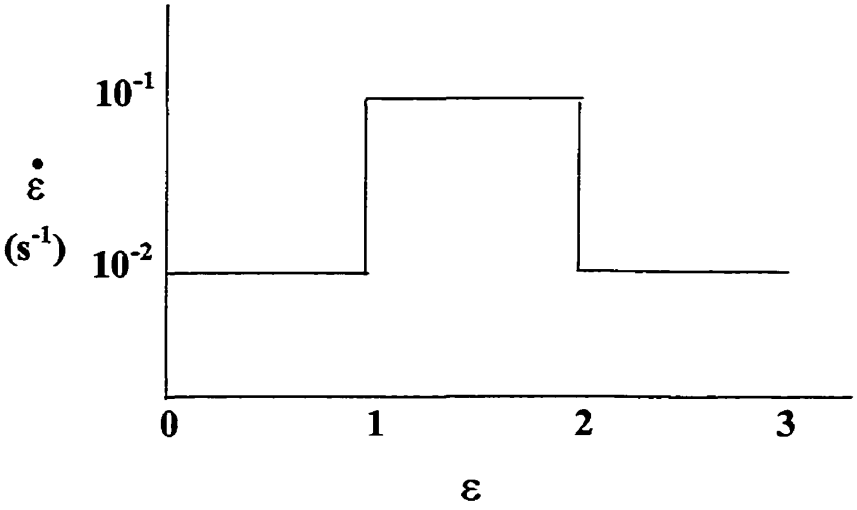

Figure 3.6: Example of the deformation cycle employed for a strain rate change test.

3.6.3 Decreasing Temperature Tests

The temperature and strain rate domain where the PLC effect, created by substitutional elements, should be observed is unknown for steel in the austenite phase. One method shown to approximate the domain was presented in section 3.5. However, another approach involves applying the model formulated by Cahn to estimate the temperatures and strain rates where the instability caused by DSA occurs[47]. It specifies the dependence of the driving force on the grain boundary velocity. Cahn's theory is similar to that proposed by Blanc and Strudel mentioned in section 2.2, although his model was constructed to account for impurity drag on *grain boundary motion* as opposed to dislocation motion in the presence of solute atmospheres. Cahn states that, with increasing impurity concentration or decreasing temperature, the grain boundary may undergo a transition due to a change in the interaction with its impurity atmosphere. At this transition, the boundary may experience jerky boundary motion due to the existence of a range of conditions where two different boundary velocities are possible. His model was adapted to the case of dislocation motion to model the dislocation velocity as a function of temperature, composition and driving force. For brevity, only the resulting curves of the model are illustrated (see **Figure 3.7**) in this section. To review the equations and constants used for the model, the reader is directed to section 4.5 for further explanation and comprehension.

From **Figure 3.7**, it can be seen that the dislocation velocity and correspondingly, the strain rate, spans a range of several orders of magnitude for temperatures between 900 and 1200°C. Therefore, in order to locate the area of instability, a good approach would be to apply a given strain rate and continuously change the temperature in hopes of crossing an instability boundary and then repeating the process at another specified strain rate. This method or procedure is quick and minimizes the number of samples needed to find the temperature and strain rate combination that induces the instability.

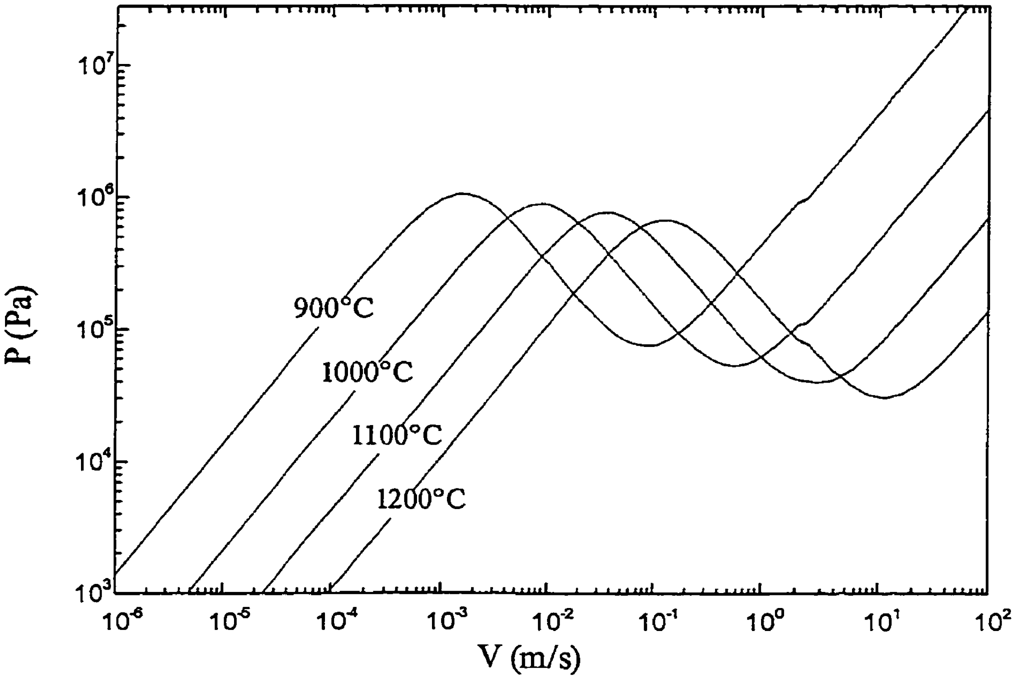

Figure 3.7: Force versus dislocation velocity profile calculated using the model formulated by Cahn at different temperatures.

The material selected for this set of tests was steel C because it was one of the materials which exhibited the most stress scatter (see section 4.1) and there was an abundant number of samples available. The strain rates explored were 10^{-2}, 10^{-3}, and 10^{-4} s^{-1}. Each specimen was strained to the steady state stress at a constant temperature before the cooling process commenced. **Table 3.2** provides the particular details of each individual experiment.

Table 3.2: Experimental details of the decreasing temperature tests.

Strain Rate (s^{-1})	Steady State Strain	Final Strain	Starting Temp. (°C)	Finishing Temp. (°C)	Data Acquisition Rate (s^{-1})	Cooling Procedure
10^{-2}	0.6	3.7	1200	1050	100	0.5°C/s
10^{-3}	0.6	3.8	1250	1050	4	0.67°C/s
10^{-4}	0.33	2.5	1200	950	0.5	0.012°C/s

3.6.3 Constant Stress Rate Tests

There have been several techniques utilized to examine the conditions for the occurrence of DSA in solid solutions. The most common methods involve constant strain rate tests described in the sections above. There have also been studies that use a constant stress rate to investigate and determine the conditions for the onset of plastic instability as a result of DSA[9,33]. This entails increasing the stress at a constant rate and observing the effect on the strain rate. The principle is the reverse of constant strain rate tests in that the stress rate is now held constant and the strain becomes the variable. The idea is that, as the stress increases, the strain rate must increase in order to maintain the applied stress rate. However, if DSA is occurring, the stress can continue to increase without an increase in the strain rate. Again, this principle is elaborated in the Results and Discussion chapter of this thesis. It was believed that this form of testing might draw out evidence of DSA. Steel C and iron were tested at a temperature of 950°C. The constant stress rate chosen was 0.5 MPa/s, equivalent to a torque of 5.42 N-mm.

3.6.5 Low Ratio Strain Rate Change Tests

Another test that was developed to try to extract evidence of DSA was a modified strain rate change test, only this time, the strain rate ratio was kept much smaller. From the scatter/noise level tests, as described in section 3.6, it was deduced that a smaller strain rate change may be more appropriate for the reasons explained in section 4.6.

Steel C was tested at 950°C with the same thermal cycle shown in **Figure 3.4**. There were several strain rate jumps performed in one experiment with varying holding times at each strain rate, and therefore, the use of the specimen was maximized. **Figure 3.8** illustrates one of the strain rate cycles to which a sample was subjected.

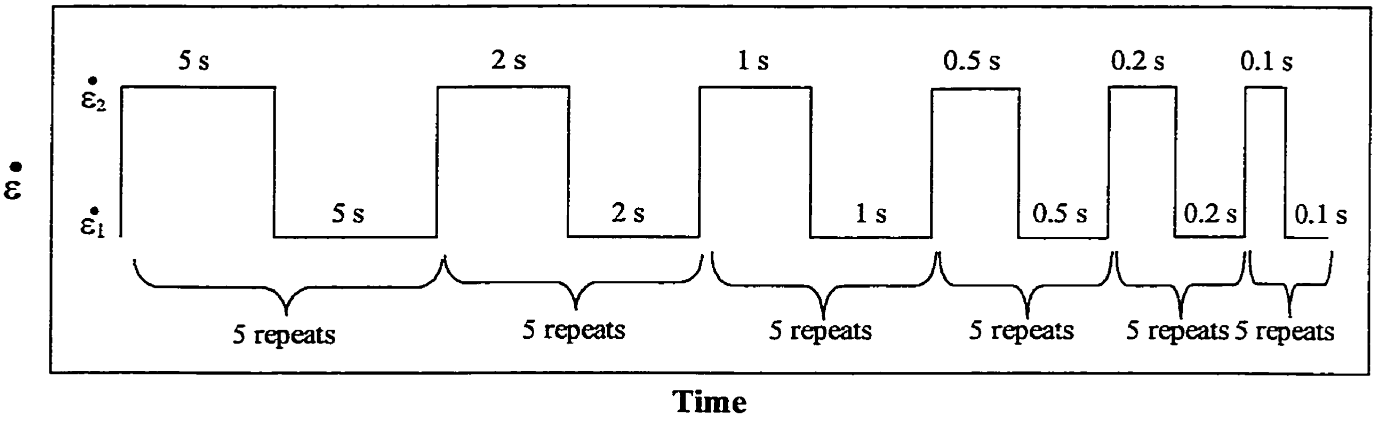

Figure 3.8: Strain rate cycle applied to a sample.

CHAPTER IV

RESULTS AND DISCUSSION

The first results presented are those of the 'noise' tests (section 4.1). That is, five steels, as well as 'pure' iron, were examined to evaluate the level of 'jerky flow' on the stress-strain curves so as to establish a link with their chemical compositions. The stress-strain curves that follow (section 4.2) are those of the simple torsion tests. Because some unexplainable results were obtained, strain rate change tests were then performed so that the latter results could be interpreted more accurately. The stress-strain curves obtained in this way are displayed and discussed in section 4.3. The sections that follow are comprised of the results from further attempts made at extracting evidence of DSA: for this purpose, a constant stress rate test (section 4.4), a varying temperature test (section 4.5), and a modified strain rate change test (section 4.6) were used.

4.1 Stress Scatter Level Results

The purpose of the stress scatter level tests was first, to establish the noise level of the torsion machine and second, to compare the average scatter level on various grades of steel. For the latter, steels containing different combinations of alloying elements were tested, all under the same conditions: at a temperature of 1050°C and a strain rate of 10^{-3}

s^{-1}. In addition, a test was run with no sample in the machine in order to obtain a base curve and to compare it to the other results. **Figure 4.1** shows the 'normalized' stress (i.e. instantaneous stress over the mean stress) versus time curves of all the materials tested, including the no-sample test, in increasing order of stress scatter level. The normalized stress was plotted so as to allow for direct comparison between the different grades of steel. The twist rates, as well as the twist angles in radians, are also presented in **Figure 4.1**. The twist rate was obtained by taking the derivative of the angle versus time curve. Note that the data were plotted such that the starting angle, 6.1 radians, was the same in all the figures. This was done deliberately in order to provide and maintain consistency.

Aside from the no-sample curve, the 'pure' iron possesses the smoothest stress-time curve, despite substantial fluctuations in the twist rate and, accordingly, the strain rate. The steels exhibit considerably more scatter on the normalized stress-time curves than the iron. In order to interpret these results with respect to their relative chemistries, **Table 4.1** was drawn up to provide the pertinent chemical compositions of the experimental materials in ascending order of stress scatter level on the stress-time curves. In addition to the relative amounts of alloying elements, features that affect the solubility, such as the atomic size factor and crystal structure, are also important in determining the effectiveness of an element in producing DSA. As stated in section 2.6, the solubility, diffusion coefficient and interaction energy between the solute atom and dislocation are the characteristics that determine the extent of DSA.

Table 4.1: Chemical compositions of the experimental materials in wt%, given in ascending order of stress scatter.

Steel	C	Cr	Mo	Mn	Ni	Si	V	Nb	S	P
Iron	0.003	0.022	<.017	0.054	0.009	<.001	N/A	<.002	<.003	<.002
D	0.155	N/A	N/A	0.01	30.5	0.03	N/A	0.005	0.001	0.002
E	0.28	0.83	0.15	0.52	N/A	0.22	N/A	N/A	0.004	0.016
B	0.45	0.99	0.96	0.67	0.47	0.19	0.12	0.014	0.005	0.0014
F	0.05	N/A	N/A	0.37	N/A	0.03	N/A	0.03	0.006	0.006
C	0.07	N/A	0.01	0.27	N/A	0.2	N/A	< .001	0.004	0.028

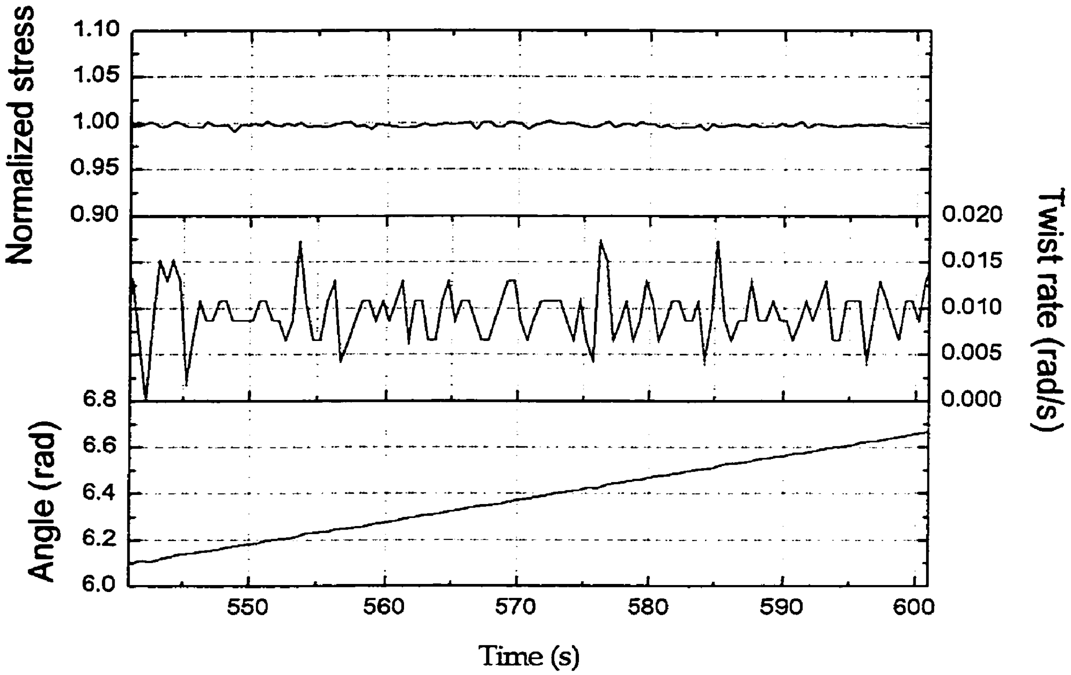
Normalized stress
1.10
1.05
1.00
0.95
0.90
Twist rate (rad/s)
0.020
0.015
0.010
0.005
0.000
Angle (rad)
6.8
6.6
6.4
6.2
6.0
550
560
570
580
590
600
Time (s)

(a)

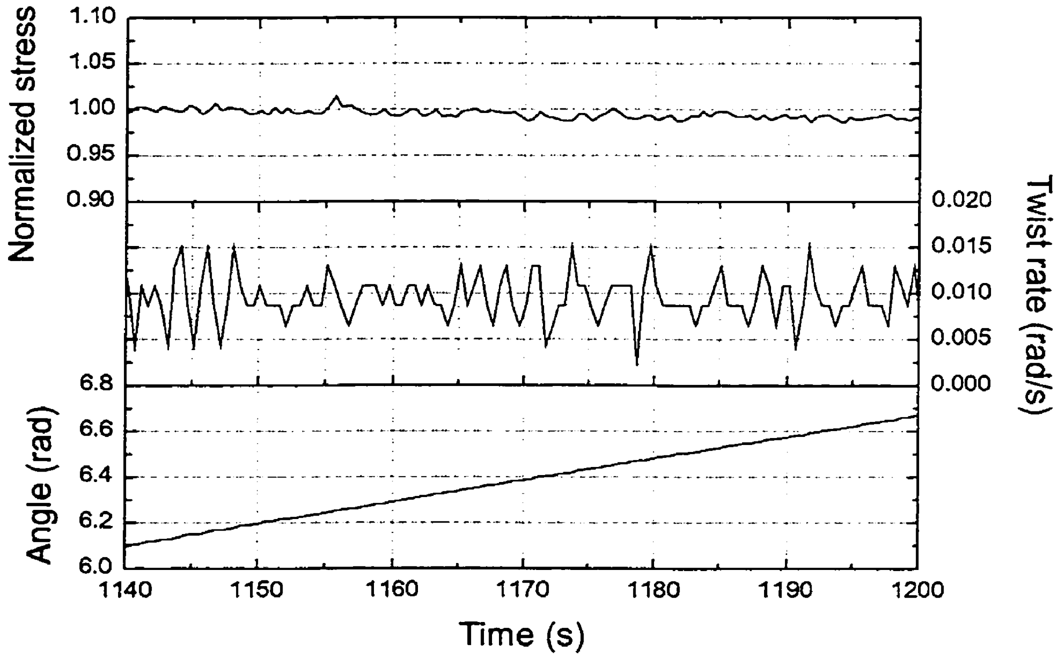
Normalized stress
1.10
1.05
1.00
0.95
0.90
Twist rate (rad/s)
0.020
0.015
0.010
0.005
0.000
Angle (rad)
6.8
6.6
6.4
6.2
6.0
1140
1150
1160
1170
1180
1190
1200
Time (s)

(b)

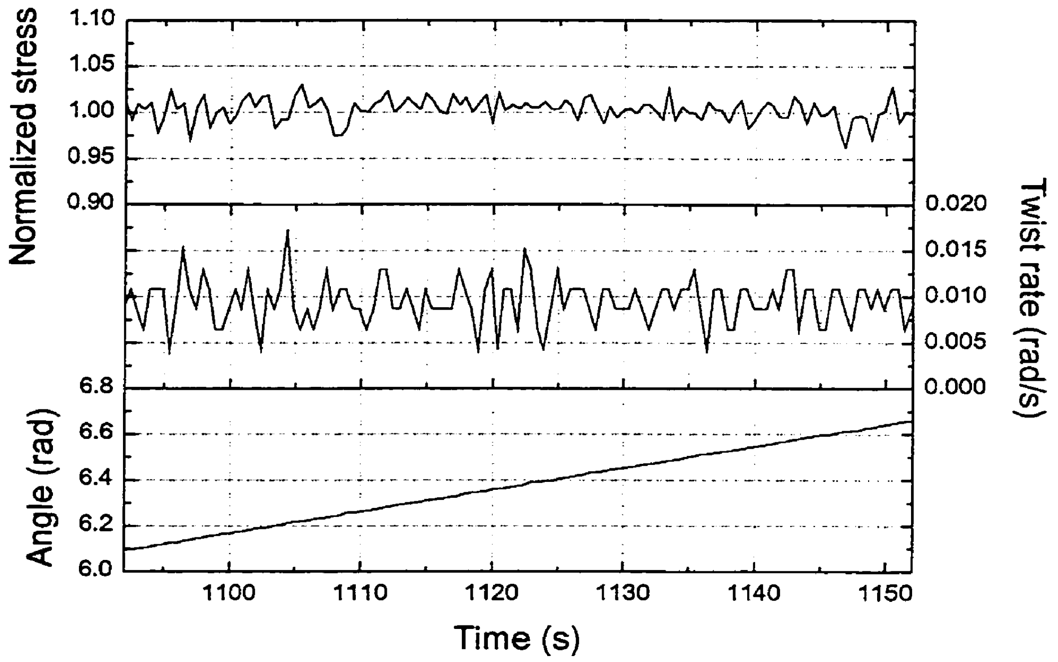
Normalized stress
1.10
1.05
1.00
0.95
0.90
Twist rate (rad/s)
0.020
0.015
0.010
0.005
0.000
Angle (rad)
6.8
6.6
6.4
6.2
6.0
1100
1110
1120
1130
1140
1150
Time (s)

(c)

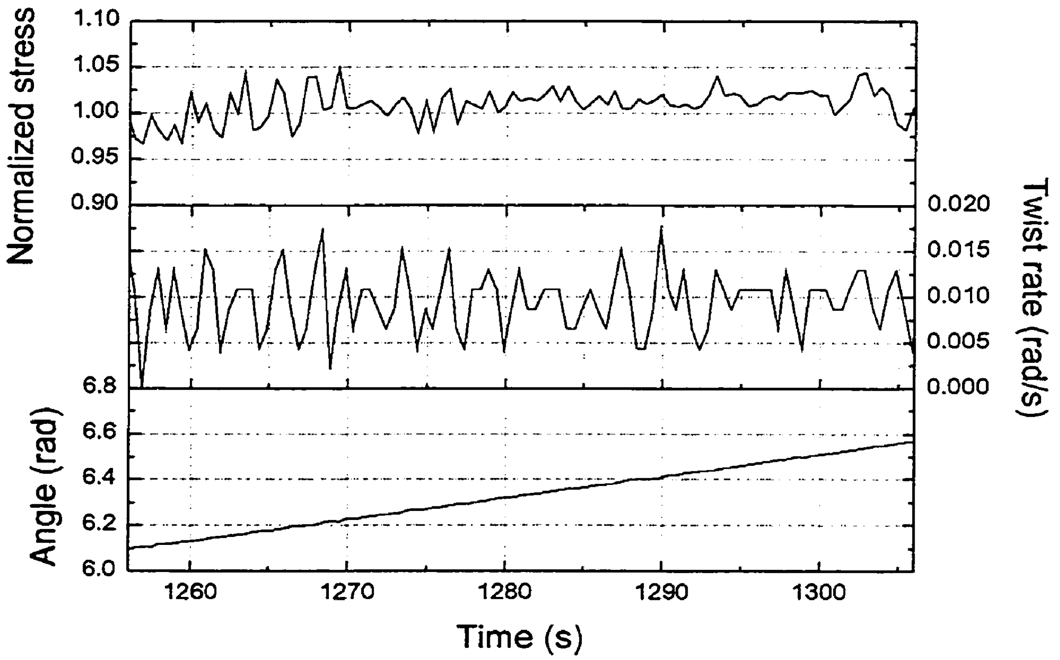
Normalized stress
1.10
1.05
1.00
0.95
0.90
Twist rate (rad/s)
0.020
0.015
0.010
0.005
0.000
Angle (rad)
6.8
6.6
6.4
6.2
6.0
1260
1270
1280
1290
1300
Time (s)

(d)

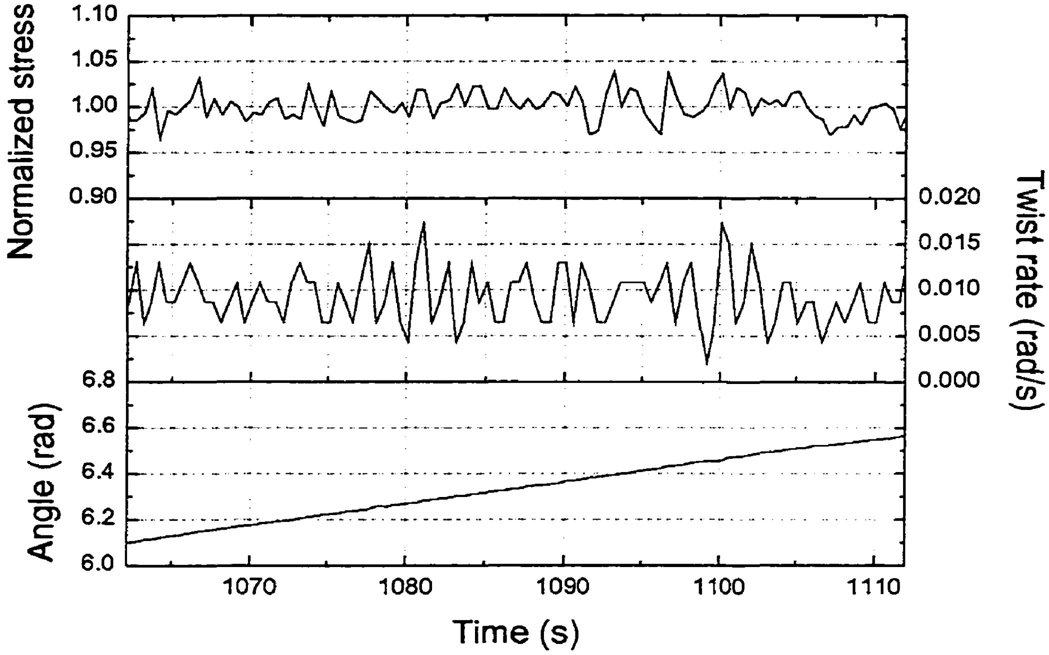
Normalized stress
1.10
1.05
1.00
0.95
0.90
Twist rate (rad/s)
0.020
0.015
0.010
0.005
0.000
Angle (rad)
6.8
6.6
6.4
6.2
6.0
1070
1080
1090
1100
1110
Time (s)

(e)

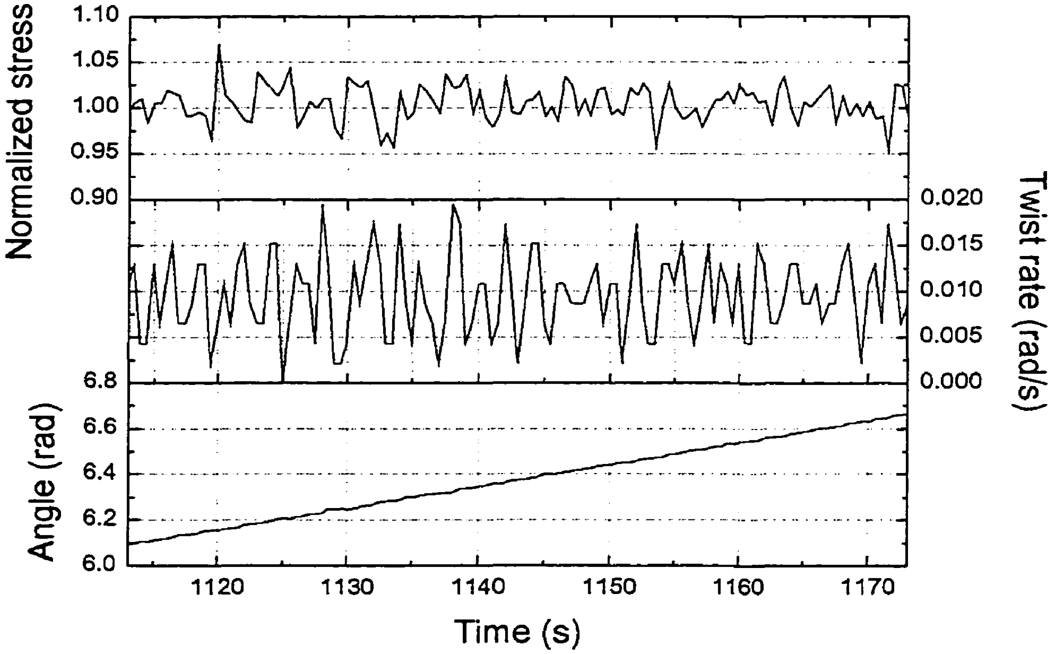
Normalized stress
1.10
1.05
1.00
0.95
0.90
Twist rate (rad/s)
0.020
0.015
0.010
0.005
0.000
Angle (rad)
6.8
6.6
6.4
6.2
6.0
1120
1130
1140
1150
1160
1170
Time (s)

(f)

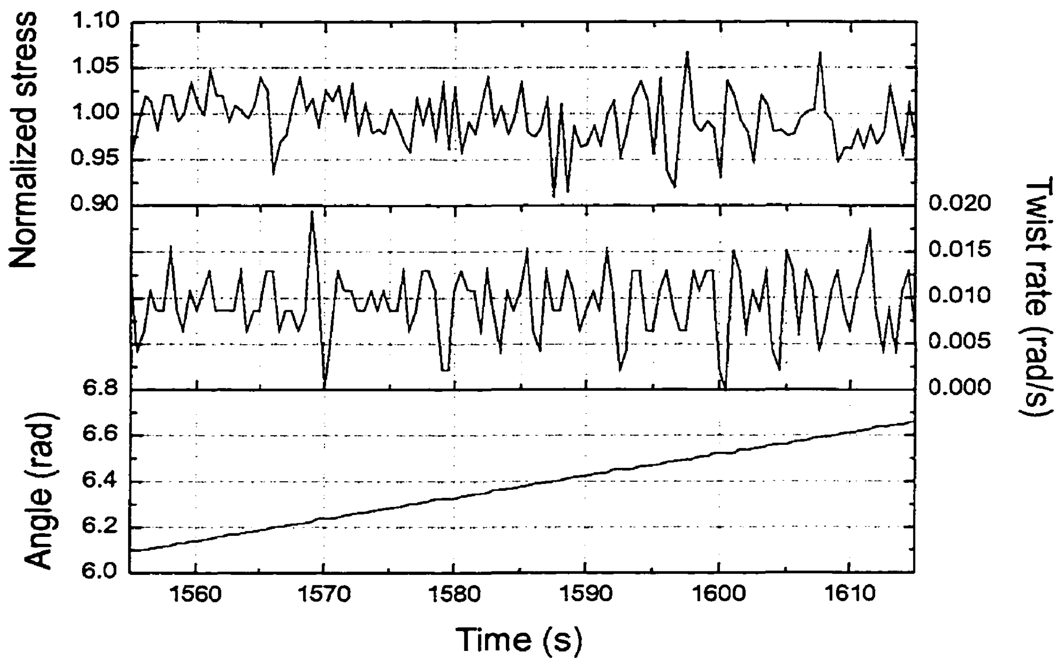

(g)

Figure 4.1: Normalized stress, twist rate and angle versus time curves obtained at 1050°C and a strain rate of 10^{-3} s^{-1} for (a) no sample, (b) 'pure' iron, (c) steel D, (d) steel E, (e) steel B, (f) steel F and (g) steel C.

Deciphering the normalized stress curves is difficult when only the chemical compositions are to be considered. This is because the increase in scatter is not a direct function of the amount of any one element. Unfortunately, it was not possible to isolate the effect of any single element because the chemical compositions of the steels varied so much. As the content of one element went down, that of another increased. Direct comparison of the steels was therefore difficult. However, information about the relationship between each substitutional element and the steel is very helpful. For example, the interaction energy between a solute atom and a dislocation indicates how strongly the atom is attracted to the dislocation. A high interaction energy implies that the atom has a strong affinity for the dislocation and, hence, will have a higher pinning effect than an element with a lower interaction energy. Although the interaction energies between solute atoms and dislocations are not known in detail, approximate values of the binding energy between a solute atom and a grain boundary in γ-Fe of certain elements are given in **Table 4.2**. These values are assumed here to be comparable to the binding energy between an atom and a dislocation. Phosphorus has the strongest attraction to a grain boundary after sulphur. Their values are well above the others at –55 and –88 kJ/mole, respectively.

Table 4.2: Binding energies between solutes and grain boundaries in γ-Fe[48].

Element	**Binding Energy (kJ/mole)**
Mo	-20
Nb	-20
P	-55
S	-88
Si	-17

The final property of importance in solute-dislocation interactions is the diffusivity of the solute element in γ-Fe. From **Figure 3.3**, the substitutional element with the highest diffusion coefficient is sulphur, followed by silicon and phosphorus. These elements display significantly higher diffusivities, at least half an order of magnitude higher, than other elements such as niobium, molybdenum, and manganese. Therefore, the elements that are expected to have the strongest effect on dislocation movement, based on their diffusivities and binding energies, are sulphur, phosphorus and, to a lesser degree, silicon.

Going back to **Table 4.1** and focusing on the concentrations of these three elements, there does appear to be a tendency for the scatter level to increase with increasing amounts of these elements. As the general concentration level of these three elements increases, the magnitude of the oscillations on the normalized stress curves increases, with the exception of steel F. Steel F produces one of the 'noisiest' stress curves, despite containing only 0.03 % silicon and 0.006% each of sulphur and phosphorus. A possible explanation for this anomaly is that it contains the highest level of niobium (0.03%). The niobium may therefore be responsible for the pinning and unpinning of dislocations (despite the relatively low *grain boundary* binding energy) and impede dislocation motion in this way. The 'noisiest' material, steel C, contains at least twice as much phosphorus as any of the other steels and notable levels of silicon and sulphur.

For all the materials, the normalized stress and twist rate oscillate to an increasing degree together, although the extent is not so pronounced in the twist rate. The fact that the twist rate displays jerky flow could signify a continuous 're-adjustment' of the strain rate as a result of the pinning and unpinning of dislocations, causing the stress variations. This hypothesis can also be reversed in that it is the 'natural' fluctuations in strain rate that are causing the oscillations on the stress-time curves. One point supporting the latter argument is that even when there was no sample in the machine (see **Figure 4.1a**), quite significant fluctuations in twist rate were still observed. Nevertheless, no clear conclusion can be drawn regarding the parameter that is producing the fluctuations and, therefore, affecting the other parameters.

The exact effect of each element on dislocation movement is unknown at this point. It appears that the influence of phosphorus and sulphur (and perhaps silicon) is greater than that of the other substitutional elements since they possess higher diffusivities and reasonably strong binding energies. This assessment is supported by the increase in scatter level when the amounts of these elements are increased. A more detailed study, using steels with less complex chemistries, would be required to lead to firm conclusions.

It should be noted that the stress oscillations could also be produced by solute-*grain boundary* interactions. The interaction between solutes and dislocations is similar to that with grain boundaries. Solutes are also attracted to grain boundaries so that they can reduce the strain field in the lattice; consequently, they impose a drag force on the boundary when it attempts to move. Hence, the statements made above with regard to the elements responsible for the stress variations could also be applied to solute-grain boundary interactions.

4.2 Simple Torsion Results

4.2.1 Simple Torsion Results for Steel A

The flow curves for steel A determined over the temperature range 900 to 1100°C and at strain rates beginning at 10^{-4} s^{-1} and ending at 5 s^{-1} are presented in **Figures 4.2** to

4.5. In the case of the higher strain rates, 5 and 1 s^{-1}, the material exhibits continuous softening as the temperature is increased. However, at a strain rate of 10^{-2} s^{-1}, the flow curve at 1050°C falls below that of the flow curve at 1100°C. Similarly, for the tests performed at a strain rate of 10^{-4} s^{-1}, the material appears to be softer at 1000°C than at 1050 and 1100°C. These findings will be discussed later in this section.

4.2.1.1 General Appearance of the Stress-Strain Curves

The amplitude of the serrations increases as the strain rate is decreased. This is commonly observed when the strain rate is lowered. It should be noted that certain flow curves, such as the 900 and 1100°C curves at 10^{-2} s^{-1} and the 1100°C curve at 10^{-4} s^{-1}, appear darker or more condensed because a higher data acquisition rate was employed during these experiments. As for the general appearance of the serrations at each specified strain rate, they are similar over the temperature range studied, with the exception of the 900 and 950°C curves at a strain rate of 1 s^{-1}. These exceptions display a unique type of serration that is quite distinct and intermittent in the case of the 900°C flow curve. This phenomenon has also been observed in the work of Balíc and Lukác, who studied PLC instabilities in an aluminum alloy (Al-3Mg)[49]. They reported that their stress-strain curves exhibited flow regime transitions from serrated to smooth and back to serrated, as reproduced in **Figure 4.6**.

Schwink and Nortmann have also studied the characteristics of DSA in binary FCC copper alloys[34,50,51]. They have constructed deformation mechanism maps of stable and unstable deformation over different temperature intervals. These maps, shown in **Figure 4.7**, display the reduced critical flow stresses (σ_i - σ_o) for the onset and termination of unstable flow as a function of temperature and alloy concentration. The reduced critical stress is simply the critical stress for the onset or termination of serrations, σ_i, less the yield stress, σ_o. The maps also delineate isolated boundaries of stable flow and establish the existence of three PLC domains involving three different DSA processes. Schwink and Nortmann believe that the three PLC domains result from the operation of different diffusion processes (i.e. diffusion via vacancies, diffusion via interstitials, etc.). It is therefore possible to have stress-strain curves with two regions of unstable flow at one temperature, as was the case for steel A tested at 900°C and a strain rate of 1 s^{-1}.

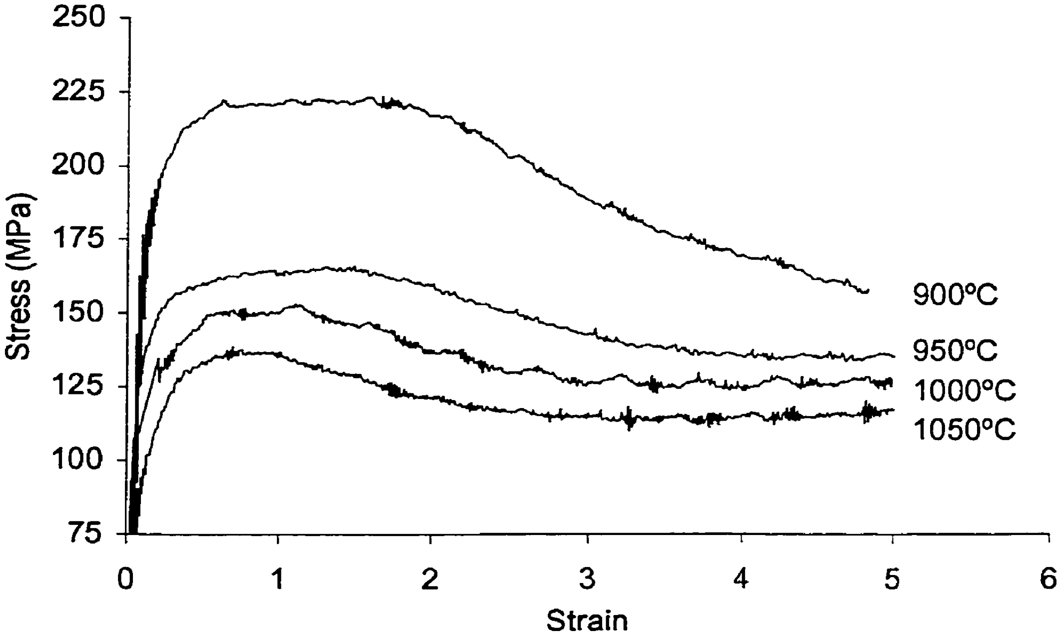

Figure 4.2: Stress-strain curves determined over the temperature range 900 to 1050°C at a strain rate of 5 s^{-1}.

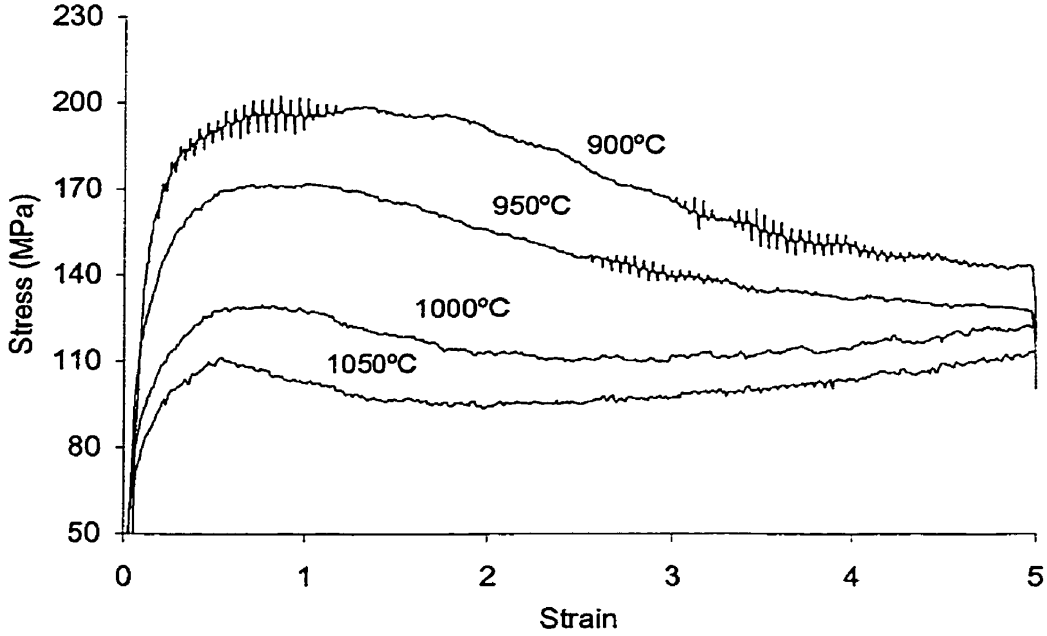

Figure 4.3: Stress-strain curves determined over the temperature range 900 to 1050°C at a strain rate of 1 s^{-1}.

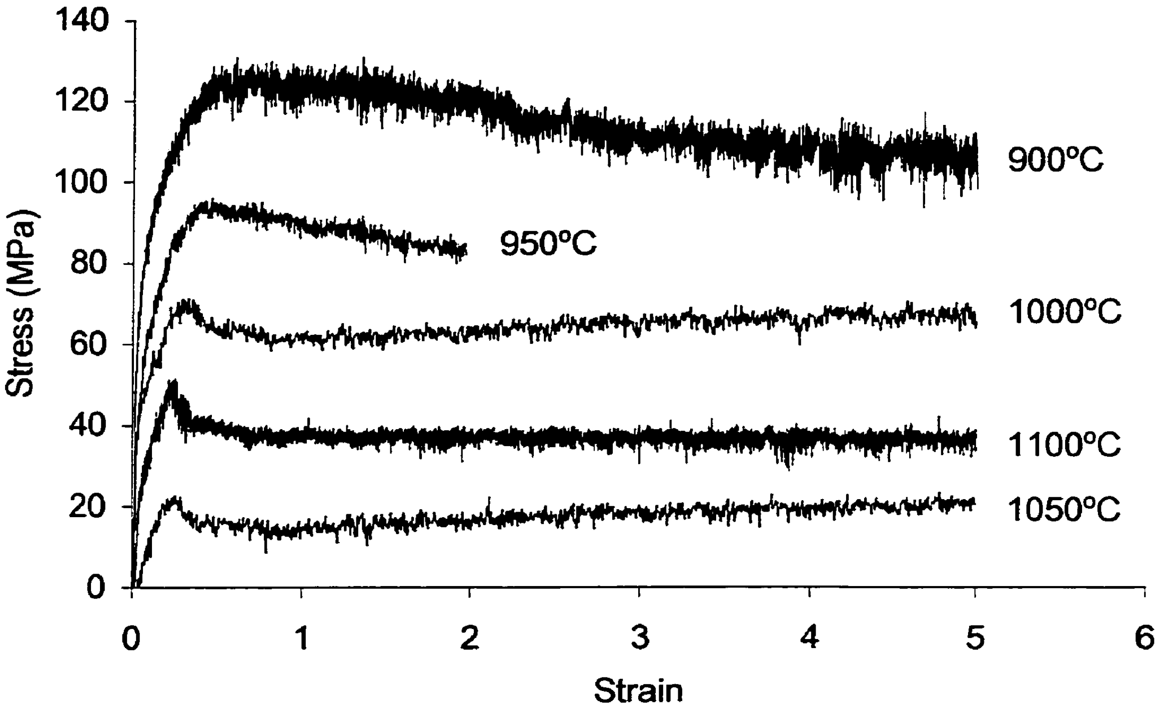

Figure 4.4: Stress-strain curves determined over the temperature range 900 to 1100°C at a strain rate of 10^{-2} s^{-1}.

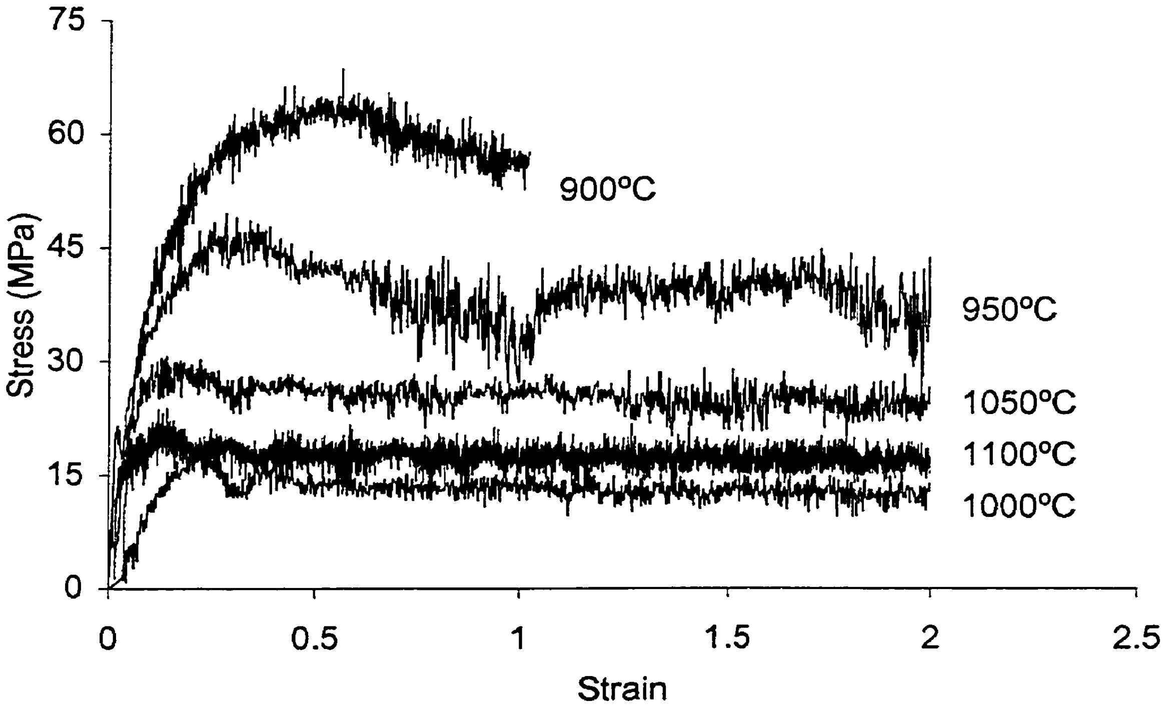

Figure 4.5: Stress-strain curves determined over the temperature range 900 to 1100°C at a strain rate of 10^{-4} s^{-1}.

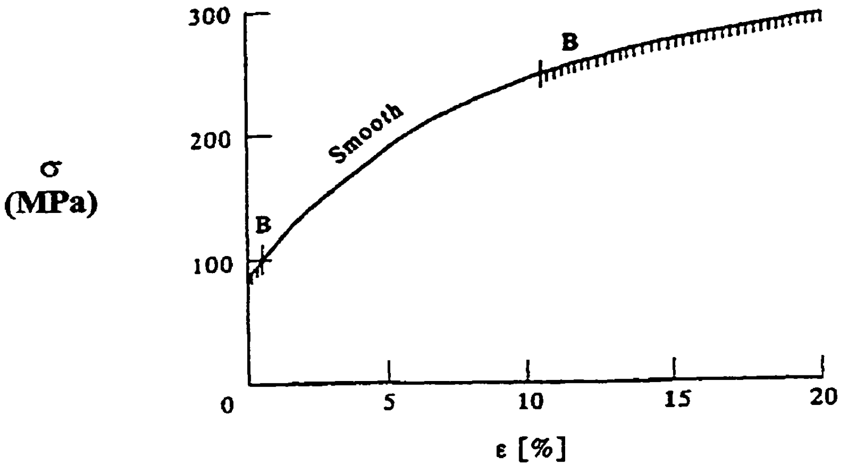

Figure 4.6: True stress-strain curve of Al-3Mg alloy tested at a strain rate of 3.3 x 10^{-6} s^{-1} showing the transitions from type B serrations to smooth curve and back to type B serrations[49].

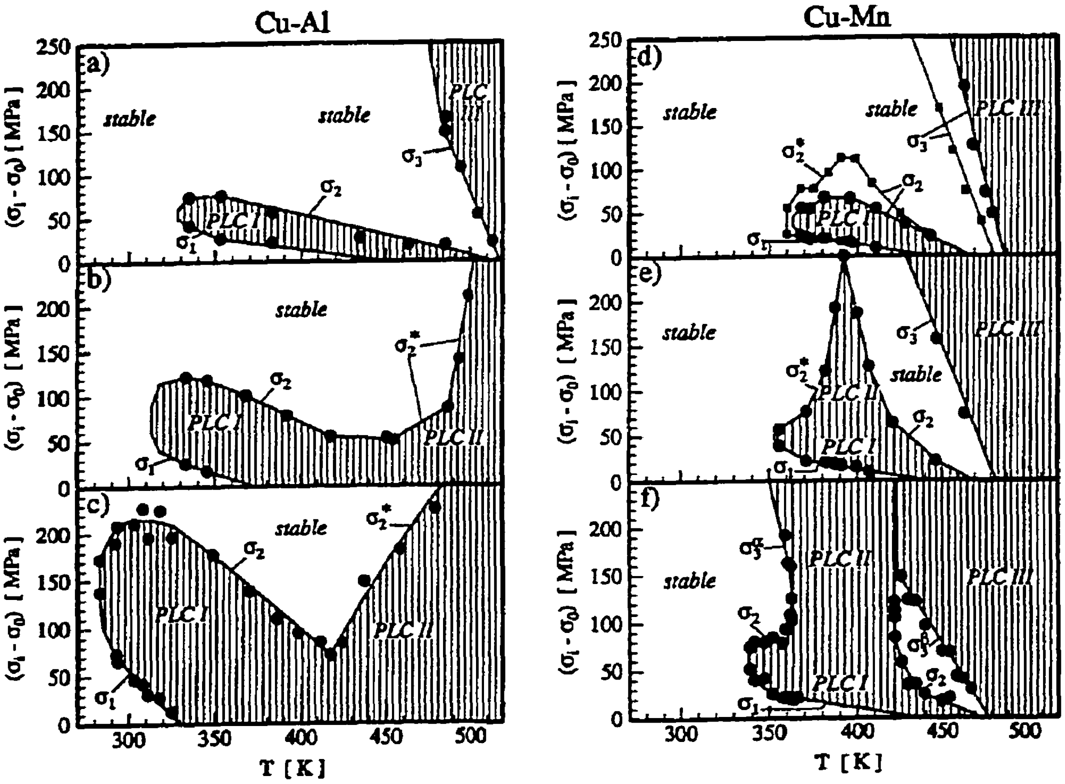

Figure 4.7: Deformation mechanism maps for CuAl (a-c) and CuMn (d-f) determined at a strain rate of 2.5 x 10^{-6} s^{-1}. (a) 5 at.% Al, (b) 7.5 at.%Al, (c) 10 at.% Al (d) 0.63 at.% Mn (●) and 0.95 at.% Mn (■), (e) 1.1 at.% Mn, and (f) 2.1 at.% Mn[51].

4.2.1.2 Test Reproducibility

The reproducibility and reliability of results is an important factor when analyzing and comparing flow curves. To verify and validate some of the unusual results (i.e. peculiar serrations) obtained in this investigation, some of the tests carried out under certain conditions were re-executed, namely, at a temperature of 900°C and a strain rate of 1 s^{-1}. The results of these tests are shown in **Figure 4.8**.

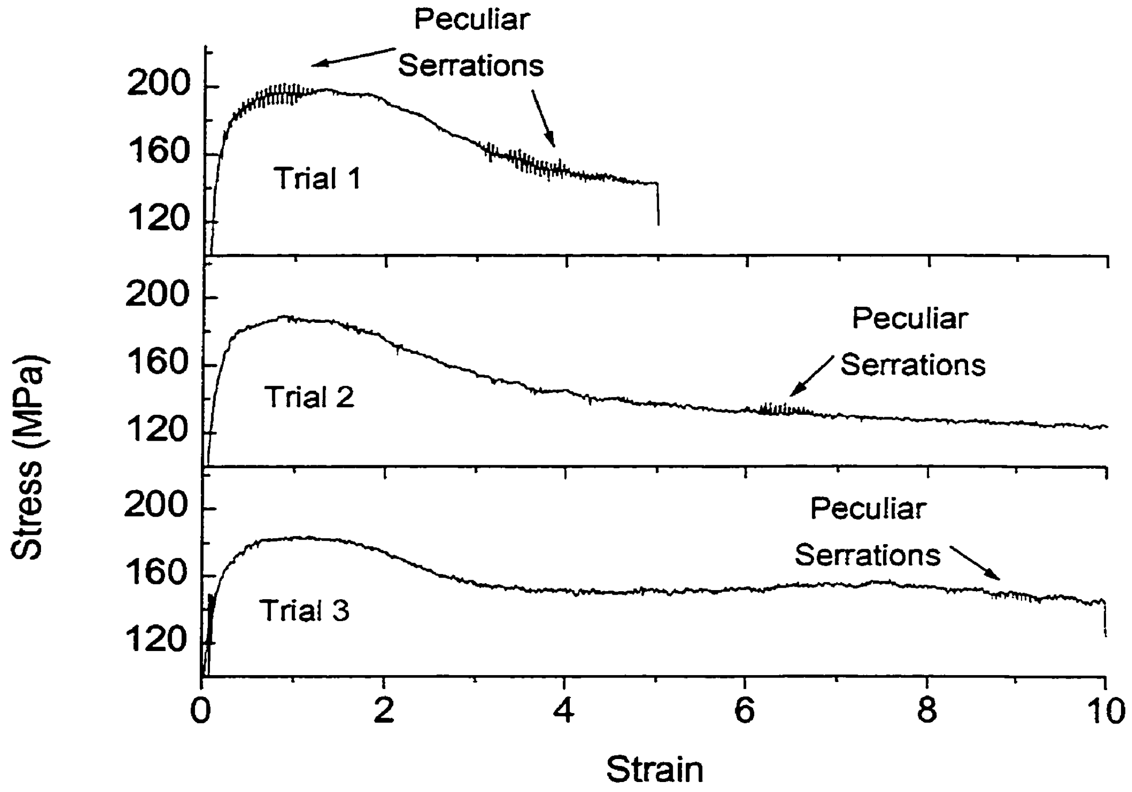

Figure 4.8: Stress-strain curves of three trials run at 900°C and a strain rate of 1 s^{-1} for steel A.

The shape and flow stress levels differ slightly, about ±10 MPa, from the initial flow stress detected (i.e. trial 1 of **Figure 4.8**). Moreover, the peculiar serrations are not reproduced at similar strains, but appear at slightly higher strains in the later tests. The lack of reproducibility was somewhat disturbing, albeit many factors could be invoked to explain the non-repeatability of the results. For one, even though the conditions in terms of temperature and strain rate were the same, changes in some of the other conditions and/or testing procedures could have affected the results. These include the argon flow rate, the thermocouple placement and the holding time at testing temperature prior to the experiment. The material may also contain some inhomogeneities that can cause the results to vary from sample to sample. Lastly, shortening and/or lengthening occurring during an experiment alters the flow stress and strain data. When the specimen gauge length shortens, from the law of constant volume in plastic deformation, the gauge diameter will increase accordingly. When the angular rotation and torque are converted to equivalent von Mises strain and stress, respectively, the variables (gauge length and diameter) are held constant in the calculation. That is, the gauge length and diameter are assigned their initial values without taking into account any changes that occur during the experiment. The flow stress versus strain curves generated can therefore contain some inaccuracies, since any changes in the gauge length and diameter were not considered in the stress and strain conversions.

4.2.1.3 Flow Stress as a Function of Temperature

We return now to the unusual 'hardening' experienced at 1100°C and a strain rate of 10^{-2} s^{-1} and at 1050°C and strain rate of 10^{-4} s^{-1} where the behavior suggests that, perhaps, DSA was manifesting itself through a negative strain rate sensitivity (SRS). It should be recalled from section 2.5 that DSA is often accompanied by negative SRS and a hump in the flow stress versus temperature curve. However, when the peak stresses were plotted versus temperature for all strain rates, as shown in **Figure 4.9**, the humps in the curves at strain rates of 10^{-2} and 10^{-4} s^{-1} were not as distinct. If the curves are extrapolated to 1500°C, the approximate melting point, it appears that there is more of a valley at 1050°C than the beginnings of a hump at 1100°C at a strain rate of 10^{-2} s^{-1}. As for the 10^{-4} s^{-1} curve, a hump does seem to surface although, to a very modest degree. If the humps are actual manifestations of DSA, the shift of the hump to higher temperatures as the strain rate is increased is logical. A higher strain rate implies a higher dislocation velocity and, therefore, a higher temperature is required to increase the solute diffusion rate and induce DSA. Unfortunately, further examination of the humps observed at 10^{-2} and 10^{-4} s^{-1} was not possible because the number of samples of steel A was limited.

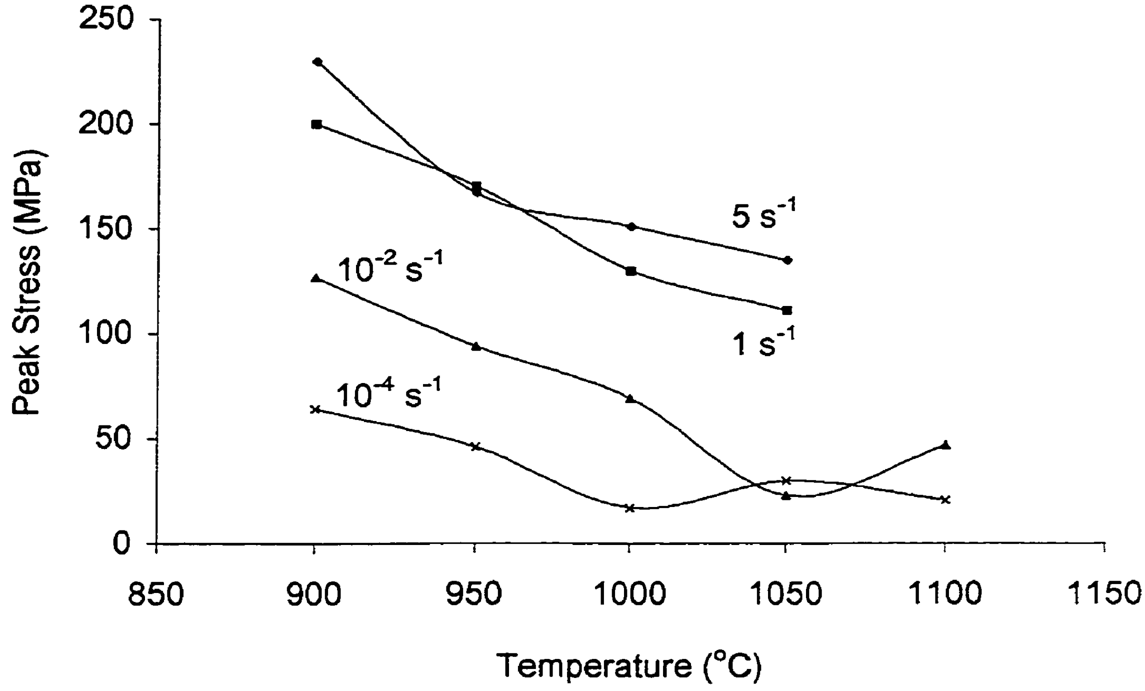

Figure 4.9: Peak stress versus temperature for all strain rates investigated for steel A.

Another interpretation of the anomalies found at strain rates of 10^{-2} and 10^{-4} s^{-1} is related to the occurrence of dynamic recrystallization (DRX). From **Figure 4.9**, it could be concluded that the 'humps' at 1050°C and 10^{-4} s^{-1} and 1100°C and 10^{-2} s^{-1} are not really 'humps' but 'valleys' at 1000°C and 10^{-4} s^{-1} and 1050°C and 10^{-2} s^{-1}. According to this view, they occur as a result of the transition from single peak to multiple peak DRX. This transition is accompanied by softening, which could explain what is observed. Multiple peaks can be clearly seen in the stress-strain plots, beginning at a temperature of 1000°C at a strain rate of 10^{-4} s^{-1}. In the case of 10^{-2} s^{-1}, the periodic oscillations are not so evident.

In **Figure 4.9**, there is a slight overlap of the 5 and 1 s^{-1} curves at 950°C. Deformation heating may have occurred at the higher strain rate and this could explain the overlap. Another explanation, also applicable to the 'humps' observed at the lower strain rates, could be the margin of error involved in the present experiments.

4.2.1 Simple Torsion Results for Steel B

Because of contradictory results obtained early during the testing of steel A as well as the inability to reproduce the results, the author became more meticulous and systematic in her approach for the subsequent tests. Much more attention was paid to the details and specifics of the experiments (i.e. holding time prior to deformation, observations during heating and soaking).

Figures 4.10 to **4.13** summarize the flow curves obtained for steel B over the temperature range 900 to 1200°C at strain rates beginning at 10^1 s^{-1} and continuing down to 10^{-3} s^{-1}. At a strain rate of 1 s^{-1}, distinct serrations are observed along sections of the stress-strain curves at test temperatures of 950, 1000, 1050 and 1200°C. This behavior is similar to that observed in steel A at temperatures of 900 and 950°C and a strain rate of 1 s^{-1}.

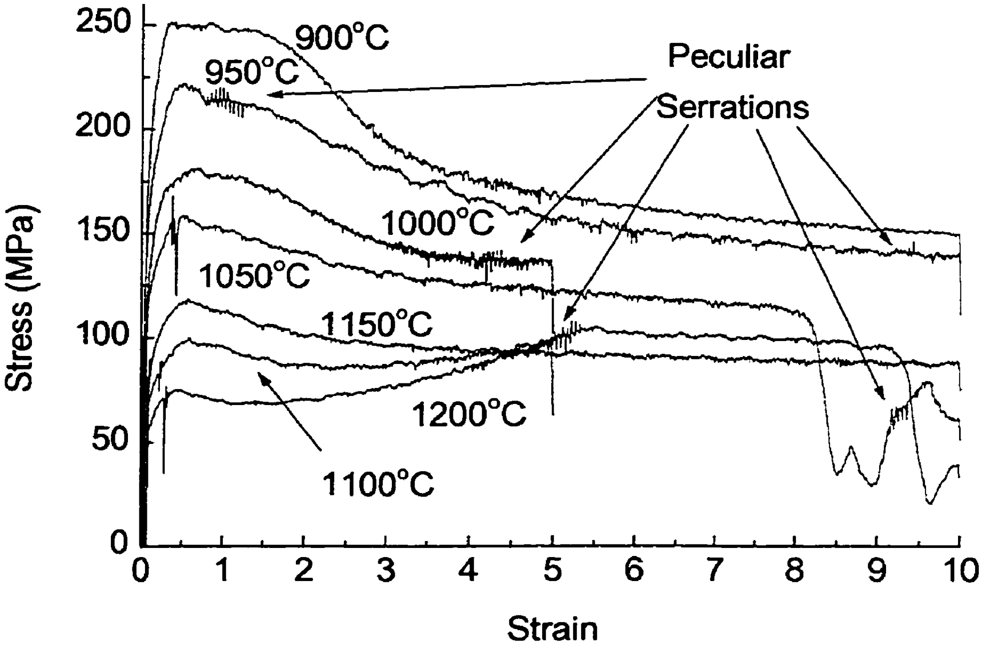

Figure 4.10: Stress-strain curves for steel B determined over the temperature range 900 to 1200°C at a strain rate of 1 s^{-1}.

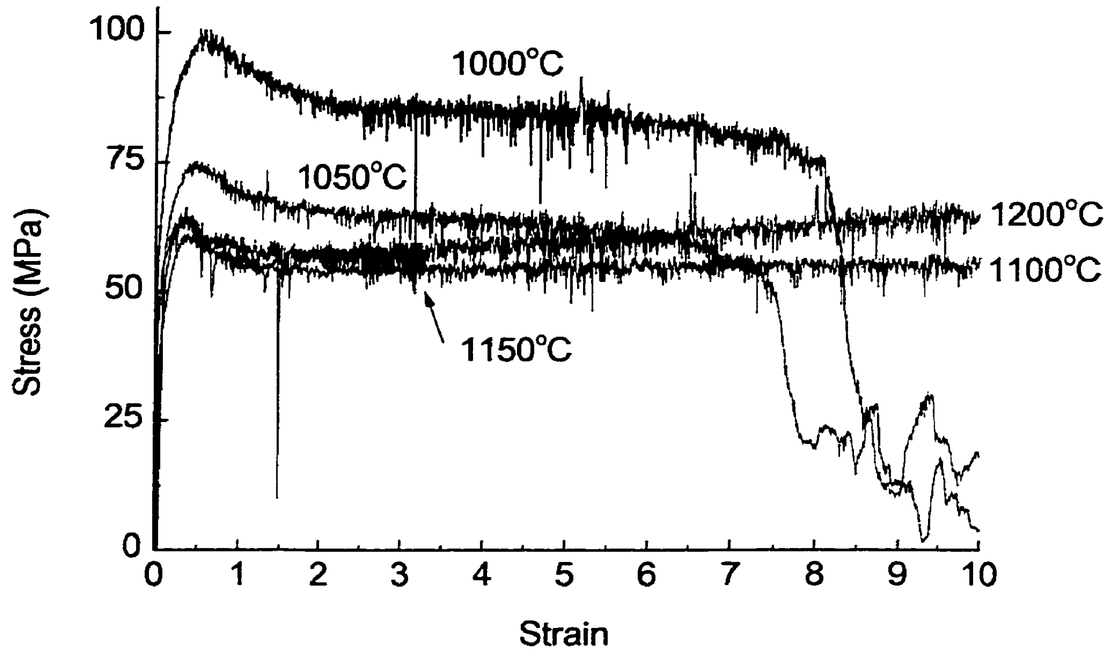

Figure 4.11: Stress-strain curves for steel B determined over the temperature range 1000 to 1200°C at a strain rate of 10^{-1} s^{-1}.

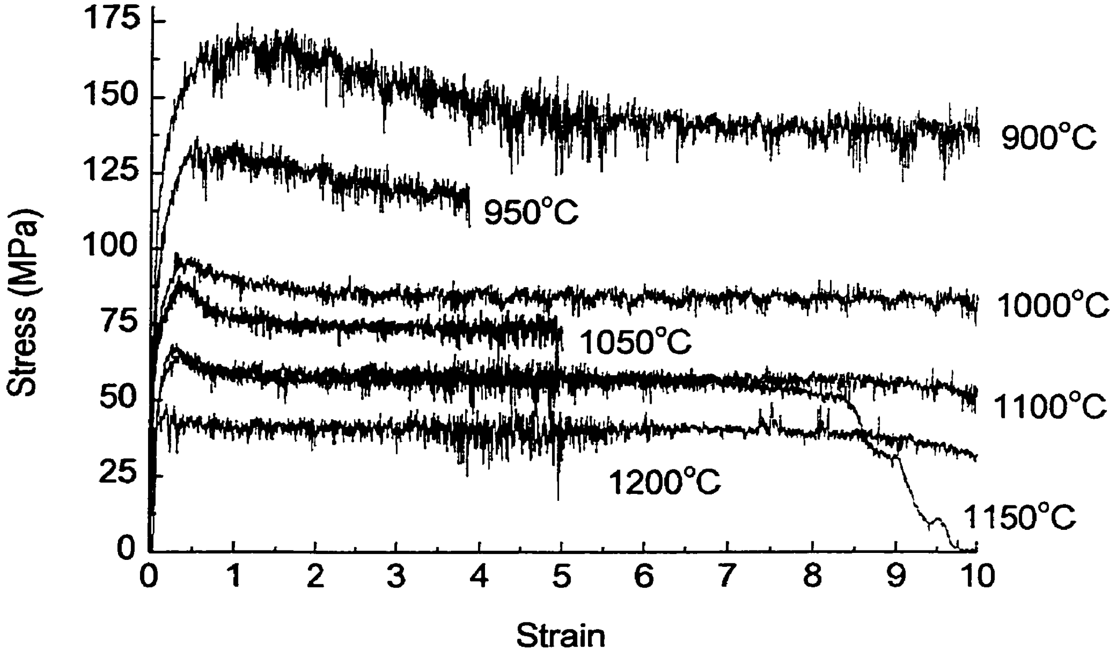

Figure 4.12: Stress-strain curves for steel B determined over the temperature range 900 to 1200°C at a strain rate of 10^{-2} s^{-1}.

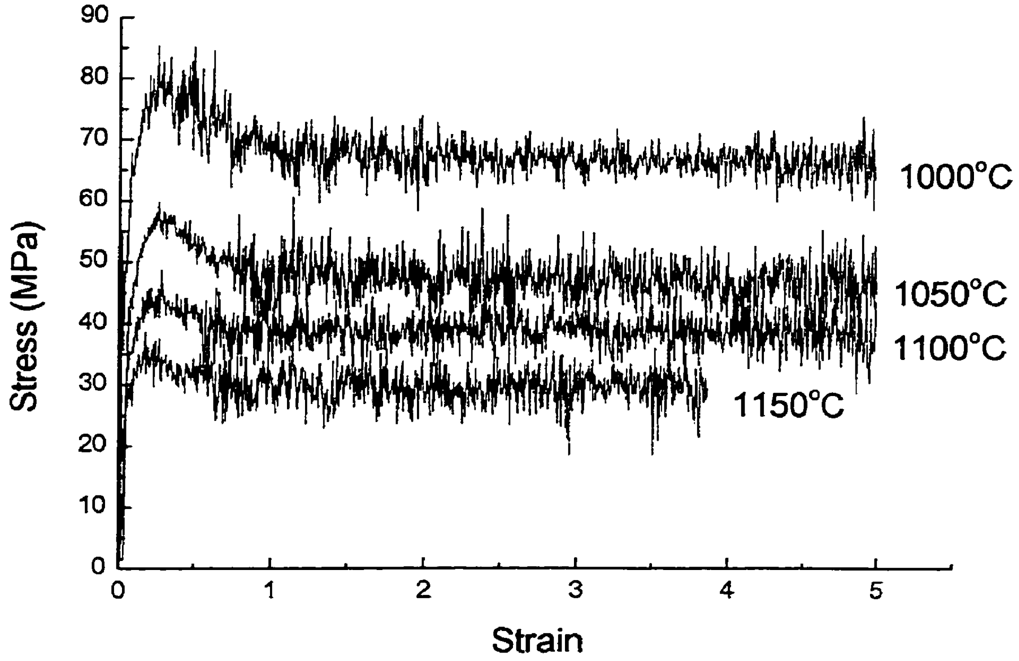

Figure 4.13: Stress-strain curves for steel B determined over the temperature range 1000 to 1150°C at a strain rate of 10^{-3} s^{-1}.

4.2.2.1 General Appearance of the Stress-Strain Curves

The general appearance of the stress-strain curves is similar to those of steel A in that the amplitude of the oscillations increases as the strain rate is decreased. In addition, peculiar serrations appear at certain temperatures at a strain rate of 1 s^{-1}, as was found with steel A. Again, this could be due to the operation of different diffusion processes, which results in the appearance of different types of serrations. It must now be recalled from section 2.10.1 that the appearance of the serrations can vary significantly and that more than one type can occur simultaneously. One phenomenon that was not observed in steel A, since the strains attained were not as high, was that the amplitude of the oscillations in steel B tended to increase at strains of around 5 for certain temperatures at strain rates of 10^{-1} and 10^{-2} s^{-1}. No reasonable explanation was found for this behavior.

Large drops in flow stress occurred at low strains, such as those in the 1050 and 1200°C flow curves. These can be explained by slippage of the threaded end of the sample in the stationary grip of the torsion machine. When a sample is not sufficiently tightened into the stationary grip and it slips during testing, the rotating grip rotates without the 'normal' resistance to deformation. Therefore, the torque cell, located at the end of the stationary grip, records a lower torque.

4.2.2.2 Flow Stress as a Function of Temperature

The peak stresses obtained at all the temperature and strain rate combinations tested are summarized in **Figure 4.14**. Beginning with the highest strain rate, 1 s^{-1}, continuous softening is noted until a temperature of 1000°C is reached. The peak stress then rises quite sharply at 1150°C before decreasing again at higher temperatures. The points at both 1100 and 1200°C do not appear to follow the trend of the curve; they are lower than expected. It could be that the points are legitimate and are manifestations of DSA, being associated with slight humps in the stress versus temperature curve. When going to lower strain rates, the 'hump' should shift to lower temperatures since, at lower strain rates, the dislocation velocity is reduced. This is not the case, however. Some tests were repeated and different values of the peak stresses were determined. The values of the peaks relative to one another therefore do not necessarily represent the true difference and determination of the trends becomes difficult. The variability could have resulted from the inhomogeneities in the material referred to above. This could have caused the flow curves to differ from one test to another under the same conditions. Another explanation is that test parameters such as thermocouple placement and set-up conditions may have altered enough to cause flow curve variances. Consequently, no inferences can be drawn from these results without a more extensive investigation employing other testing methods (i.e. strain rate change tests).

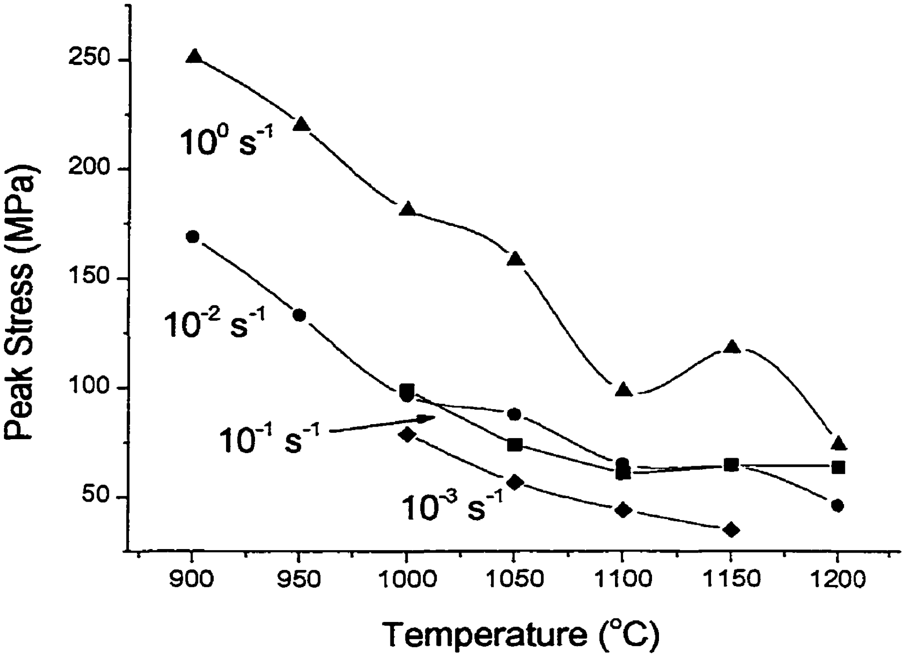

Figure 4.14: Peak stress versus temperature for all strain rates examined for steel B.

4.3 Strain Rate Change Results

Strain rate change tests were carried out in order to remove the problems of sample and test variability. By performing strain rate changes on a single sample, the issue of sample to sample variability is resolved; the change in stress can be taken as the true change resulting from a strain rate change and not from any material inhomogeneities. It also maintains the testing set-up, such as the thermocouple placement, and allows for direct comparison from one strain rate to another without questioning whether the conditions were the same. Basically, the test can be employed to conclude whether the material exhibits positive or negative strain rate sensitivity under the conditions of testing.

Figure 4.15 shows some of the stress-strain curves obtained in this way. Beginning with **Figure 4.15a**, a general increase in flow stress is observed when the strain rate is increased from 10^{-1} to1 s^{-1}. At the initiation of the strain rate change, there is a stress drop at each temperature studied. This apparent softening or relaxation seems to have resulted from programming problems associated with the torsion machine software. A similar response is noted when the reverse change in strain rate is made. At higher temperatures, the steady state flow stress level is preserved upon returning to the lower strain rate. At lower temperatures, the second steady state flow stress level at 10^{-1} s^{-1} increased compared to the initial steady state flow stress at 10^{-1} s^{-1}. This can be attributed to the changes in specimen size, as discussed in section 4.2, which were not taken into account.

The appearance of each curve in terms of oscillations shows that the scatter level is comparable throughout the temperature range studied, with the exception of the 1150°C flow curve. The latter exhibits distinct oscillations at the highest strain rate, 1 s^{-1}, which were also observed in the simple torsion tests of steel A and B (see **Figures 4.3** and **4.10**). The sudden drops in flow stress are most likely due to slippage of the sample in the fixed grip.

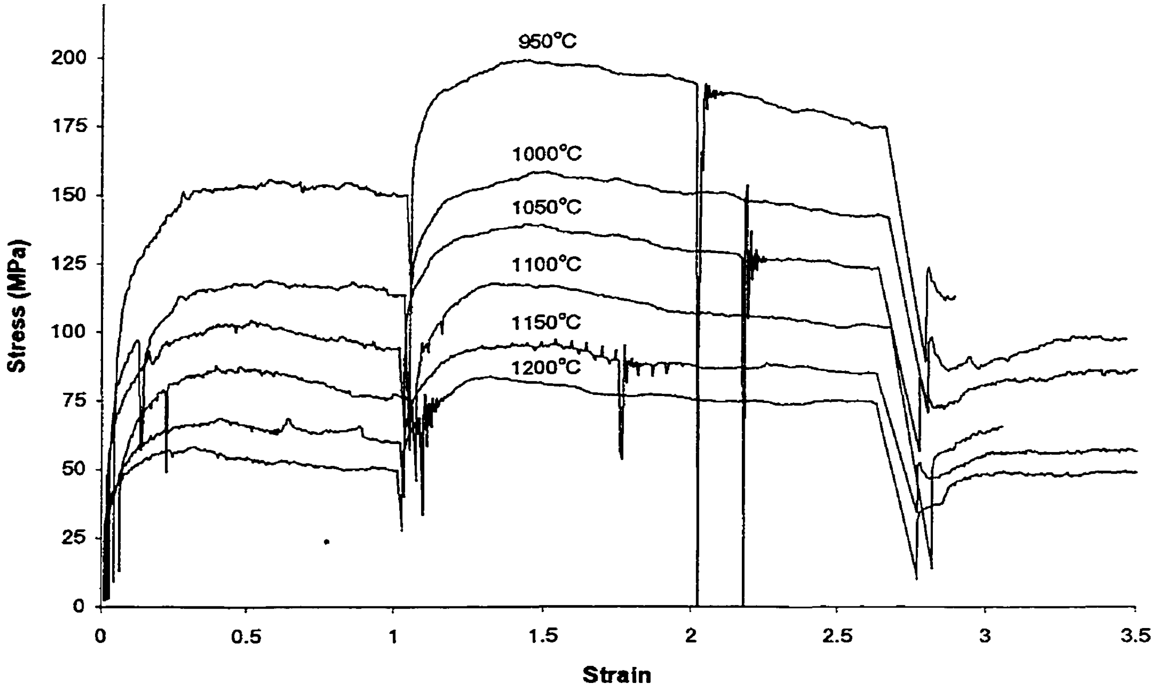

(a)

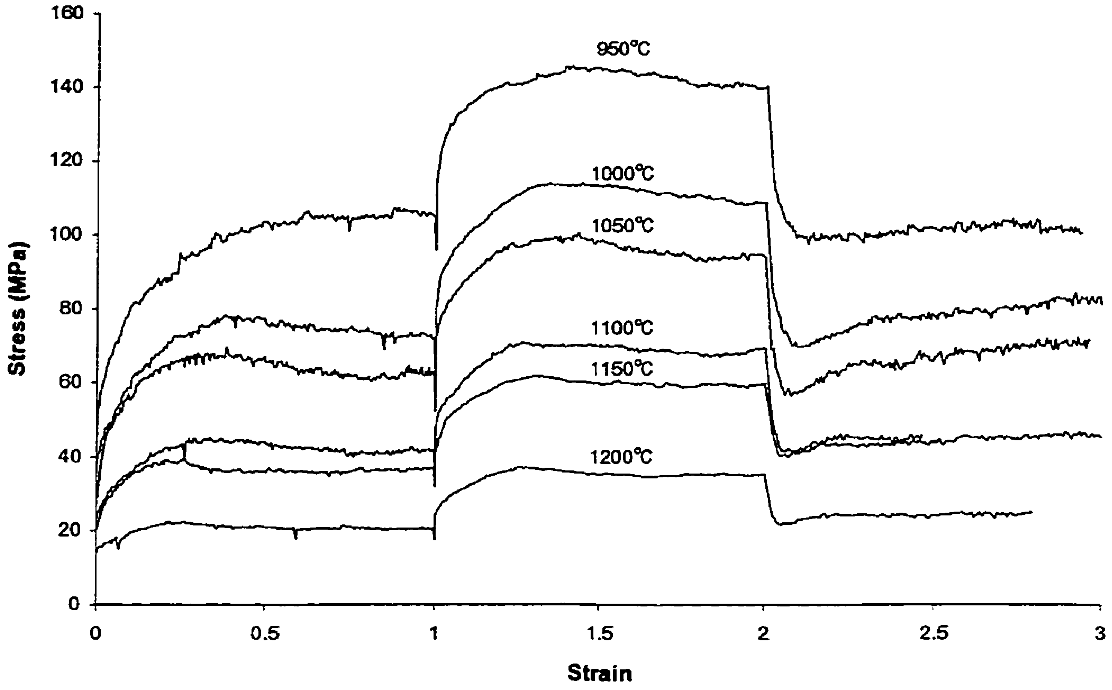

(b)

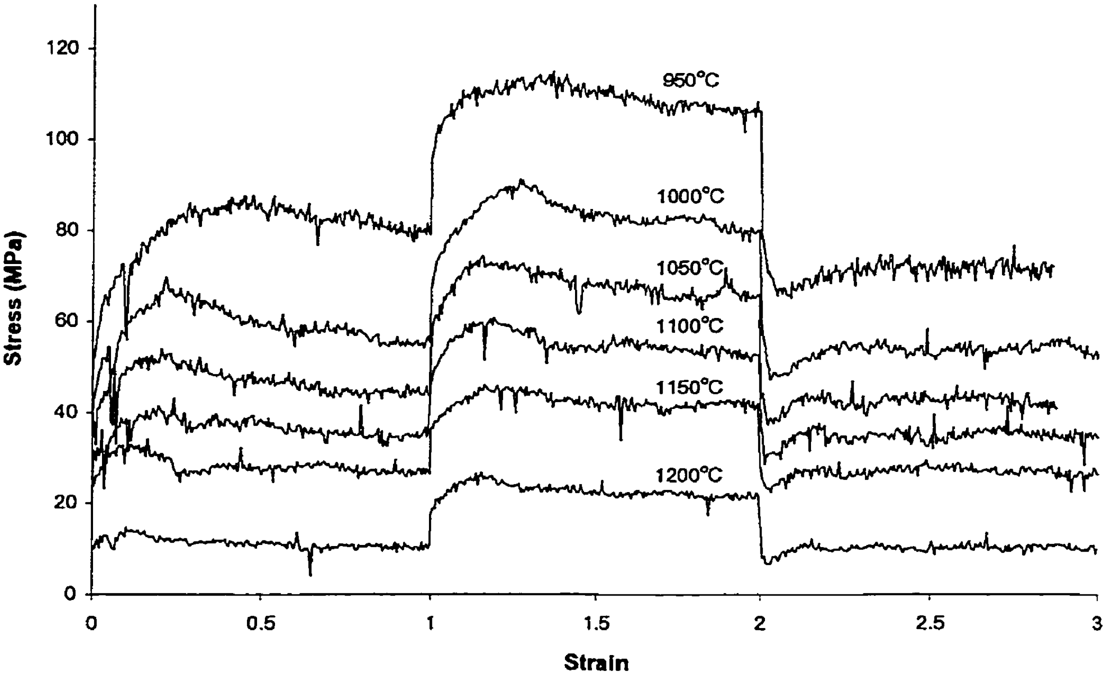

(c)

Figure 4.15: Stress-strain curves determined in the strain rate change tests (a) 10^{-1} to 10^{0} and back to 10^{-1} s^{-1}, (b) 10^{-2} to 10^{-1} and back to 10^{-2} s^{-1}, and (c) 10^{-3} to 10^{-2} and back to 10^{-3} s^{-1}.

When going to the next set of strain rate change tests, from 10^{-2} to 10^{-1} and back to 10^{-1} s^{-1}, the amplitudes of the serrations are similar all along the curves. Again, the flow curves display a drop in stress at the onset of a strain rate increase or decrease. The drop, however, is not as severe, especially after the decrease in strain rate. In general, the steady state stress level associated with the lower strain rate is resumed after the strain rate decrease.

In the last set of strain rate change tests, shown in **Figure 4.15c**, the oscillations in the curves are more pronounced. In addition, there is no visible drop in stress upon the strain rate increase and only a small dip is discernible after the strain rate decrease. This is probably because the strain rates are both quite low in this case and the machine software is better able to accommodate the changes.

One important fact that was revealed through these tests was that, under the conditions studied, there was no evidence of negative strain rate sensitivity. The response to every increase and decrease in strain rate was an overall increase and decrease in flow stress, respectively. Although, negative rate sensitivities were not found, this does not necessarily imply that DSA is not occurring. When testing at high temperatures in the presence of dynamic recrystallization, significant work hardening is prevented. The absence of appreciable work hardening makes it particularly difficult to detect when dislocations are able to escape from their solute atmospheres as a result of a strain rate increase.

4.4 Constant Stress Rate Results

Several studies have been conducted using constant stress rate tests to demonstrate discontinuous yielding[33,52-56]. These studies have shown that, rather than displaying a serrated shape, the curve is characterized by a stepped appearance, as shown in **Figure 4.16**. The mechanics of the test procedure have been demonstrated to alter the form of the stress–strain curve[53-56]. The stepped or stair-shaped curve featured under constant stress (creep) and constant stress rate conditions is said to result from the propagation of a plastic deformation wave front, otherwise referred to as a Lüders band, along the specimen[52,56]. Each horizontal section of the curve corresponds to the propagation of a deformation wave. Each time the stress is increased, an instability condition is reached in a section of the specimen and yielding begins. The deformation band then moves to unyielded regions under constant stress until it has propagated along the whole specimen. The material is now strain hardened and the stress must be increased before another deformation band can be generated. The process is then repeated and, between the occurrences of such waves, almost no strain is produced, hence creating a 'step' on the stress-strain curve. It is of interest that, during each stress increase, the plastic strain rate is very low, while during each strain increase, it is very high. Thus, this curve displays the type of negative SRS normally associated with DSA behavior.

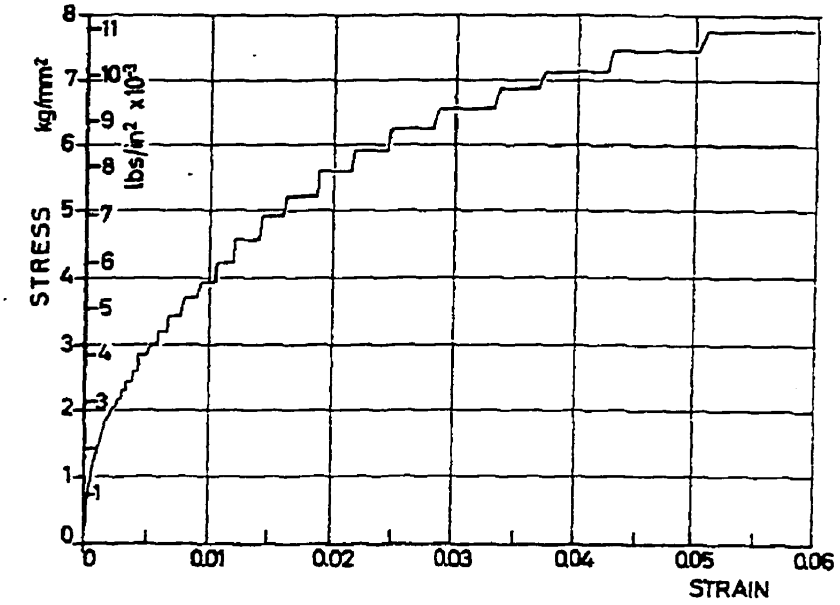

Figure 4.16: Typical stepped stress-strain curve for annealed, commercially pure, aluminum (at room temperature) under slowly applied dead weight tensile loading[53].

Another explanation given by Reynolds is that, as the material is strained, lattice vacancies are created which enhance diffusion and precipitation in their immediate vicinity[56]. The material is then hardened and, consequently, movement of the deformation band is prevented. The stress must therefore be increased to initiate another band at some other point along the gauge length of the specimen. Another band is formed and extends until the hardening from precipitation of solutes becomes substantial enough to stop spreading of the band.

The idea of performing a constant stress rate test was based on this established method of demonstrating that discontinuities on stress-strain curves originate from solute-dislocation interactions. The result of a constant stress rate test carried out on steel C, tested at a stress rate of 0.5 MPa/s at 950°C, is presented in **Figure 4.17**. The curve clearly displays discontinuities, although these are not in the classical form of steps. The discontinuities are grouped in bunches of three or four and persist, although to a smaller degree, to relatively high strains. These peaks may or may not be attributable to solute-dislocation interactions. Cyclic dynamic recrystallization may also be responsible for this behavior since the experiments were performed at a high temperature, where recrystallization becomes an issue.

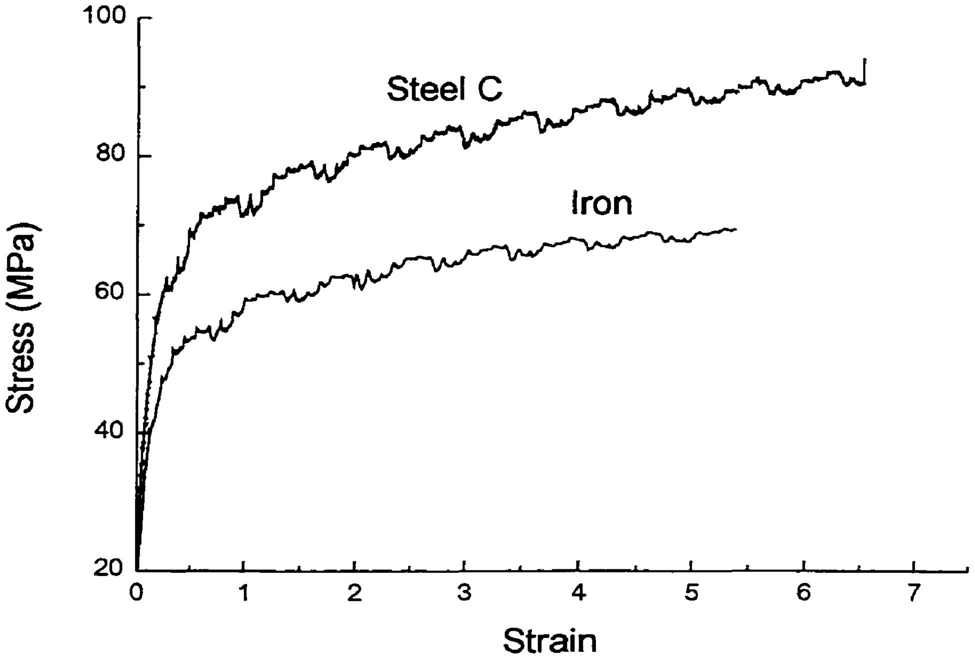

Figure 4.17: Stress-strain curves of steel C and iron tested at a constant stress rate of 0.5 MPa/s at 950°C.

Dynamic recrystallization (DRX) involves the nucleation and growth of new grains during deformation. When periodic DRX occurs, the material is work hardened sufficiently so as to induce DRX; subsequently, the material is softened and drops in flow stress are observed. The material is then strengthened again by deformation until it recrystallizes once more. This process is repeated several times over the course of the deformation process. The softening experienced during periodic DRX could explain the dips observed on the upper stress-strain curve of **Figure 4.17**. If, indeed, these discontinuities are caused by cyclic DRX, then a purer material, such as iron, should manifest this behavior to a stronger degree. For a purer material, the drops should be much more pronounced as there are fewer obstacles to impede grain boundary movement. In addition, the number of stress drop cycles should also increase as the kinetics of the recrystallization process will be faster. Pure iron was therefore also tested under the same conditions to verify this hypothesis. The stress-strain curve of the iron is shown together with the steel C curve in **Figure 4. 17**.

The iron displays the same peculiar breaks although with fewer bumps, which are also slightly smaller, though the relative drops are about the same. According to workers such as Jonas and Sakai, a single peak flow curve signifies that grain refinement is occurring, while multiple peak flow curves indicate grain coarsening[57]. Whether refinement or coarsening of the grains will occur is determined by the initial grain size relative to the stable dynamic grain size. If the initial grain size is finer than the stable dynamic grain size, coarsening will occur and the flow curve will exhibit multiple peaks. Conversely, if the initial grain size is larger than the stable dynamic grain size, the grain structure will be refined and the flow curve will display only one stress peak. A schematic diagram depicting multiple and single peak flow is reproduced here in **Figure 4.18**.

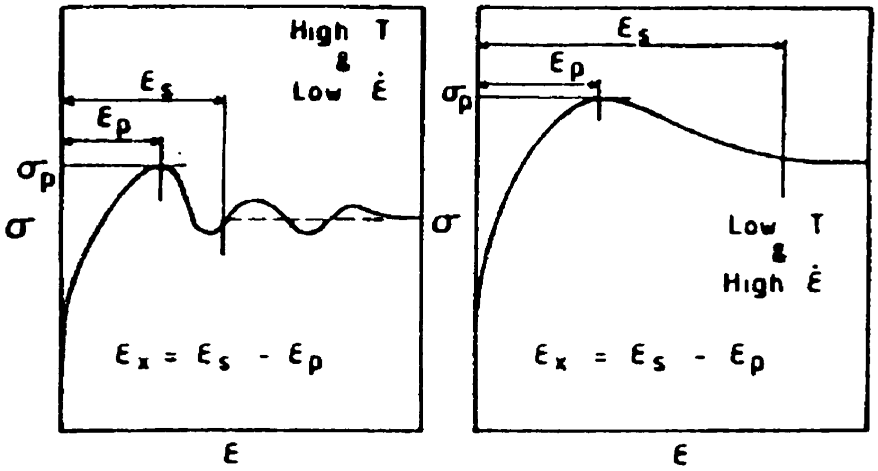

Figure 4.18: Schematic diagram of (a) periodic recrystallization and (b) single peak recrystallization[57].

With the aid of this information, we can now return to the case of the iron and of steel C. It can be imagined that the iron might have possessed an initial grain size closer to its stable dynamic grain size than steel C. Unfortunately, the initial grain sizes were not measured as it was only recognized later that the grain sizes might have played an important role. If the iron had a larger grain size prior to deformation, this would explain why it did not exhibit as large or as many drops in flow stress as steel C. That is, it did not require as many cycles of recrystallization to reach its stable dynamic grain size. This interpretation is based on the observation that larger grains were present in the iron after a 15-minute soak at 1200°C than in the steel. During this time, grain growth occurred and the iron, with fewer solutes and particles to inhibit grain growth, attained a larger average grain size than steel C, which contained many more impurities. This scenario can explain the present observations, as indicated in more detail below.

To investigate the discontinuities further, a plot of the strain rate versus the strain was superimposed onto the stress-strain curves, as shown in **Figures 4.19** and **4.20**. In both cases, the strain rate curves are consistently synchronized with the flow stress curves. Dips in the strain rate coincide with decreases in the flow stress. This means that the material was displaying *positive* SRS under the present testing conditions, unlike the negative SRS that characterized the material of **Figure 4.16**. That is, when the curves of **Figures 4.19** and **4.20** are smoothed, the peak stresses coincide with the peak strain rates and vice versa. Thus, it appears that cyclic dynamic recrystallization can provide a rationalization for the appearance of the dips in the flow curve. Clearly, further investigation of this phenomenon is called for. Nevertheless, it can be concluded at least tentatively that the 'large strain' fluctuations are due to cycles of dynamic recrystallization, while the fine scale ones (i.e. the 'noise' or scatter) may be due to DSA.

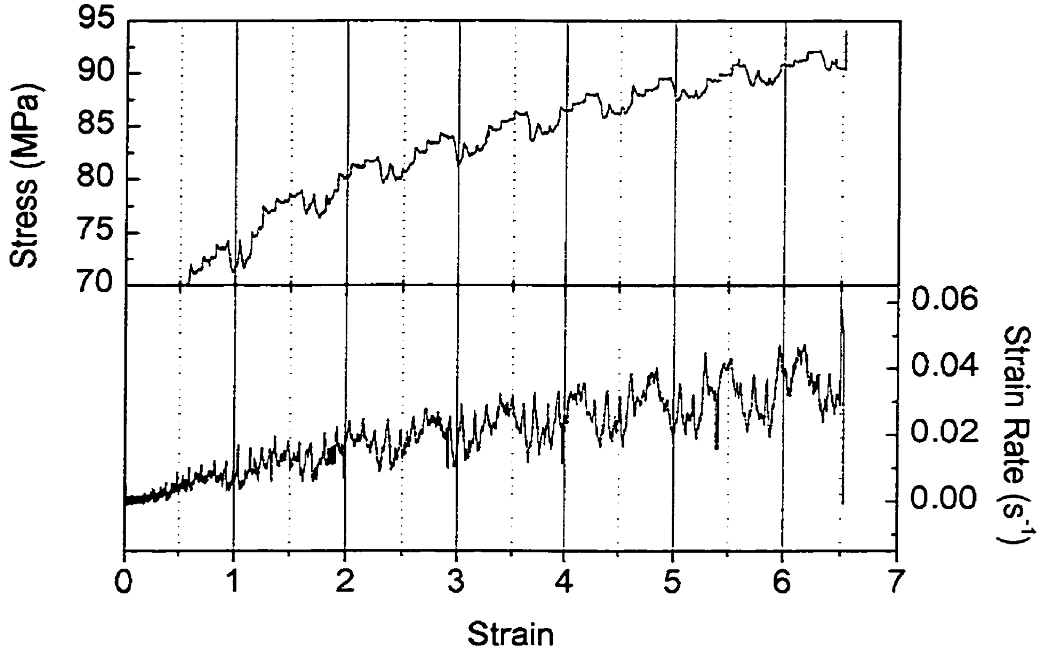

Figure 4.19: Stress and strain rate versus strain curves for steel C, determined at a constant stress rate of 0.5 MPa/s at 950°C.

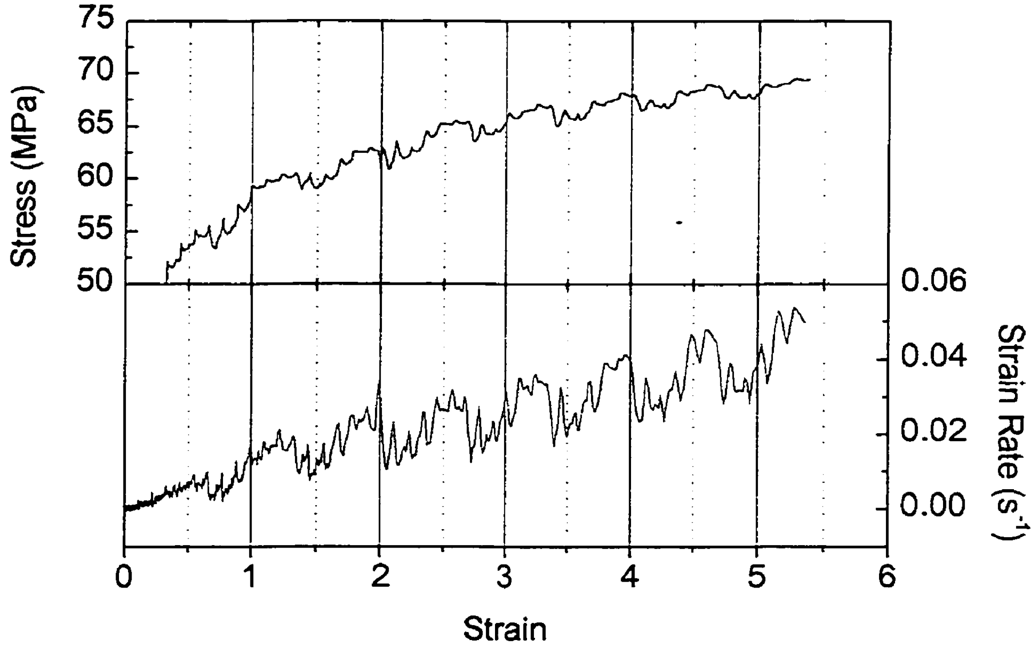

Figure 4.20: Stress and strain rate versus strain curves for iron, determined at a constant stress rate of 0.5 MPa/s at 950°C.

4.5 Decreasing Temperature Results

Cahn's model, as discussed in section 3.6.3, was adapted for the case of dislocation motion to estimate the temperatures and strain rates at which an instability could arise as a result of a transition in the interaction between solute atoms and dislocations. At low velocities, the dislocation velocity is considered to be determined by an impurity drag effect in which the impurities are dragged along by the dislocations[47]. At high velocities, the dislocations break away from the solute atmospheres and their velocity is now dependent on the rate of diffusion of solute atoms across the dislocations[47]. At the transition point between these two extremes, there is an instability, which forms because two velocities are possible at a given driving force. The following equation, taken from Cahn was used to locate this instability[47]:

$$P = \lambda V + \frac{\alpha C_o V}{1 + \beta^2 V^2} \qquad (4.1)$$

Here P is the driving force, λ is the intrinsic drag coefficient or the reciprocal of the intrinsic (pure metal) mobility ($m = m_o \exp(-Q/RT)$) , V is the grain boundary velocity, or for our case, the dislocation velocity, and C_o is the bulk concentration of the solute species. The parameters α and β are variables given by the following:

$$\alpha = \frac{N_v (k T)^2}{E_o D} \left(\sinh \frac{E_o}{R T} - \frac{E_o}{R T} \right) \qquad (4.2)$$

$$\beta^2 = \frac{\alpha k T \delta}{2 N_v E_o^2 D} \qquad (4.3)$$

Here N is the number of iron atoms per unit volume, k is Boltzmann's constant, T is the absolute temperature, E_o is the interaction energy between the grain boundary and the solute atom, or for our case, the interaction energy between the dislocation and the solute atom, D is the diffusion coefficient of the solute species, R is the ideal gas constant and δ is the interaction width. One of the solute elements most likely to be responsible for the instability in the present case is phosphorus, based on the results obtained in the stress scatter level tests (see section 4.1). This is why it is selected here for the instability calculation. The values assigned to the variables in the model are listed in **Table 4.3**.

Table 4.3: Constants used to calculate the driving force, P.

Parameter	Value Assigned	Reference
λ (m^4/J s)	$1/[\,4.4 \times 10^6 \exp(-276\,000 / RT)\,]$	58*
N_v (atoms/m^3)	9.17×10^{28}	
k (J/atom K)	1.38×10^{-23}	
E_o (J/mole K)	- 55 000	48
D (m^2/s)	$8.7 \times 10^{-4} \exp(-200\,000 / RT)$	44
R (J/mole K)	8.134	
δ (m)	13×10^{-10}	58*

*values for nickel

Using the adapted model and the values given in **Table 4.3**, the force versus velocity plots of **Figure 4.21** were obtained. Here, unstable flow will occur when the velocity increases while the force is *decreasing*. Between 900° and 1200°C, unstable dislocation velocities defined in this way span the range from 1.5×10^{-3} to 12 m/s. To find the approximate strain rates to which these velocities correspond, the following relationship was used:

$$\dot{\varepsilon} = \frac{b \rho \bar{v}}{\sqrt{3}} \qquad (4.4)$$

where b is the Burgers vector, ρ the dislocation density and v the mean dislocation velocity[5]. However, the dislocation density will vary with stress according to:

$$\rho = \frac{\sigma^2}{\alpha^2 G^2 b^2} \qquad (4.5)$$

where σ is the stress, α is a numerical constant between 0.3 and 0.6 and G is the shear modulus[13].

Assuming a stress of 40 MPa for steel C, a Burgers vector of 2.5×10^{-10} m, a shear modulus of 50 GPa, and an α constant of 0.4, the strain rate range was estimated to fall between 13.8 and 110 666 s^{-1}. These are very high strain rates, and since the calculation involved many assumptions, it can be concluded that the model did not provide the exact locations of the expected instabilities. Nevertheless, it does demonstrate the existence of the instability produced by the transition from the solute drag to the 'lattice friction' regime (as denoted by Blanc and Strudel[14]). A test was therefore designed to provoke this transition under the conditions where serrated yielding had previously been reported by Kirihata et al.[3], that is, at strain rates of 10^{-2}, 10^{-3} and 10^{-4} s^{-1} and at temperatures between 900° and 1200°C. To eliminate the need to perform tests at a series of temperatures, each test was conducted under continuous cooling conditions. The stress-strain curves obtained in this way, along with their respective temperature profiles during deformation, are shown in **Figures 4.22** to **4.24** for steel C. The flow stress in **Figure 4.22** does not immediately increase upon a temperature decrease; in fact, it decreases. This is most likely due to a time lag between the thermocouple and sample temperatures.

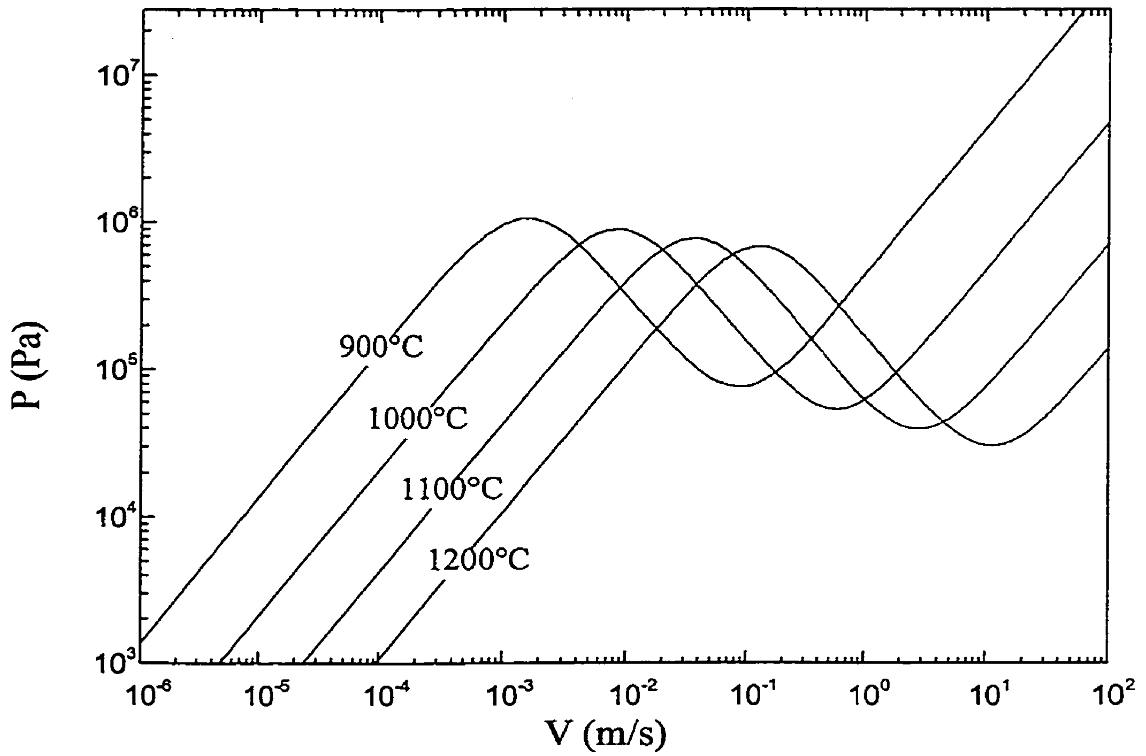

Figure 4.21: Force versus dislocation velocity profile calculated using the model formulated by Cahn.

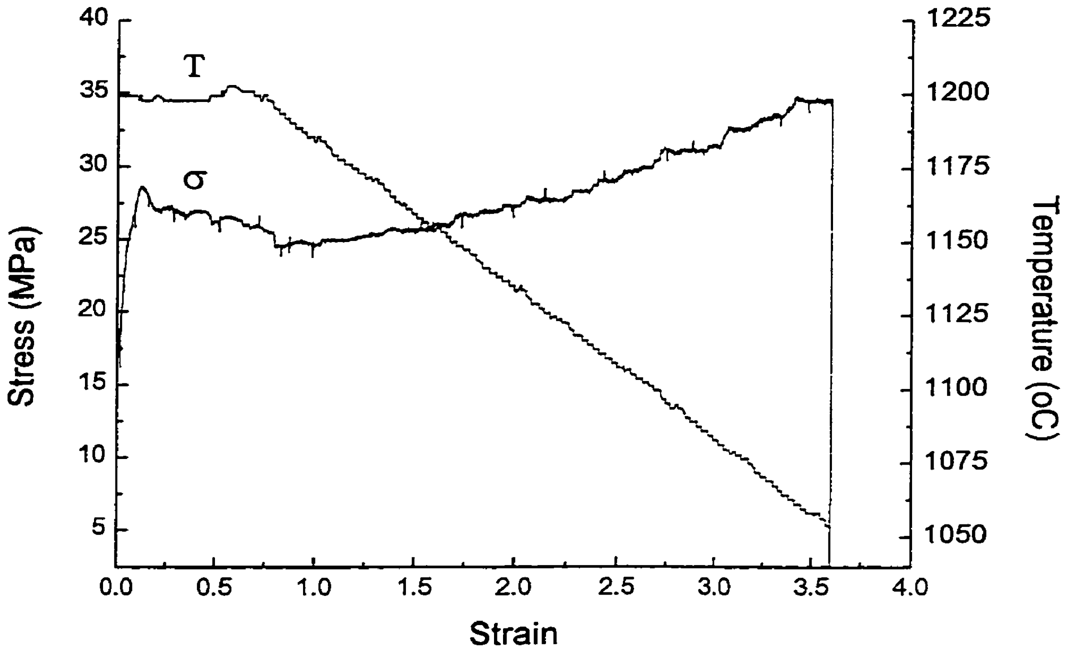

Figure 4.22: Stress-strain curve and temperature profile for steel C. Test carried out at ε rate = 10^{-2} s^{-1}.

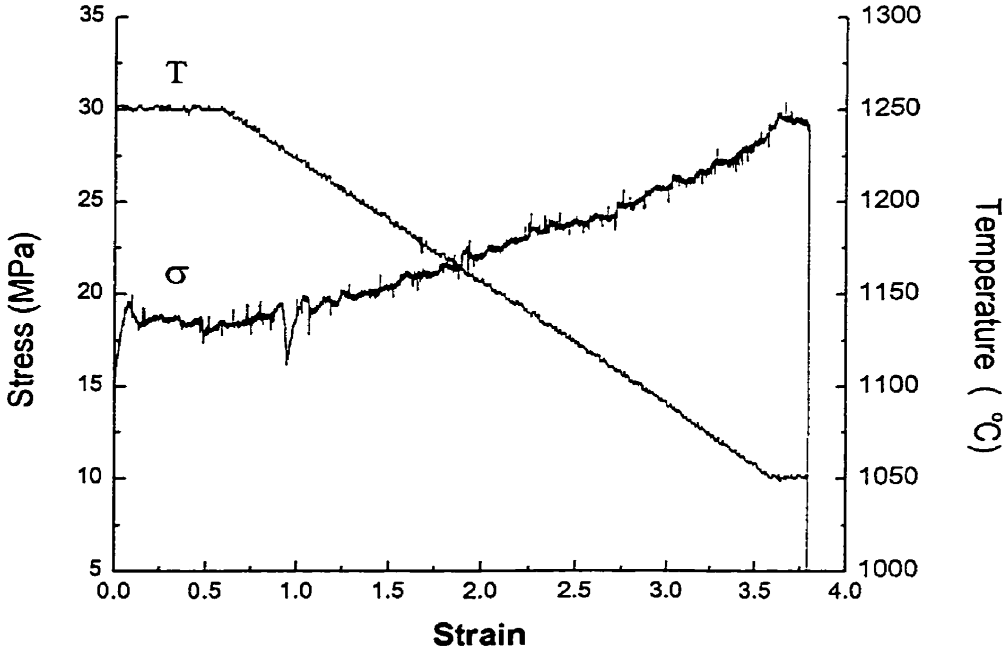

Figure 4.23: Stress-strain curve and temperature profile for steel C. Test carried out at ε rate = 10^{-3} s^{-1}.

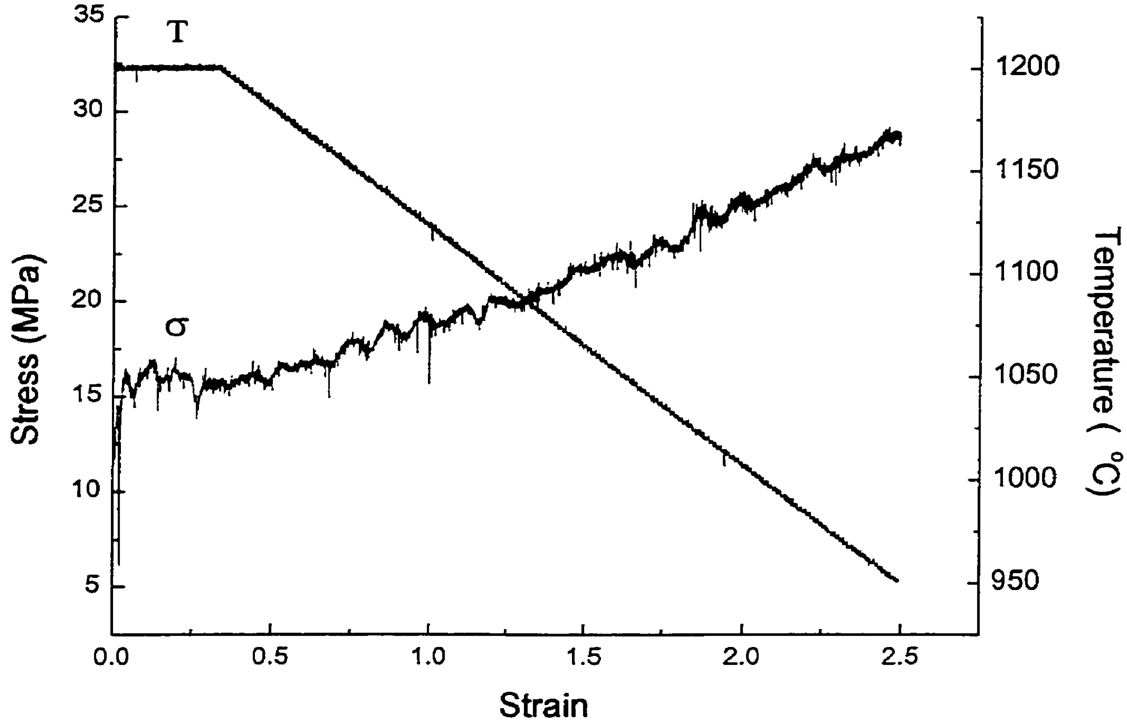

Figure 4.24: Stress-strain curve and temperature profile for steel C. Test carried out at ε rate = 10^{-4} s^{-1}.

The amplitudes of the serrations on the stress-strain curves of **Figures 4.22** and **4.24** appear to increase as the temperature is lowered. To inspect this trend more closely, the difference between the instantaneous stress and the smoothed average stress, obtained by averaging 100 points at a time (a 'running' average), was plotted versus strain for all the conditions studied. These curves are shown in **Figures 4.25**, **4.26** and **4.27**. An increase in the stress difference with strain would imply that the 'noise' level is increasing as the temperature is decreasing. Such an increase could indicate that DSA or some other type of solute-dislocation interaction is taking place. At a strain rate of 10^{-2} s^{-1}, **Figure 4.25**, the amplitude of the serrations clearly increases as the temperature is decreased. At a strain rate of 10^{-3} s^{-1}, **Figure 4.26**, the change in the stress difference amplitude is not so evident. At the final and lowest strain rate, 10^{-4} s^{-1}, **Figure 4.27**, once again, there is an increase in the amplitude as the temperature is decreased.

The amplification of the oscillations with decreasing temperature suggests that there may be an increasing drag effect of the solute elements on the dislocations. The substitutional atoms may begin to impose a higher drag force, caused by the temperature decrease, which results in a lower diffusion rate. This could act to create a larger degree of pinning and unpinning of the dislocations and could provide a possible explanation for observed behavior.

Figures 4.22 to **2.25** clearly do not display any sharp instabilities in flow stress. A plot of log stress versus inverse absolute temperature was therefore prepared to try to draw out evidence for the instability, as was done in the work of Le Gall and Jonas[59]. They studied the effect of sulphur segregation to grain boundaries in nickel and found that there was a discontinuity in the log stress versus inverse absolute temperature plot for data taken from hot compression tests. Unfortunately, there was no evidence for a similar discontinuity in the data obtained on steel C tested under the present conditions.

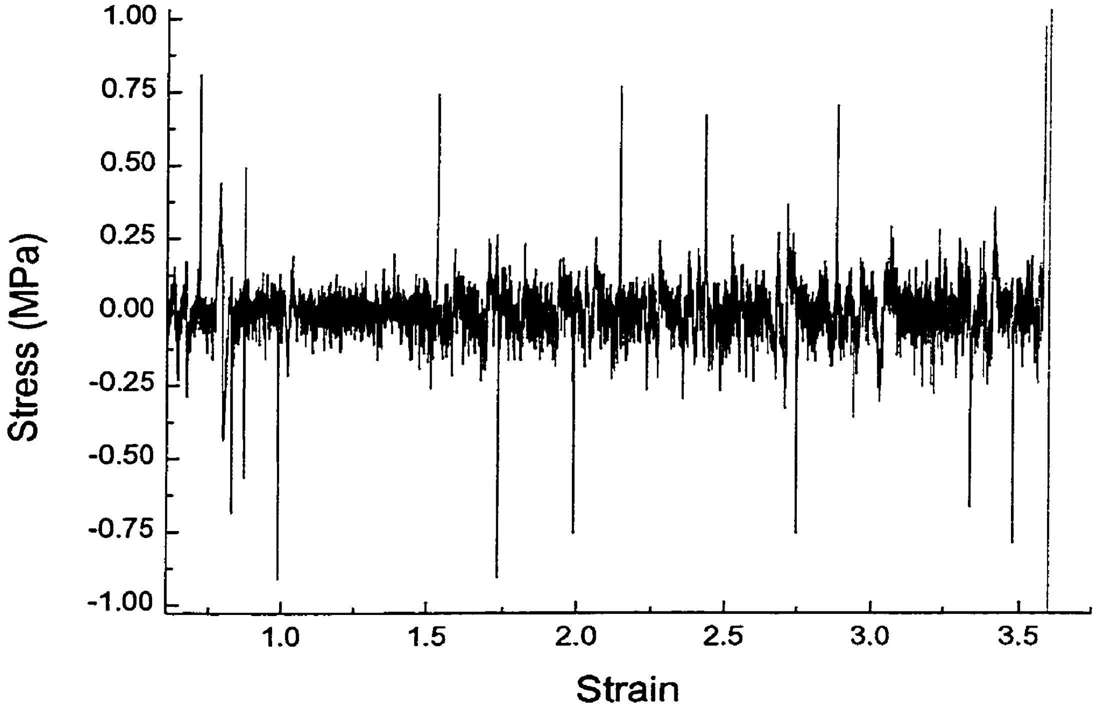

Figure 4.25: Difference between the instantaneous stress and the smoothed average stress, obtained by taking running averages of 100 points, versus the strain at ε rate = 10^{-2} s^{-1}.

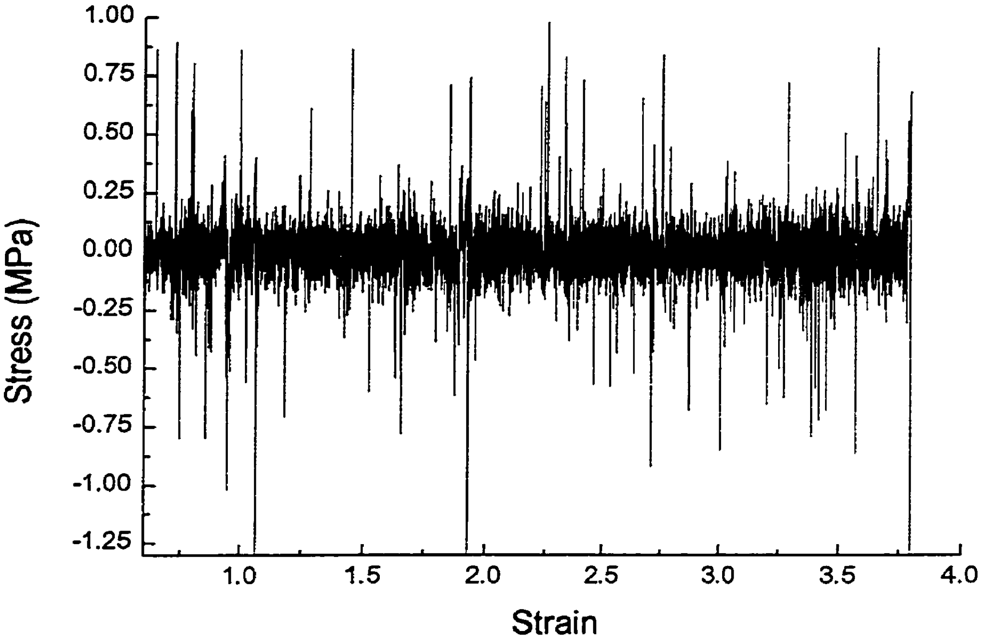

Figure 4.26: Difference between the instantaneous stress and the smoothed average stress versus the strain at ε rate = 10^{-3} s^{-1}.

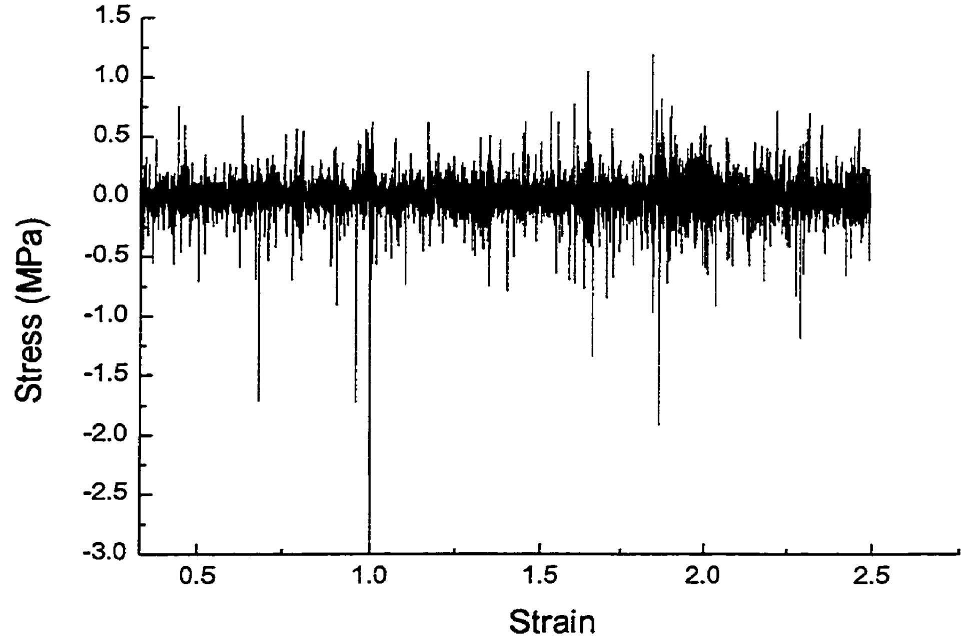

Figure 4.27: Difference between the instantaneous stress and the smoothed average stress versus the strain at ε rate = 10^{-4} s^{-1}.

4.6 Results of the Low Ratio Strain Rate Change Tests

The final tests that were carried out in the attempt to extract evidence regarding the occurrence of DSA consisted of modified strain rate change tests. The strain rate change ratio was reduced from the usual one order of magnitude down to about 1.3. It was reasoned that if the stress oscillations in **Figure 4.1** are the result of solute-dislocation interactions, the critical 'holding time' for pinning and unpinning is in the order of seconds or fractions of a second. In addition, it appears that only small strain rate fluctuations are needed to cause jerky flow at high temperatures. In an effort to obtain more solid evidence for DSA behavior, low ratio strain rate change tests, using steel C, were performed with varying holding or cycle times. The expected or projected response to a change in strain rate that can be considered to provide evidence for the pinning and unpinning of dislocations is illustrated in **Figure 4.28**.

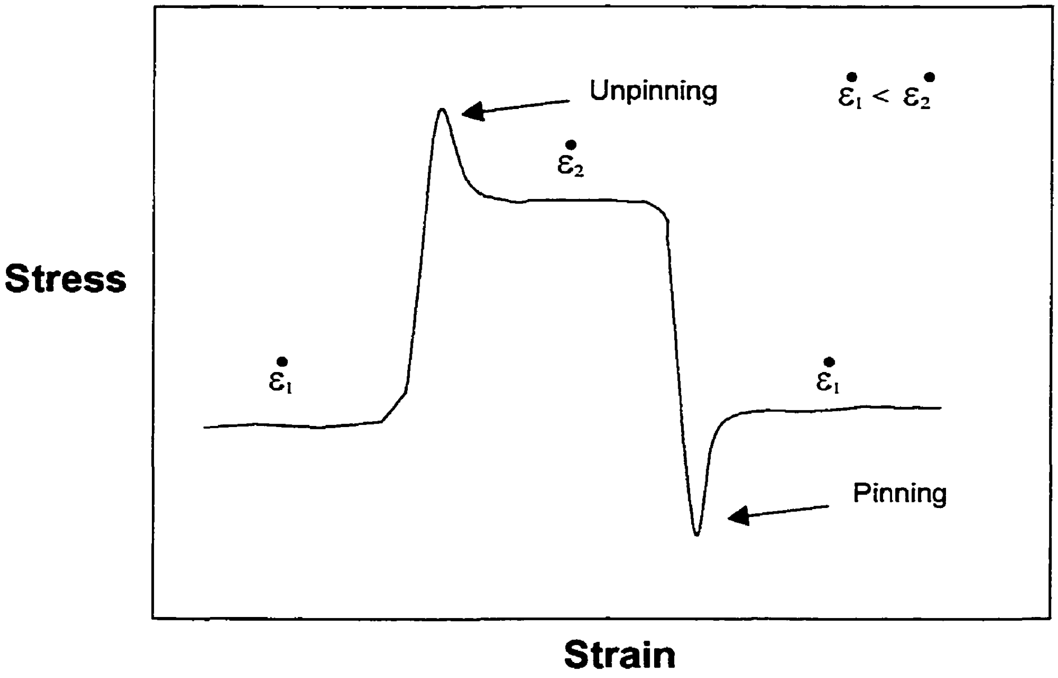

Figure 4.28: Schematic diagram showing the expected effect of the pinning and unpinning of dislocations during low ratio strain rate changes.

In order to maximize the use of each sample, several strain rate change tests were carried out on each specimen. Once a strain rate change sequence was completed, the next series of strain rate change tests was executed at the next set of assigned strain rates.

The stress and strain rate versus time curves of the first test are shown over the entire strain range in **Figure 4.29**, while **Figure 4.30** displays the curves in sections for better viewing and analysis. For clarity, an average strain rate curve, obtained by taking a running average of 50 data points, is also shown in the figures. In reality, however, the variability in strain rate is fairly large, producing an overlap between the two strain rates. In the case of the flow curves, **Figure 4.29** shows the actual curve with no alterations, whereas in **Figure 4.30**, the flow stress is again smoothed by taking a running average of 50 data points for clarity. Looking at **Figure 4.30**, it is evident that the strain rate changes are not abrupt; that is, the wave is not square, but rather in between a triangle and a square wave. The sluggish response was even more pronounced when the holding time was decreased. The strain rate did not have time to reach its designated value before it decreased again to the lower rate.

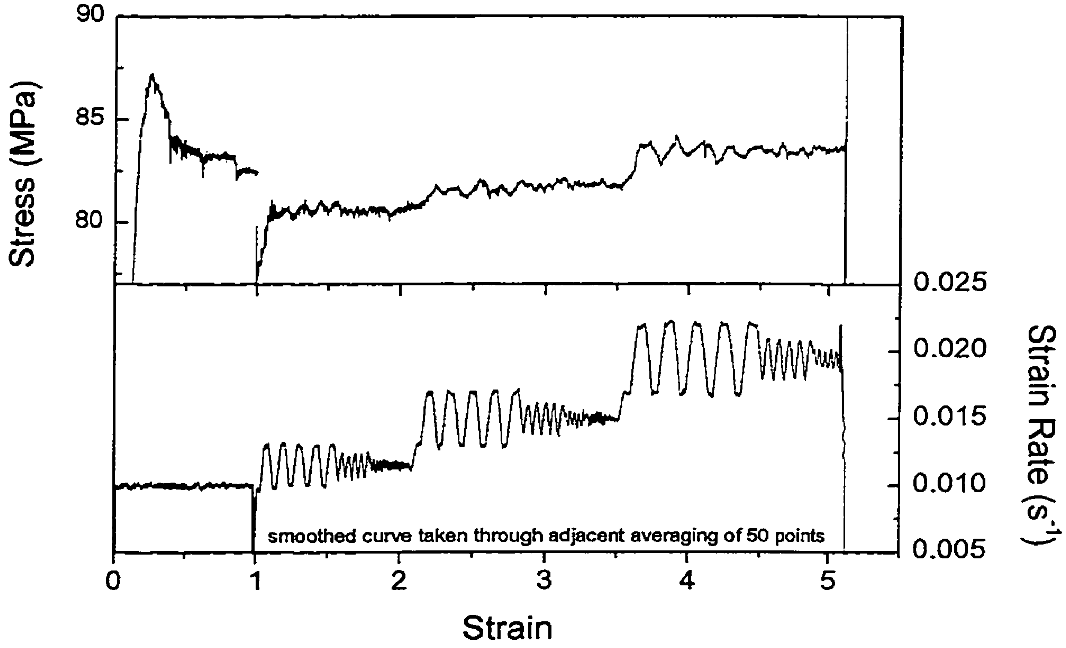

Figure 4.29: Stress and strain rate versus strain curves determined at 950°C for steel C in test 1 of the low ratio strain rate change tests.

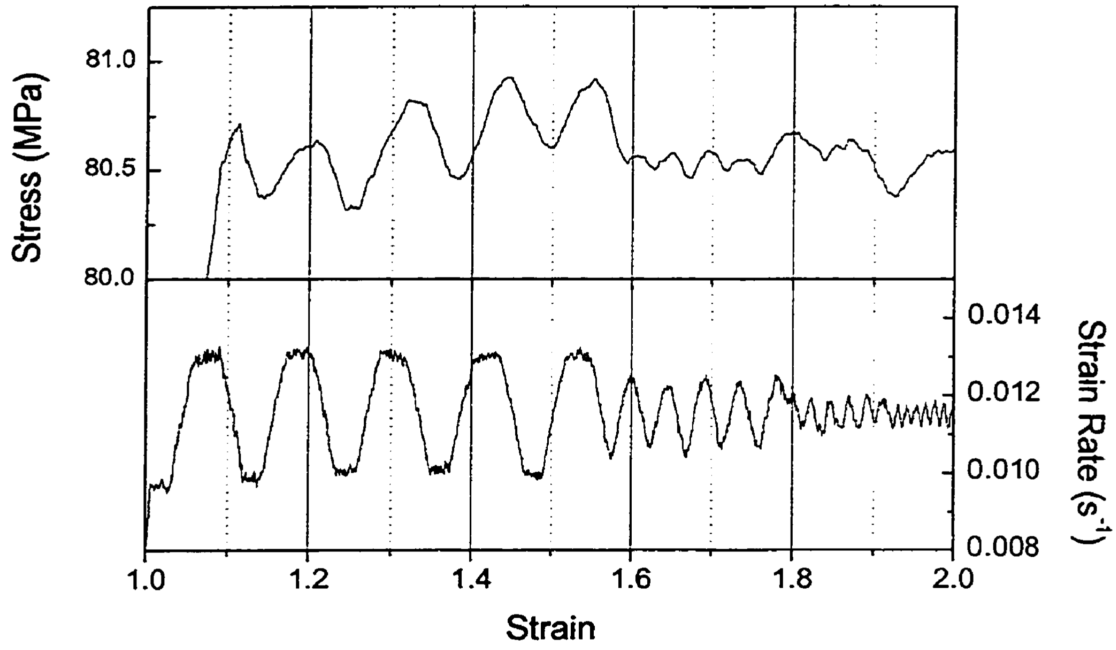
Stress (MPa)
81.0
80.5
80.0
0.014
0.012
0.010
0.008
Strain Rate (s^{-1})
1.0
1.2
1.4
1.6
1.8
2.0
Strain

(a)

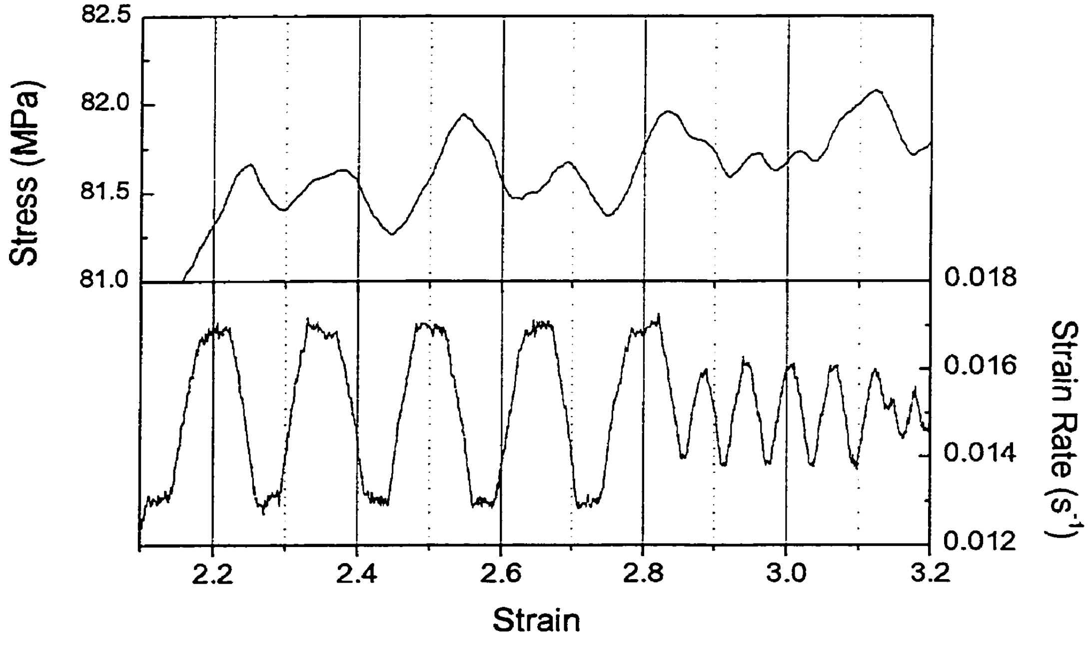
Stress (MPa)
82.5
82.0
81.5
81.0
0.018
0.016
0.014
0.012
Strain Rate (s^{-1})
2.2
2.4
2.6
2.8
3.0
3.2
Strain

(b)

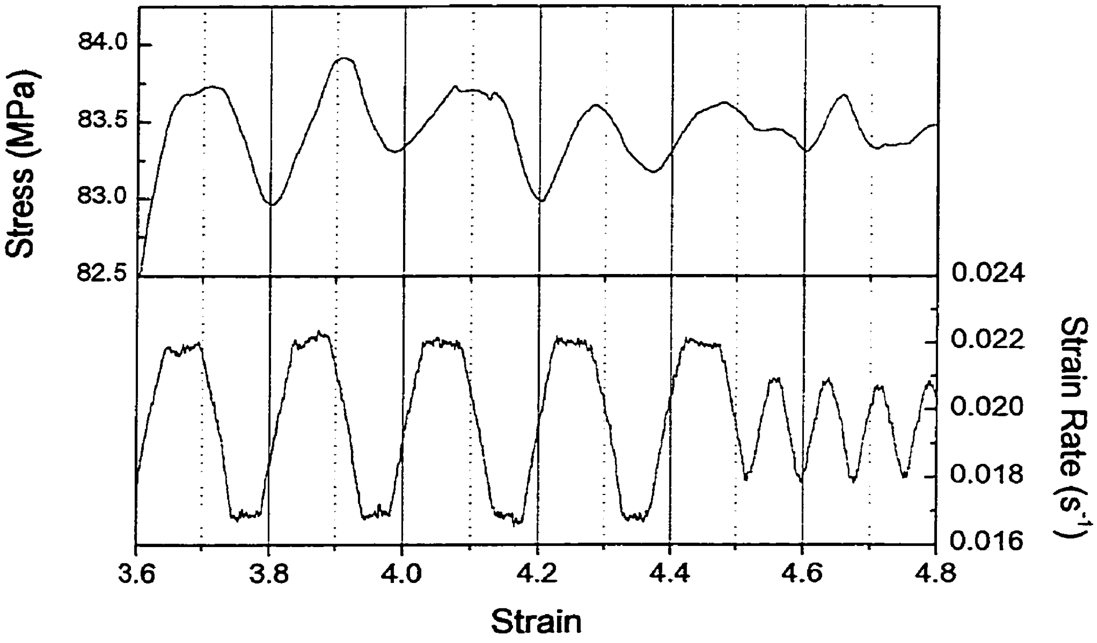

(c)

Figure 4.30: Magnified smoothed stress and smoothed strain rate versus strain curves determined at 950°C for steel C in test 1 of the low ratio strain rate change tests from (a) $\varepsilon = 1$ to $\varepsilon = 2$, (b) $\varepsilon = 2.1$ to $\varepsilon = 3.2$ and (c) $\varepsilon = 3.6$ to $\varepsilon = 4.8$.

In these diagrams, the flow stress exhibits positive strain rate sensitivity, although the response is rather slow. The two are not well synchronized, the flow stress changes lagging behind the strain rate changes. At the longest holding time, 5 seconds, there are as many peaks and dips in flow stress as there are changes in strain rate. This is not the case for the shorter holding times; under the latter conditions, it appears that there was insufficient time for the steady state flow stress to be reached.

The conditions of the test were then repeated with only a few changes. First, the strain rate change program was altered such that it provided sharper changes in strain rate and the shorter holding times were omitted as they provided little information. The other modification was that the data acquisition rate was increased to 100 data points per second. **Figure 4.31** summarizes the results of the experiment, while **Figure 4.32** provides more detailed information about each sequence of the strain rate changes. Although the strain rate changes were more abrupt, there was no apparent change in the flow curve. The response to the strain rate changes is similar to that of the first test, with the exception of the peculiar drops and rises in flow stress all along the curve, as illustrated in **Figure 4.31**. It is of interest that the 'rises' tend to occur at the high strain rate and the 'drops' at the low strain rates. These anomalies do not, however, appear in the curves of **Figure 4.32** because this curve displays the smoothed running average obtained using 50 data points. No explanation can be offered as yet for these unusual dips and rises in flow stress.

The third test, shown in **Figures 4.33** and **4.34**, again produced comparable results, with no obvious pinning and unpinning at the beginning of each strain rate change. This experiment, however, displayed the fastest response to the changes in strain rate. The flow stress began to change immediately upon a strain rate change. The maximum and minimum flow stresses followed after a strain interval associated with work hardening and flow softening, respectively.

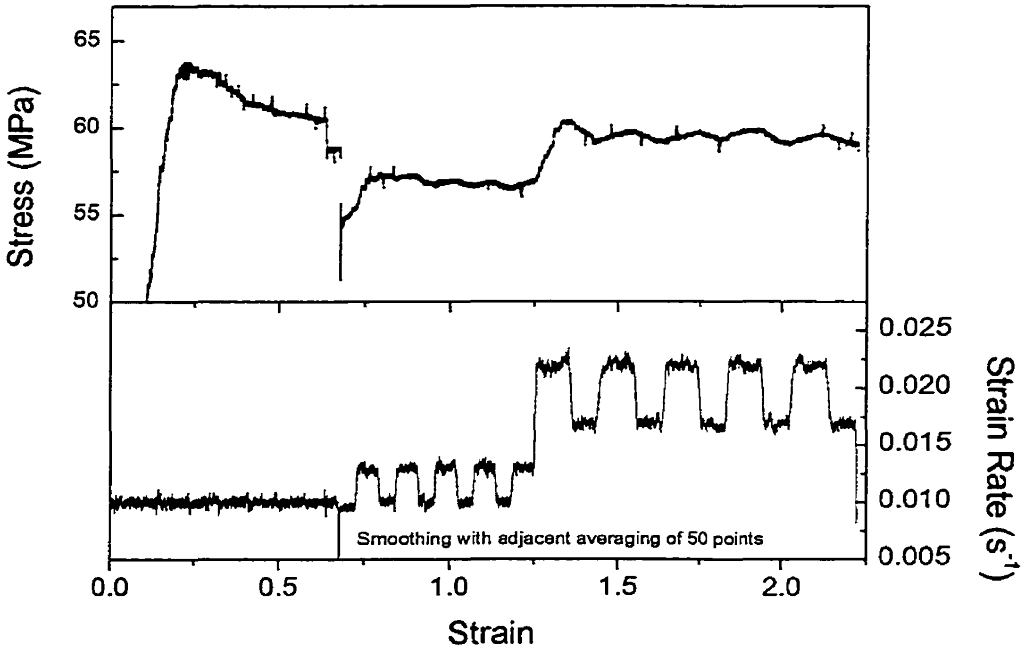

Figure 4.31: Stress and strain rate versus strain curves determined at 950°C for steel C in test 2 of the low ratio strain rate change tests.

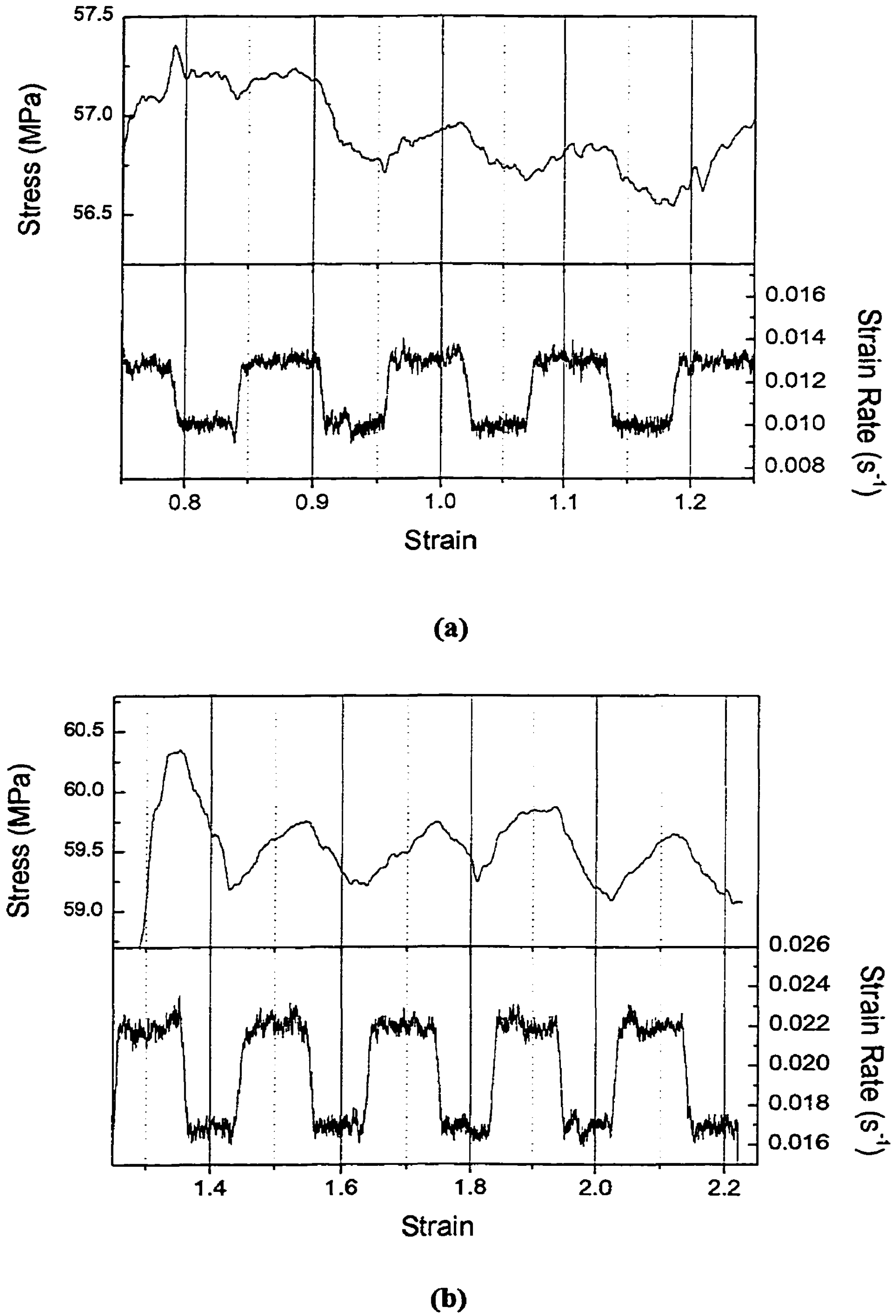

Figure 4.32: Magnified smoothed stress and smoothed strain rate versus strain curves determined at 950°C for steel C in test 2 of the low ratio strain rate change tests from (a) $\varepsilon = 0.75$ to $\varepsilon = 1.25$ and (b) $\varepsilon = 1.32$ to $\varepsilon = 2.25$.

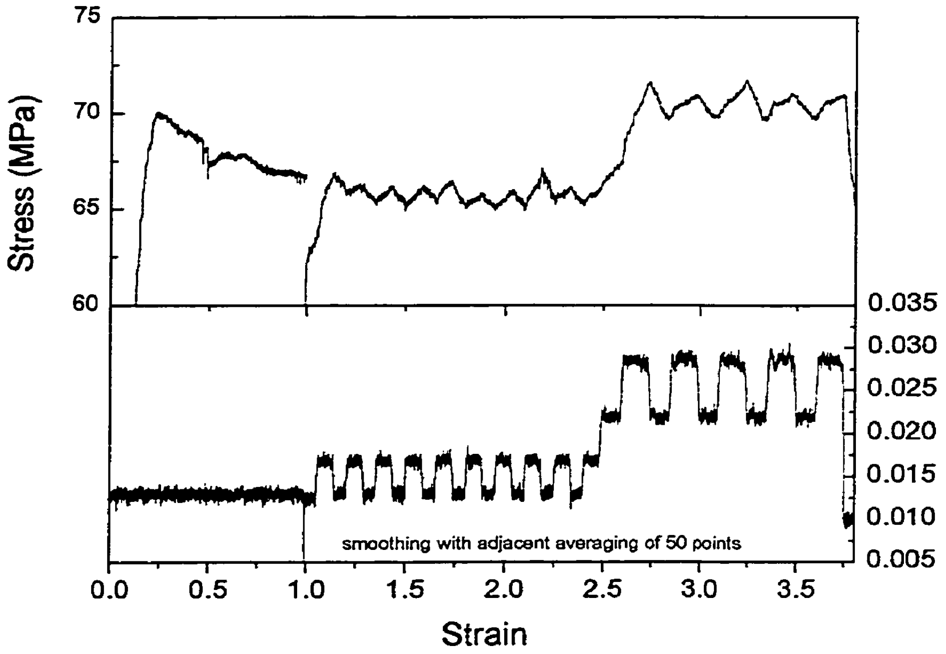

Figure 4.33: Stress and strain rate versus strain curves determined at 950°C for steel C in test 3 of the low ratio strain rate change tests.

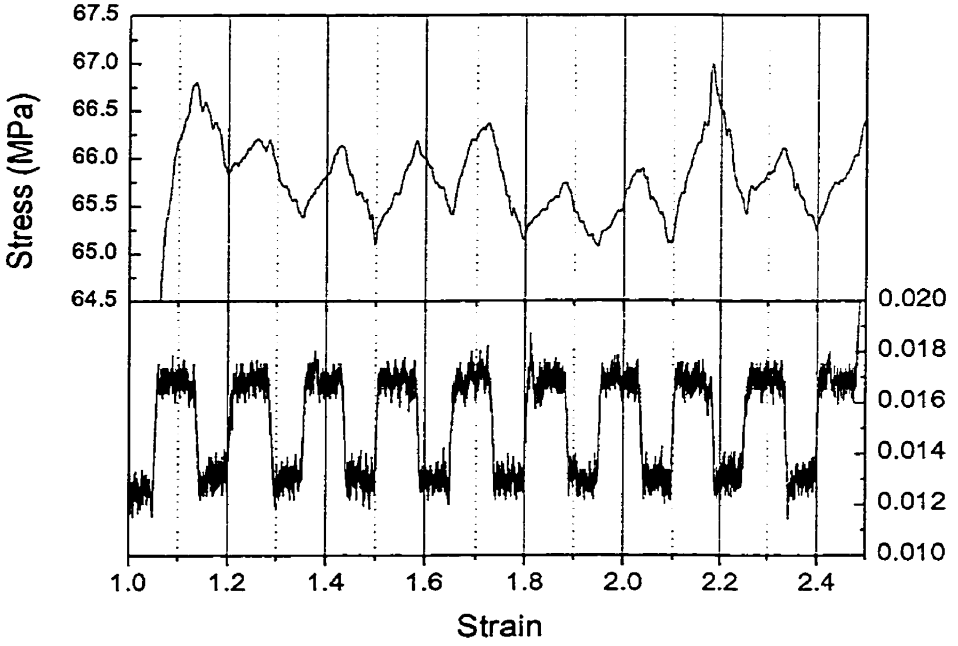

(a)

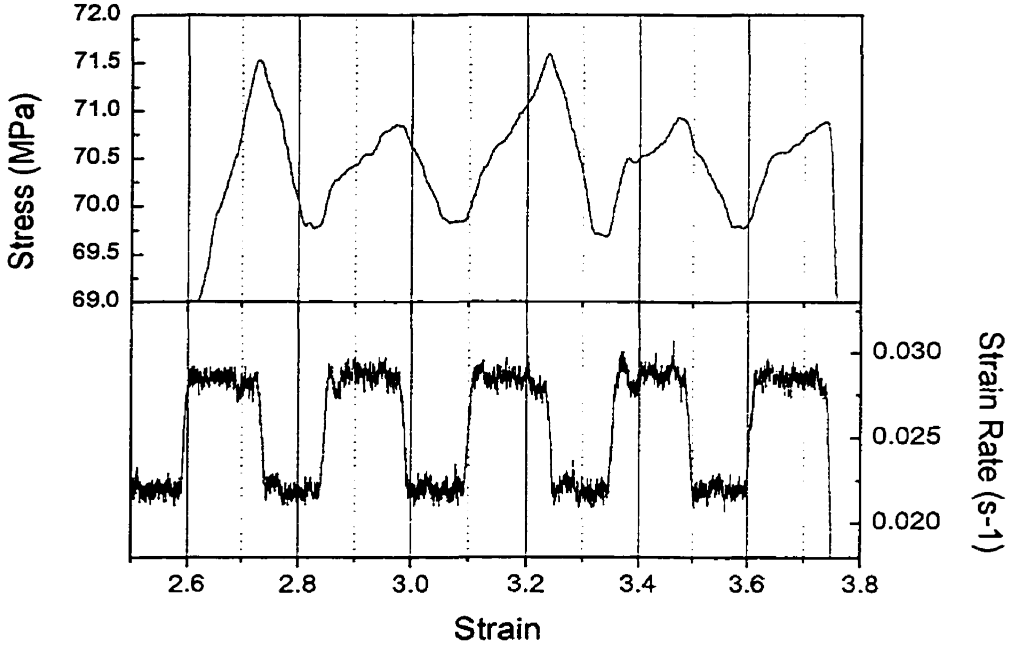

(b)

Figure 4.34: Magnified smoothed stress and smoothed strain rate versus strain curves determined at 950°C for steel C in test 3 of the low ratio strain rate change tests from (a) $\varepsilon = 1$ to $\varepsilon = 2.5$ and (b) $\varepsilon = 2.5$ to $\varepsilon = 3.8$.

No evidence of pinning and unpinning was obtained using this type of testing. Only positive rate sensitivities were observed. The conditions may not have been suitable for producing evidence of this phenomenon, if it occurs. Another possible explanation is related to the mode of testing. In torsion, the torque measured by the load cell sums up the contributions of all the rings or shells in the specimen, with the weight of the outermost ring being the highest. Such averaging will result in the suppression of possible flow peaks or drops in any one ring. In addition, the noise level of the machine with respect to strain rate was very high. Consequently, the flow stress 'noise' was also high and events such as pinning and unpinning may have been 'drowned out' by the noise.

CHAPTER V

CONCLUSIONS

The effect of substitutional elements on dynamic strain aging in steel is not well researched. The purpose of this study was to investigate and hopefully to determine the conditions under which DSA occurs as a result of the presence of substitutional elements. Several tests were formulated in attempting to extract evidence for this phenomenon. The following conclusions can be drawn from this work.

1. Stress Scatter Tests

- The 'pure' iron sample possessed the smoothest stress-time curve, followed (in order) by steels D, E, B, F and C.
- No single element could be isolated as the sole cause of the stress variations. Analysis and comparison of the stress-time curves as a function of their chemical compositions were difficult as the chemistries of the steels were so different.
- Nevertheless, the effects of silicon, phosphorus and sulphur on the amplitude of the oscillations were greater that those of the other elements. This conclusion is consistent with their higher interaction energy levels with grain boundaries and with their higher diffusivities.

It was assumed in this work that the values of the former are comparable to the interaction energies of a solute and a dislocation.

- It could also be concluded that, rather than the solute-dislocation interactions causing the stress fluctuations, the latter could result from solute-grain boundary interactions.
- The twist rate, obtained by taking the derivative of the angle-strain curve, was found to vary significantly, indicating that the testing machine does not provide a constant strain rate for testing.

2. Simple Torsion Tests

- There were peculiar serrations observed in both the steel A and steel B tests carried out at various temperatures at a strain rate of 1 s^{-1}.
- In one case, the peculiar serrations were intermittent with the serrations appearing, disappearing and then appearing again. Other workers have also observed this behavior in between isolated stable deformation regimes[34,50,51]. Different diffusion processes have been considered to be responsible for this phenomenon (i.e. diffusion via vacancies, diffusion via interstitials, etc.).

3. Strain Rate Change Tests

- Under the conditions examined, there was no evidence of negative strain rate sensitivity.
- Dynamic recrystallization probably eliminated the effect, if any, of the work hardening contribution made by solute-dislocation interactions.
- The low dislocation densities present at high temperatures may make it difficult to obtain evidence for DSA.

4. Constant Stress Rate Tests

- Constant stress rate tests have often been utilized to demonstrate the occurrence of discontinuous yielding. It was therefore hoped that this type of testing could extract evidence for DSA at elevated temperatures.

- The iron and steel C specimens did not display the classical step-shaped stress-strain curves observed at lower temperatures. The stress-strain curves for both materials contained similar cyclic discontinuities.
- The cycles are probably caused by repeated intervals of dynamic recrystallization.
- The data indicated that the materials were characterized by *positive* rate sensitivities under the current testing conditions.

5. Decreasing Temperature Tests

- No distinct stress instability was found when the temperature was decreased at all the strain rates investigated.
- At two of the strain rates explored, 10^{-2} and 10^{-4} s^{-1}, the amplitudes of the serrations increased when the temperature was decreased. This was taken as an indication that the solute atoms were imposing higher drag forces as the temperature was decreased. The higher degrees of pinning and unpinning probably produced greater fluctuations in stress.

6. Low Ratio Strain Rate Tests

- This test was employed to attempt to demonstrate the pinning and unpinning of dislocations when small strain rate changes are made. Unfortunately, the occurrence of such events could not be verified.
- The conditions may have been unsuitable for revealing this phenomenon. It could also be that torsion may not be the most suitable testing mode as it sums up the torque contributions of each incremental shell of the specimen. The torque peak produced in a single ring may get suppressed or obscured when all of the rings are considered.

- Another explanation is that the strain rate noise level of the machine is simply too high to permit fine scale effects such as the pinning and unpinning of dislocations to be observed.

Although this study was not successful in producing firm evidence for the occurrence of DSA caused by substitutional elements in steel, this does not imply that the phenomenon is not taking place. The work simply demonstrated that perhaps torsion testing is not the most suitable mode of testing, especially with the equipment and software currently available. In order to reveal DSA, the sensitivity of the machine must be high with a very high signal-to-noise ratio. Unfortunately, the torsion machine available for this investigation did not exhibit these features. Moreover, the fact that these tests were carried out within the dynamic recrystallization temperature range may have reduced the dislocation densities to levels that are too low to permit evidence for DSA to be obtained. More work must therefore be done in order to further our understanding of DSA in steel at elevated temperatures and perhaps to find a method that is suitable for establishing firm evidence for this phenomenon.

REFERENCES

1. J.M. Robinson & M.P. Shaw, *International Materials Reviews*, V. 39, No. 3, 1994, p. 113.
2. S. Lou & D.O. Northwood, *Materials Forum*, V. 17, No. 2, 1993, p. 153.
3. A. Kirihata, F. Siciliano Jr., T.M. Maccagno & J.J. Jonas, *Iron and Steel Institute of Japan International*, V. 38, No. 2, 1998, p. 187.
4. D.Q. Bai, J.J. Jonas, P.R. Hastings & N. Nickoletopoulos, *Metallurgical Transactions*, V. 29A, No. 5, 1998, p. 1384.
5. G. Dieter, Mechanical Metallurgy, Third Edition, McGraw-Hill, 1986.
6. J.D. Baird, *Iron and Steel*, May 1963, p. 186.
7. J.D. Baird, *Iron and Steel*, July 1963, p. 368.
8. C.C. Li & W.C. Leslie, *Metallurgical Transactions*, V. 9A, No. 12, Dec. 1978, p. 1765.
9. L.J. Cuddy & W.C. Leslie, *Acta Metallurgica*, V. 20, Oct. 1972, p. 1157.
10. J.D. Baird, "Chapter 8: Dynamic Strain Aging" in The Inhomogeneity of Plastic Deformation, ASM, 1973, p. 191.
11. A.S. Keh, Y. Nakada & W.C. Leslie, "Dynamic Strain Aging in Iron and Steel" in Dislocation Dynamics, McGraw-Hill, 1968, p. 381.
12. J.D Baird, *Metallurgical Reviews*, Review 149, V. 16, 1971, p. 1.
13. R.E. Reed-Hill, Physical Metallurgy Principles, Third Edition, PWS-Kent Publishing Company, 1992.
14. D. Blanc & J.L. Strudel, Proceedings of the 7th International Conference of Strength on the Strength of Metals and Alloy, Pergamon Press, p. 349.
15. B.J. Brindley & P.J. Worthington, *Metallurgical Reviews*, Review 145, V. 15, 1970, p. 101.
16. O.N. Senkov & J.J. Jonas, *Metallurgical and Materials Transactions*, V. 27A, 1996, p. 1877.

17. N.E. Zeghib & J.R. Klepaczko, *Journal of Materials Science*, V. 31, No. 22, 1996, p. 6085.

18. G.H. Rubiolo & P.B. Bozzano, *Materials Transactions, JIM*, V. 36, No .9, 1995, p. 1124.

19. P. Hähner, *Materials Science Engineering A*, V. 207, No. 2, 1996, p. 208.

20. K.J. Draheim & J. Schlipf, *Computational Materials Science*, V. 5, No. 1, 1996, p. 67.

21. L.H. de Almeida, *Scripta Metallurgica et Materialia*, V. 31, No. 5, 1994, p. 505.

22. A. Karimi Taheri, T.M. Maccagno & J.J. Jonas, *Iron and Steel Institute of Japan International*, V. 35, No. 12, 1995, p. 1532.

23. W.R. Thomas & G.M. Leak, *Iron and Steel Institute of Japan*, V. 180, 1955, p.155.

24. K.G. Samuel, S.L. Mannan & P. Rodriguez, *Journal of Materials Science Letters*, V. 15, No. 19, 1996, p. 1697.

25. E. Bouchaud, L. Kubin & H. Octor, *Metallurgical Transactions A*, V. 22A, May 1991, p. 1021.

26. J.D. Baird & A. Jamieson, *Iron and Steel Institute of Japan*, V. 204, 1966, p. 793.

27. R. Kishore, R.N. Singh & T.K. Sinha, *Journal of Materials Science*, V. 32, No. 2, 1997, p. 437.

28. C. Weidig, M. Espindola, B. Gonzalez, P. Rodrigues & M. Andrade, *Wire Journal International*, V. 28, No. 1, 1995, p. 82.

29. B. Cao, J.J. Jonas, P.R. Hastings & N. Nickoletopoulos, Proceedings of the International Conference on Microalloying in Steel, Trans Tech Publishing, 1998, p. 543.

30. J.D. Baird, *Iron and Steel*, June 1963, p. 326.

31. A. Karimi Taheri, T.M. Maccagno & J.J. Jonas, *Metallurgical and Materials Transactions A*, V. 26A, 1995, p. 1183.

32. L.P. Kubin & Y. Estrin, *Acta Metallurgica et Materialia*, V. 38, No. 5, 1990, p. 697.

33. L.P. Kubin & Y. Estrin, *Acta Metallurgica et Materialia*, V. 33, No. 3, 1985, p. 397.

34. Ch. Schwink & A. Nortmann, *Materials Science and Engineering*, A234-236, 1997, p. 1.

35. P. Rodriguez, *Bulletin of Materials Science*, V. 6, No. 4, 1984, p. 653.

36. M.R. Winstone & R.D. Rawlings, *Journal of Materials Science*, V. 6, 1971, p. 1355.

37. A.H. Cottrell, *Philosophical Magazine*, V. 44, 1953, p. 829.

38. M.L. Weaver, *Materials Research Society Symposium Proceedings*, V. 460, 1997, p. 499.

39. D.J. Bailey, *Acta Metallurigca*, V. 13, 1965, p. 436.

40. B.J. Brindley & P.J. Worthington, *Acta Metallurgica*, V. 17, 1969, p. 1357.

41. D.J. Lloyd & P.J. Worthington, *Philosophical Magazine*, V. 24, 1971, p. 195.

42. S. Radelaar, *Scripta Metallurgica*, V. 4, 1970, p. 743.

43. D.S. Fields & W.A. Backofen, *Proceedings of ASTM,* V. 57, 1957, p. 1259.

44. www.inaba.nrm.go.jp/diff.

45. C.P. Ling, Y. Estrin & P.G. McCormick, *Acta Metallurgica et Materialia*, V. 42, No. 5, 1994, p. 1541.

46. C. Ouchi, T. Okita & S. Yamamoto, *Transactions ISIJ*, V. 22, 1982, p. 214.

47. J.W. Cahn, *Acta Metallurgica*, V. 10, 1982, p. 789.

48. P. Lejcek & S. Hofmann, *Critical Reviews in Solid State and Materials Science*, V. 20, No. 1, 1995, p. 1.

49. J. Balík & P. Lukác, *Acta Metallurgica et Materialia*, V. 45, No. 5, 1993, p. 1447.

50. A. Nortmann & Ch. Schwink, *Acta Materialia,* V. 45, No. 5, 1997, p. 2043.

51. A. Nortmann & Ch. Schwink, *Acta Materialia,* V. 45, No. 5, 1997, p. 2051.

52. S.R. Bodner & J. Baruch, *Journal of Applied Physics*, V. 43, No. 5, 1972, p. 2092.

53. S.R. Bodner & A. Rosen, *Journal of the Mechanics and Physics of Solids*, V. 15, 1967, p. 63.

54. W.N. Sharpe, *Journal of the Mechanics and Physics of Solids*, V. 14, 1966, p. 187.

55. S.R. Bodner, *Materials Science and Engineering*, V. 2, 1967, p. 213.

56. A.W. Reynolds, *Metals Transactions*, V. IV, 1949, p.32.

57. J.J. Jonas & T.Sakai, in Deformation, Processing, and Structure, 1982 ASM, Materials Science Seminar, G. Krauss, ed., p. 185.

58. R. Le Gall, G. Liao & G. Saindrenan, *Materials Science Forum*, V. 294-296, 1999, p. 509.

59. R. Le Gall & J.J. Jonas, submitted to *Metallurgical and Materials Transactions*.